The Effects of the Earth's Rotation on Internal Wave Near-resonant Triads and Weakly Nonlinear Models

by

Youna Hu

A thesis
presented to the University of Waterloo
in fulfilment of the
thesis requirement for the degree of
Master of Mathematics
in
Applied Mathematics

Waterloo, Ontario, Canada, 2007

I hereby declare that I am the sole author of this thesis. This is a true copy of the thesis, including any required final revisions, as accepted by my examiners.

I understand that my thesis may be made electronically available to the public.

Abstract

This thesis investigates the effects of the earth's rotation on internal waves from two perspectives of nonlinear internal wave theory: near-resonant triads and weakly nonlinear models.

We apply perturbation theory (multiple scale analysis) to the governing equations of internal waves and develop a near-resonant internal wave triad theory. This theory explains a resonant-like phenomenon in the numerical results obtained from simulating internal waves generated by tide topography interaction. Furthermore, we find that the inclusion of the earth's rotation (nonzero f) in the numerical runs leads to a very special type of resonance: parametric subharmonic instability.

Through using perturbation expansion to solve separable solutions to the governing equations of internal waves, we derive a new rotation modified KdV equation (RMKdV). Of particular interest, the dispersion relation of the new equation obeys the exact dispersion relation for internal waves for both small and moderate wavenumbers (k). Thus this new RMKdV is able to model wea kly nonlinear internal waves with various wavenumbers (k), better than the Ostrovsky equation which fails at describing waves of small k.

Acknowledgements

This thesis could not have been written without Dr. Kevin Lamb who not only supervised but also encouraged and challenged me throughout my master's studies. I would like to thank all the members in our environmental and geophysical fluid dynamics group, especially Dr. Francis Poulin and Dr. Marek Stastna for their guidance and help. Last but not least, I would like to thank Dr. Serge D'Alessio for reading and commenting on my thesis.

Contents

List of Figures

List of Tables

CHAPTER 1

THEORETICAL BACKGROUND

1.1 Internal Waves Studies

Research on internal waves has undergone a great revolution over the years. Since the 1960's, the interplay of wave theory and experimental observations has greatly advanced our understanding of nonlinear internal waves. Recent advances in satellite technology for remote sensing and image processing have brought experimental research on internal waves into a new era. Currently available computer resources allow even small groups to do high resolution numerical simulations of internal waves. The combination of these powerful tools stimulated theoretical studies. This trend will open a new page for the understanding of internal waves.

Internal waves studies contribute to the intellectual exploration of oceanic energy, biological processes, ocean circulation and environmental enhancement, whose theoretical results are vital to aid human activities. A glimpse of the history of internal waves studies is provided in several review papers [Garrett and Munk, 1979; Staquet and Sommeria, 2002; Helfrich and Melville, 2006; Garrett and Kunze, 2007].

Garrett and Munk [1979] gave a very interesting broad review article on internal waves, where four major aspects: observational techniques, interpretations, theory and future work were briefly discussed. This paper was intended to give non-experts some idea of the basic structure of internal waves research.

Helfrich and Melville [2006] focused on nonlinear internal wave models, where equations of the Korteweg-de Vries (KdV) type are the most frequently used weakly nonlinear models and the Euler equations as well as the MCC equation (named after Miyata, Choi and Camassa) are

typically used as fully nonlinear models. They also discussed the fact that properties such as instability and breaking can not be obtained from the weakly nonlinear models and that observed results can be more accurately explained with fully nonlinear models.

A paper concentrating on the process of instability to turbulence of internal waves is Staquet and Sommeria [2002]. This paper at first studied the mechanism of wave steepening and breaking and then discussed the process of wave breaking into small-scale turbulence. In this paper many laboratory and numerical experiment results were presented. By comparing different models and different results, the paper pointed out the difficulty in matching models of widely different ranges of temporal and spatial scales.

Garrett and Kunze [2007] reviewed internal tides in the ocean. After analysing the setting and parameter space of a typical tide topography interaction model, they moved on to theoretical linear theory with assumptions of appropriate small parameters. Then, they discussed numerical models of some ideal nonlinear situations as well as some applications for real topographies, for example the Mid-Atlantic Ridge. They also talked about some layer models investigating internal tides generation as well as oceanic observation results.

In the hope of understanding the influence of the earth's rotation on internal waves, this thesis has covered two aspects: near-resonant wave triad interaction and weakly nonlinear models. In working on these two topics, we pay particular attention to including the earth's rotation and to comparing the results obtained with those obtained in the absence of rotation.

1.2 Objectives

This thesis is divided into two different topics, both of which take the earth's rotation, or more specifically, the Coriolis force into account. As mentioned in the last section, many studies have been carried out on linear and nonlinear internal waves. In order to simplify the algebra and the model itself, a large portion of the research has ignored the earth's rotation. Setting the Coriolis force to be zero works well in cases when the Rossby number (see section 1.5) is larger than one, especially when it is very large. However, when the Rossby number is small, the Coriolis force is very important and cannot be neglected. For the first topic which is covered in chapter 2 and 3, we aim to give a complete theoretical explanation and the numerical results of rotational effects for near resonant internal wave triads. On the second topic, we come up

with a weakly nonlinear model which accounts for rotational effects and keep the exact linear dispersion relation of internal waves.

1.3 Equations of Motion

The equations of motion for an incompressible, inviscid, stratified fluid, under the Boussinesq approximation, observed on the earth rotating at an angular velocity Ω ([Kundu and Cohen, 2004], Chapter 10) are

$$\nabla \cdot \mathbf{u} = 0, \tag{1.1a}$$

$$\frac{D}{Dt}\mathbf{u} + \mathbf{2\Omega} \times \mathbf{u} = -\frac{1}{\rho_0}\nabla \mathbf{p} - \frac{\mathbf{g}\rho}{\rho_\mathbf{0}}\mathbf{k}, \tag{1.1b}$$

$$\frac{D\rho}{Dt} = 0, \tag{1.1c}$$

where $\mathbf{u} = (u, v, w)$, p is the pressure and the fluid density $\rho_d(x, z, t)$ can be written as

$$\rho_d(x, z, t) = \rho_0 + \rho(x, z, t), \tag{1.2}$$

with ρ_0 being the reference density and ρ as the difference of the fluid density from the reference density.

1.4 f-plane and β-plane

In the equations of motion we have the Coriolis force $2\Omega \times \mathbf{u}$. The components of angular velocity of the earth in the local Cartesian system (figure 1.1) are

$$\Omega_x = 0, \tag{1.3a}$$

$$\Omega_y = \Omega \cos\theta, \tag{1.3b}$$

$$\Omega_z = \Omega \sin\theta, \tag{1.3c}$$

where θ is the latitude.

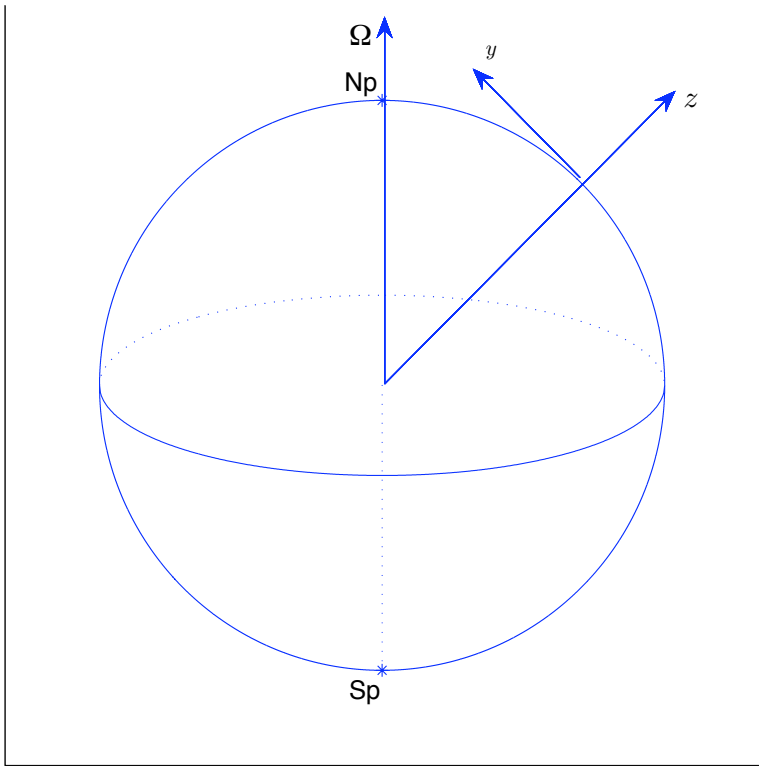

Figure 1.1: The local Catersian coordinate. $\mathbf{\Omega}$ points upward and passes through the north pole. The coordinate center is the intersection point of the y and z axis. x axis is not shown in this figure but is indicated as a line starting from the coordinate center and pointing into the plane where y and z axis are lying on. The label Np and Sp stand for north pole and south pole respectively.

As in ([Kundu and Cohen, 2004], Chapter 12), we make the traditional approximation whereby only the component perpendicular to the surface is retained, in which case the Coriolis force becomes

$$2\mathbf{\Omega} \times \mathbf{u} = (-fv, fu, 0), \tag{1.4}$$

where

$$f = 2\Omega \sin\theta. \tag{1.5}$$

The momentum equations in component form then become

$$\frac{Du}{Dt} - fv = -\frac{1}{\rho_0}\frac{\partial p}{\partial x}, \tag{1.6a}$$

$$\frac{Dv}{Dt} + fu = -\frac{1}{\rho_0}\frac{\partial p}{\partial y}, \tag{1.6b}$$

$$\frac{Dw}{Dt} = -\frac{1}{\rho_0}\frac{\partial p}{\partial z} - \frac{g\rho}{\rho_0}. \tag{1.6c}$$

As an indicator of the Coriolis force, f in equation (1.5) is called the Coriolis parameter. Varying with latitude, it is positive in the northern hemisphere and negative in the southern hemisphere. This variation is very important when the wave motion has very long time scales or very long length scales; however, for a relatively localized wave motion, the variation is negligible and we can treat f as a constant, say, $f_0 = 2\Omega \sin\theta_0$, where θ_0 is a characteristic latitude of the region under study. The approximation of using a constant f_0 is called f-plane approximation. A model using this approximation is often called an f-plane model. Of course, we can approximate f to a higher order. The aforementioned constant approximation is from truncating the taylor expansion of $f(y)$ at $O(1)$. If we include the term of $O(y)$, we will have

$$f = f_0 + \beta y, \tag{1.7}$$

where, according to taylor expansion,

$$\beta = \left(\frac{df}{dy}\right)_{\theta_0} = \left(\frac{df}{d\theta}\frac{d\theta}{dy}\right)_{\theta_0} = \frac{2\Omega\cos\theta_0}{R}. \tag{1.8}$$

Note that $d\theta/dy = 1/R$. The radius of the earth, R is nearly 6371 km. This approximation is called the β-plane approximation. A model employing β-plane approximation is called a β-plane model.

1.5 The Rossby Number

The momentum equation (1.1b) shows that the pressure and the gravitational force must be balanced by the sum of the nonlinear advection and the Coriolis force. To inspect the relative importance of these two forces, we try to write down and compare the order of each.

The order of the nonlinear force is estimated as

$$\rho_0 \mathbf{u} \cdot \nabla \mathbf{u} = O\left(\rho_0 \frac{U^2}{L}\right), \tag{1.9}$$

while the Coriolis force has the order

$$\rho_0 \mathbf{\Omega} \times \mathbf{u} = O\left(\rho_0 \Omega U\right) = O\left(\rho_0 f U\right). \tag{1.10}$$

The ratio of the order of the nonlinear force to that of the Coriolis force is written as

$$Ro = \frac{\rho_0 \frac{U^2}{L}}{\rho_0 f U} = \frac{U}{fL}, \tag{1.11}$$

which is called *the Rossby number*, used as an important parameter in many models. If $Ro \ll 1$, the Coriolis force is very important and we cannot ignore the earth's rotation; however, when $Ro \gg 1$, the nonlinear acceleration overly dominates the Coriolis force and the earth's rotation becomes negligible.

1.6 Governing Equations of Internal Waves

1.6.1 Dimensional Governing Equations of Internal Waves

Throughout this thesis, we will assume the fluid to be inviscid and incompressible and that the wave motion is homogenous in the y direction, i.e. $\frac{\partial}{\partial y} = 0$. What we need to emphasize here is that with rotation, motion in the y direction will occur; however, $\frac{\partial v}{\partial y} = 0$.

From the equations of motion, we can derive the 2-dimensional (2D) governing equations of internal waves with rotation as follows.

We can further split the density ρ in (1.2) as

$$\rho = \bar{\rho}(z) + \rho'(x, z, t), \tag{1.12}$$

where $\bar{\rho}$ is the mean of the density whearas ρ' is a small density perturbation. We also define a very important density related function called the *buoyancy frequency* given by

$$N^2 = -\frac{g}{\rho_0} \frac{d\bar{\rho}}{dz}. \tag{1.13}$$

Since the flow is incompressible (1.1a), we can introduce a streamfunction ψ, such that $(u, w) = (\psi_z, -\psi_x)$. By taking the curl of the horizontal and vertical momentum equations (1.6a and 1.6c) we obtain the vorticity equation

$$\frac{\partial}{\partial t}\nabla^2\psi + J(\nabla^2\psi, \psi) - fv_z - b_x = 0, \tag{1.14}$$

where $\nabla^2 = \frac{\partial^2}{\partial x^2} + \frac{\partial^2}{\partial z^2}$, the Jacobian J is defined by $J(A, B) = A_x B_z - A_z B_x$ and b is a density related function, defined as

$$b = g\frac{\rho'}{\rho_0}. \tag{1.15}$$

With the streamfunction ψ and the Jacobian, (1.6b) turns into

$$v_t + J(v, \psi) + f\psi_z = 0. \tag{1.16}$$

With (1.15), the density equations (1.1c) reads

$$b_t + N^2\psi_x + J(b, \psi) = 0. \tag{1.17}$$

To sum up, the governing equations for internal waves are

$$\frac{\partial}{\partial t}\nabla^2\psi + J(\nabla^2\psi, \psi) - fv_z - b_x = 0, \tag{1.18}$$

$$v_t + J(v, \psi) + f\psi_z = 0, \tag{1.19}$$

$$b_t + N^2\psi_x + J(b, \psi) = 0. \tag{1.20}$$

1.6.2 Non-dimensionalization of the Governing Equations

We have already obtained the dimensional governing equations for internal waves as in (1.18) – (1.20). The physical variables in SI (Système International d'unités) units governed by dimensional governing equations intrinsically hinder the understanding of the physical systems in a parametric way, and hence inevitably bring obstacles in applying the theories and ideas derived in one problem to another. Fortunately, non-dimensionalization, or what we called *scaling* has been developed in order to compare the relative sizes of the various terms.[1] Small non-dimensional parameters are essential to the application of perturbation theory to the physical problems, particularly the nonlinear ones.

[1] More details about scaling will be discussed in Chapter 2.

To carry out non-dimensionalization, we need different standard length scales and time scales in order to measure the physical variables. We choose L, H and U to be the horizontal length scale, vertical length scale and velocity scale respectively. We also assume that u and w are small perturbations of the velocity field, so that

$$u, w \ll U, \tag{1.21}$$

and hence we can set

$$u = \epsilon U \tilde{u}, \tag{1.22}$$

where $\tilde{u}$ is the non-dimensional horizontal velocity and ϵ is a small parameter to represent the smallness of the perturbation. Since $(u, w) = (\psi_z, -\psi_x)$, ψ can be expressed as

$$\psi = \epsilon H U \tilde{\psi}, \tag{1.23}$$

where $\tilde{\psi}$ is the non-dimensional streamfunction.

The dimensions of the other variables can be obtained from the dominant balances in the governing equations. Let

$$(x, z, t) = \left(L\tilde{x}, H\tilde{z}, \frac{L}{U}\tilde{t} \right) \tag{1.24}$$

$$(\psi, b, v) = \epsilon \left(UH\tilde{\psi}, \frac{U^2}{H}\tilde{b}, fL\tilde{v} \right) \tag{1.25}$$

$$N^2 = \frac{U^2}{H^2}\tilde{N}^2. \tag{1.26}$$

The variables with tilde are dimensionless counterparts of those without tildes.

Note that the scale of N^2 guarantees that b_x is of the same order as $\frac{\partial}{\partial t}\psi_{zz}$, or we say that the dominant balance is between these two terms. Using the above scales to non-dimensionalize the governing equations, we obtain the non-dimensional equations

$$\frac{\partial}{\partial t}\psi_{zz} - b_x = \delta v_z + \epsilon J(\psi, \psi_{zz}) - \mu \frac{\partial}{\partial t}\psi_{xx} + \epsilon\mu J(\psi, \psi_{xx}) \tag{1.27a}$$

$$v_t + \psi_z = \epsilon J(\psi, v) \tag{1.27b}$$

$$b_t + N^2\psi_x = \epsilon J(\psi, b), \tag{1.27c}$$

where

$$\mu = \frac{H^2}{L^2}, \delta = \frac{f^2L^2}{U^2}. \tag{1.28}$$

In fact, ϵ is a measure of the smallness of the amplitude, μ evaluates the hydrostaticity, and δ equals to the square of the reciprocal of the Rossby number [Kundu and Cohen, 2004]: Ro, which indicates the importance of the earth's rotation.

1.7 Internal Wave Normal Modes

Internal waves are always associated with density stratification. The simplest case is the internal waves in a two-layer fluid, where waves can be either of elevation or of depression and only mode-1 waves exist. In a three-layer fluid, internal waves are formed by coupled displacement of top interface and the bottom interface, which can be in-phase or out-of-phase. We call the former case mode-1 wave and the latter one mode-2 wave.

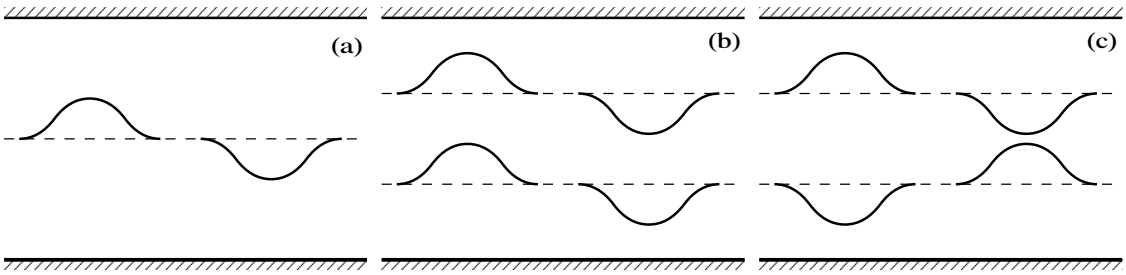

Figure 1.2: This figure gives a demonstration of the simple normal modes. (a) shows a two-layer fluid where only mode-1 wave exists and (b), (c) depict a mode-1 and mode-2 wave respectively.

Internal wave normal mode is a term we use to distinguish the properties of waves in the vertical direction. In figure 1.2, (a) and (b) demonstrate examples of mode - 1 wave, and (c) gives the mode - 2 wave of a three-layer fluid.

The normal mode of internal waves is often used to capture the vertical property of internal wave motion. Inspired by the method of separable solution in solving different equations, we characterize the wave motion in the horizontal plane and the vertical direction. To do so, fluid motion can be conveniently expressed by the multiplication of a function of x,y and t, the horizontal variables and z, the vertical variable. For instance, the horizontal velocity is often written

as

$$u(x,y,z,t) = \sum_{n=0}^{\infty} \eta_n(x,y,t) h_n(z), \tag{1.29}$$

where $u(x,y,z,t)$, in fact, has been separated into different vertical functions[2] $h_n(z)$ ($n \in \mathbb{N}$) weighted by horizontal functions $\eta_n(x)$ ($n \in \mathbb{N}$). *Normal modes* have originated from this idea of separation.

Different textbooks have their own ways of introducing the concept of normal modes of internal waves. By assuming small amplitude and hydrostaticity of the fluid motion[3] together with bringing in N, the buoyancy frequency and the Boussinesq approximation, Kundu and Cohen [2004] linearized (1.1a), (1.1c) and (1.6a) – (1.6c) into

$$\frac{\partial u}{\partial x} + \frac{\partial v}{\partial y} + \frac{\partial w}{\partial z} = 0, \tag{1.30}$$

$$\frac{\partial u}{\partial t} - fv = -\frac{1}{\rho_0}\frac{\partial p}{\partial x}, \tag{1.31}$$

$$\frac{\partial v}{\partial t} + fu = -\frac{1}{\rho_0}\frac{\partial p}{\partial y}, \tag{1.32}$$

$$\frac{\partial p}{\partial z} = -g\rho, \tag{1.33}$$

$$\frac{\partial \rho}{\partial t} - \frac{\rho_0 N^2 w}{g} = 0, \tag{1.34}$$

where N has already defined in (1.13) as

$$N^2 = -\frac{g}{\rho_0}\frac{d\bar{\rho}}{dz}.$$

Taking the solution for the density to be

$$\rho(z) = \sum_{n=0}^{\infty} \rho_n \frac{d\psi_n}{dz}, \tag{1.35}$$

[2]For simplification, we call functions of vertical variables *vertical functions* while naming the functions of horizontal variables *horizontal functions*. Horizontal variables are usually donoted by x and y and vertical variable is conventionally z.

[3]A fluid being hydrostatic is represented as in how we express the pressure in (1.33).

and substituting it into (1.34) and taking that every component of the infinite series is independent of each other due to linearity, Kundu and Cohen [2004] hence obtained the Sturm-Liouville boundary value problem [Boyce and Diprima, 1997]

$$\frac{d}{dz}\left(\frac{1}{N^2}\frac{d\psi_n}{dz}\right)+\frac{1}{c_n^2}\psi_n=0, \tag{1.36}$$

where c_n is the constant from solving (1.34) and (1.35) by the method of separation of variables.

In order to construct a complete Sturm-Liouville problem from (1.36), we need two boundary conditions, which can be obtained from the rigid lid at the top and the bottom of the fluid.

Gill [1982], however, explained the normal modes of internal waves by acquiring two equations relating w and p from the linearized equations which can be given by setting $f=0$ in (1.30) – (1.34)

$$\frac{\partial^2 w}{\partial z\partial t} = \frac{1}{\rho_0}\left(\frac{\partial^2}{\partial x^2}+\frac{\partial^2}{\partial y^2}\right)p, \tag{1.37}$$

$$N^2 w = -\frac{1}{\rho_0}\frac{\partial^2 p}{\partial z\partial t}, \tag{1.38}$$

then, by solving these two equations with separable solutions, he obtained an equation of the Sturm-Liouville form similar to (1.36).

In fact, we can also try to understand the normal modes by manipulating the governing equations (1.27a) – (1.27c). As has been done in the textbooks, we also assume that the wave motion is of infinitesimal amplitude[4]. However, we do not make the hydrostaticity assumption but take $\mu=1$, then the 2D governing equations read

$$\frac{\partial}{\partial t}\nabla^2\psi - b_x = \delta v_z, \tag{1.39a}$$

$$v_t+\psi_z = 0, \tag{1.39b}$$

$$b_t+N(z)^2\psi_x = 0. \tag{1.39c}$$

It is easy to simplify (1.39a) – (1.39c) into one single equation

$$\frac{\partial^2}{\partial t^2}\nabla^2\psi+N(z)^2\psi_{xx}+\delta\psi_{zz}=0. \tag{1.40}$$

[4]Leblond and Mysak [1978] has made a good point in justifying the linearization of equations. They suggested to use a/c to measure if the wave can be assumed to be linear, where a is the amplitude of wave amplitude and c is the typical phase speed of the wave.

In the ocean, the displacement at the surface is much smaller than that in the fluid column, hence we can make the rigid lid approximation, which says that the vertical velocity w is approximately zero at the surface $z = 0$. While at the bottom, we apply the no normal flow boundary condition, so that we obtain $w = 0$ at $z = -H$. These rigid lids are described by figure 1.3.

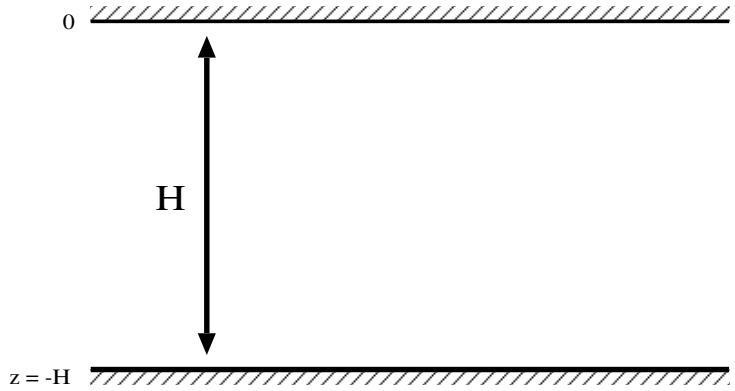

Figure 1.3: Rigid lid approximation means that the vertical velocity is nearly zero at the surface. This figure also demonstrates a flat bottom where there is no normal flow. At the bottom, w is also zero.

The property of streamfunction $\psi_x = -w$ and the two boundary conditions for w yield

$$\psi(x, 0) = 0, \tag{1.41}$$

$$\psi(x, -H) = 0, \tag{1.42}$$

if Substituting $\psi = e^{i(kx-\omega t)}\phi(z)$ into (1.40) gives

$$\frac{d^2}{dz^2}\phi - \left(\frac{\omega^2 - N^2}{\omega^2 - \delta}\right) k^2\phi(z) = 0, \tag{1.43}$$

$$\phi(0) = \phi(-H) = 0. \tag{1.44}$$

The DE (1.43) together with boundary conditions (1.44) form a boundary value problem[5], whose solutions usually require numerical computation. However, to simply the problem, we can assume $N(z)$ is a constant and $f < \omega < N$, hence we obtain its theoretical solution

$$\psi(x, z) = A\cos(mz) + B\sin(mz), \tag{1.45}$$

[5]In a more mathematical context, a boundary value problem is referred as a Sturm-Liouville problem.

where $m^2 = k^2 \frac{N^2-\omega^2}{\omega^2-\delta} > 0$. To meet the boundary conditions (1.44), we need $A = 0$ and

$$m_n = \frac{n\pi}{H}. \qquad n = 0, 1, 2 \cdots , \tag{1.46}$$

which is the equation expressing the normal modes of internal waves. This expression of m_n is consistent with the result derived by Kundu and Cohen [2004] and Gill [1982].

1.8 Tidal Frequency

The tides, referring to the cyclic rise and fall of ocean levels (especially the coastal sea water levels), result from the gravitational force and centrifugal force from the earth-moon system and the earth-sun system. Mellor [1996] has explained the underlying mathematics and physics of tides. He also showed that the moon plays a more important role than the sun in the generation of tides.

There are many different types of tides all over the world. Even though some people tend to classify the tides into many small categories [Doodson, 1921], in fact, it is more convenient to think of these two fundamental types of tides: the diurnal tides (K_1 tides) and the semi-diurnal tides (M_2 tides). In some areas of the gulf of Mexico and Southeast Asia, we can see tides having one high and one low per day. These tides are usually called *diurnal tides*, or K_1 tides. However, what is more common along the Atlantic and Arctic coast are the *semidiurnal tides*, called M_2 tides. The other types of tides are usually classified as the *mixed tides* of K_1 and M_2 tides, where we see higher high water, lower high water, higher low water as well as lower low water in the tides.

The M_2 tide is the dominant tide throughout the world since its tidal potential is the largest; therefore, a very large portion of tides research and studies have been focused on this specific type of tide.

Consequently, the *tidal frequency* is conventionally taken to be the M_2 tide, which is

$$\omega_{M_2} = \frac{2\pi}{T_{M_2}} = 1.4075 \times 10^{-4}\ s^{-1}, \tag{1.47}$$

with M_2 tidal period: $T_{M_2} = 12.42$ hr. We refer to Mellor [1996] for details of the derivation of T_{M_2} and ω_{M_2}.

CHAPTER 2

NEAR-RESONANT INTERNAL WAVE TRIADS

2.1 Resonance and Perturbation Theory

Resonance is an interesting phenomenon in oscillatory problems, such as the motion of a mass-spring system, the R-L-C circuit and so on. Jeffrey [1999] introduces resonance using the second-order ordinary differential equation (ODE) given by

$$\frac{d^2y}{dt} + 2\zeta\frac{dy}{dt} + \Omega^2 y = A\cos(\omega t). \tag{2.1}$$

It can be shown that the amplitude of the steady state solution of this ODE is

$$P(\omega) = \frac{A}{\left(\left(\Omega^2 - \omega^2\right)^2 + 4\zeta^2\omega^2\right)^{1/2}}. \tag{2.2}$$

$P(\omega)$ obtains its maximum when

$$\omega^2 = \omega_c^2 = \Omega^2 - 2\zeta^2, \tag{2.3}$$

in which case

$$P_{max} = \frac{A}{2\zeta\left(\Omega^2 - \zeta^2\right)^{1/2}}. \tag{2.4}$$

The system is said to experience *resonance* at ω_c, when the *external forcing frequency*[1] is the same as the *inertial frequency*[2]. The most extreme effect of resonance occurs when there is no damping ($\zeta = 0$), in which case the amplitude is unbounded. To be more specific, on setting $\zeta = 0$ in (2.1) and solving for $y(t)$ subject to (2.3), we obtain

$$y(t) = t\sin(\Omega t). \tag{2.5}$$

However, this extreme example is unphysical, since any physical system will invariably experience dissipation and damping. Nonlinearity will also modify the behaviour of the system.

In dealing with nonlinearity, among the most effective techniques are perturbation methods, the idea of which was originated in 17th century celestial mechanics and thereafter had been introduced in order to solve many differential equations from various branches of mechanics. The premise of perturbation theory is to find an approximate solution in the form of a power series form in a small parameter. First, we need to solve the lowest order problem and then use its result to obtain a sequence of higher order solutions. For instance, in a wave-wave interaction problem ([Leblond and Mysak, 1978],[Craik, 1985]), we have the nonlinear term in the material derivative term

$$\frac{Du}{Dt} = \frac{\partial u}{\partial t} + u\frac{\partial u}{\partial x} + v\frac{\partial u}{\partial y} + w\frac{\partial u}{\partial z}, \tag{2.6}$$

in the momentum equation, which appears in (1.6a) back into chapter 1.

The nonlinear terms make it hard to find exact solutions of u in (1.6a) given appropriate conditions. Perturbation theory suggests us to assume the solution u as the form of a power series as

$$u = \epsilon u_0 + \epsilon^2 u_1 + \epsilon^3 u_2 + \mathrm{O}(\epsilon^4). \tag{2.7}$$

If the amplitude of u is very small, we can define a small parameter ϵ and claim that u is the same order of ϵ, the small parameter [3], while the nonlinear terms, say, $u\frac{\partial u}{\partial x}$ is at the order of ϵ^2 and we can claim that $u\frac{\partial u}{\partial x} \ll u$. Therefore, in solving u_0, we can ignore higher order terms,

[1]External forcing are the terms on the right hand side that makes the ODE in-homogeneous. In (2.1), $A\cos(\omega t)$ is the external forcing term and ω is the forcing frequency.

[2]Inertial frequency is defined as the oscillation frequency of the corresponding homogenous equation, which is $\frac{d^2y}{dt} + 2\zeta\frac{dy}{dt} + \Omega^2 y = 0$ for (2.1).

[3]Mathematically, we call $a(x)$ is in the same order of $b(x)$ if we have $\lim_{x\to x_0}\frac{a(x)}{b(x)} = c$, where c is a nonzero and bounded constant.

and at the next step, when solving u_1, we can use the already computed value of u_0. At the end, if the power series in (2.7) actually converges, it can be taken as a valid asymptotic solution for the problem. However, if the series diverges, for example, $\lim_{x \to x_0} u(x) = \frac{1}{\epsilon}$, we call this a *secular term* and the perturbation series is not able to provide a valid solution. The regular perturbation method [Lamb, 2005; Bender and Orszag, 1999; Nayfeh, 1973] fails at this point and we need to try a singular perturbation method [Lamb, 2005; Bender and Orszag, 1999; Nayfeh, 1973].

Figure 2.1 shows the infinitely growing amplitude of function $y(t) = t\sin(t)$ as in (2.5). This amplitude characterizes resonant phenomena and the term is a *secular term*[4] in perturbation theory. This term is unphysical since it would allow a system to possess an unbounded amount of energy. According to perturbation theory, secular terms are not allowed in the perturbation power series since a divergent series does not give a valid approximation to the actual solution. However, the singular perturbation method provides us the method of multiple scales [Bender and Orszag, 1999] to deal with cases where secular terms appear. Later in this thesis, we will apply this method to deal with resonant and near-resonant behaviours in internal wave triads.

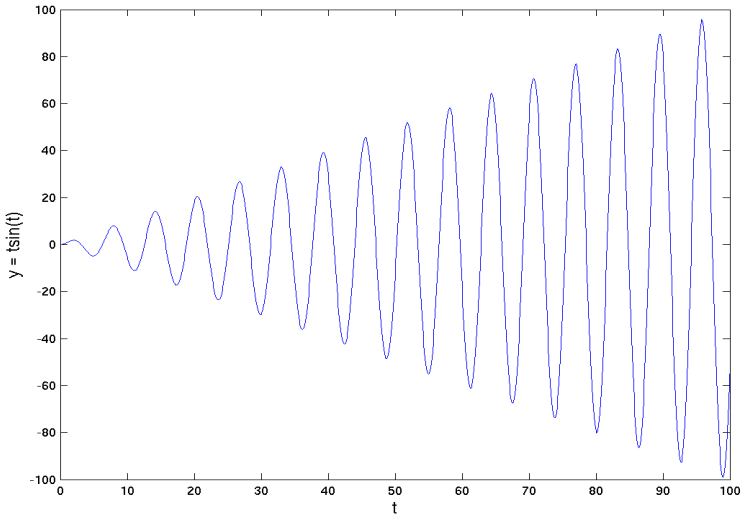

Figure 2.1: The infinitely growing amplitude of the secular term: $t\sin(t)$.

[4]Secular terms are also known as resonant terms.

2.2 On Near-resonant Water Waves

2.2.1 Water Wave Resonance and its Development

Resonance in water waves is a typical example of "weak wave-wave interaction" [Leblond and Mysak, 1978], the theory of which is the outgrowth of the application of perturbation theory in water waves. Following Craik [1985], we introduce resonance by investigating the interaction of several waves with dominant wave modes under *resonant conditions*. Resonance usually occurs among a group of waves. If there are only three waves in this group, we get a *resonant triad*, which is the most basic resonant wave. In order to obtain the resonant condition, we take the conventional wave form[5] as

$$Re\{a_j(x)e^{-i(\vec{k}\cdot\vec{x}-Re\{\omega_j t\})}\}, \qquad (j=1,2,3), \tag{2.8}$$

with amplitude a_j being small. Interaction of any of the two waves, say, the first and second wave[6] in terms of the nonlinear terms yields a term like

$$e^{-i\{(\vec{k}_1+\vec{k}_2)\cdot\vec{x}+Re(\omega_1+\omega_2)t\}}, \tag{2.9}$$

which comes from taking the sum product into account. When (2.9) acts as a forcing term, resonance would occur if we have

$$\vec{k}_1+\vec{k}_2 = \vec{k}_3, \tag{2.10a}$$

$$Re\{\omega_1\}+Re\{\omega_2\} = Re\{\omega_3\}, \tag{2.10b}$$

which drives (2.9) into the family of the third wave[7]. Note that $(\vec{k_j},\omega_j)(j=1,2,3)$ satisfy the given dispersion relation of the physical problem under study. Similar to the forcing term on the right hand side of the ODE given by (2.1), here, (2.9) can be viewed as an external forcing characterized by wave-vector $\vec{k_1}+\vec{k_2}$ and frequency $Re\{\omega_1\}+Re\{\omega_2\}$, and the wave-vector and inertial frequency of the physical system is given by $\vec{k_3}$ and $Re\{\omega_3\}$. If (2.10a) and (2.10b) are

[5]For generality, Craik [1985] used complex ω_j $(j=1,2,3)$. Most of the time in this thesis, we are working with real ω_j $(j=1,2,3)$.

[6]We use subindices to denote the n^{th} wave.

[7]If wave a has same frequency and wavenumber of wave b, we say they are in the same wave family.

satisfied, external forcing resonate with wave 3; (2.10a) – (2.10b) are called *the resonant triad condition*.

The resonant triad condition can be also found in Pedlosky [1987] and is summarized as

$$\vec{k}_1 + \vec{k}_2 + \vec{k}_3 = 0, \tag{2.11a}$$

$$\omega_1 + \omega_2 + \omega_3 = 0, \tag{2.11b}$$

where k_j $(j = 1, 2, 3)$ and $\omega_j (j = 1, 2, 3)$ are the wavenumber vector and frequency of the resonant triad. Notice that (2.11a) – (2.11b) can be viewed as the same as (2.10a) – (2.10b), if we allow k_j and ω_j to have $\pm$ signs.

Phillips [1960] and Hasselmann [1962] are the pioneers on the studies of resonant water waves. They independently worked out that resonant triads for inviscid surface gravity waves do not exist. Three waves must interact to produce a fourth wave and they satisfied the resonant quartets condition

$$\vec{k}_1 + \vec{k}_2 + \vec{k}_3 + \vec{k}_4 = 0, \tag{2.12a}$$

$$\omega_1 + \omega_2 + \omega_3 + \omega_4 = 0. \tag{2.12b}$$

Following their work, McGoldrick [1965, 1970, 1972] showed that even though there is no resonant triads for inviscid surface gravity waves, the interaction of the capillary-gravity waves is able to embrace resonant triads.

For internal gravity waves, Thorpe [1966] claimed that resonant triads are possible for any stable stratification and McComas and Bretherton [1977] discussed them in detail. Martin et al. [1972] carried an experiment on linearly stratified internal wave triads and presented its theoretical explanation. The possibility of a resonant triad formed by a pair of surface gravity waves and an internal gravity wave was shown by Thorpe [1966].

2.2.2 From Resonance to Near-resonance

In the last section, we glanced at the development on resonant water wave theory. We also need to mention that for waves in other fields, for example, optics, electronics. there is also a series of literature devoted on resonance studies [Armstrong et al., 1962]. Nayfeth [1971]; Armstrong et al. [1962] are among the earliest scientists to use the concept of *near-resonance* and try to

link and compare between exact resonance and near-resonance. Two recent pieces of work on near-resonance can be found in [Smith and Lee, 2005; Lamb, 2007b].

Resonance exists when (2.11a) – (2.11b) or (2.12a) – (2.12b) are satisfied perfectly; however, when there is a small detuning of frequency and wavenumber, near-resonance occurs. Craik [1985] defined a frequency mismatch in resonant triads as

$$\omega_1 + \omega_2 + \omega_3 = \Delta\omega, \tag{2.13}$$

and named this case as near-resonance when $\Delta\omega$ is very small. Also, Armstrong et al. [1962] named the resonant like physical phenomenon near-resonance when there is a small mismatch for the horizontal wavenumber

$$k_1 + k_2 + k_3 = \Delta k. \tag{2.14}$$

To sum up, if three waves satisfy the following relations

$$-\vec{k_3} + \Delta\vec{k} = \vec{k_1} + \vec{k_2}, \tag{2.15}$$

$$-\omega_3 + \Delta\omega = \omega_1 + \omega_2, \tag{2.16}$$

$$\omega_j = \omega(k_j), \qquad j = 1, 2, 3 \tag{2.17}$$

and when $\Delta\vec{k}$ and $\Delta\omega$ are relatively small, they form a near-resonant triad.

2.2.3 Near-resonant Triads in Internal Waves

The general theory of near-resonance can be applied to internal waves, where the dispersion relation is specified by the theory of internal waves. For internal waves, there are two important stages: the generation and the propagation of internal waves. Internal waves are usually generated by the combined effects of the earth's rotation and the stratification of the medium. A typical example is internal waves generated by the interaction of barotropic tides and topography. In this case, most of the energy in the internal wave field resides in waves of tidal frequency, which is called *internal tides.* The significance of the earth's rotation on inertial tides can be found in [Gerkema and Zimmerman, 1994] and [Gerkema, 1996]. During the propagation of internal waves, if the frequency is small, the earth's rotation is important as well. However, for some other problems, for example, the propagation of internal solitary waves, the earth's rotation can be treated as not important and hence neglected except for over long time scales, the case

when the tiny influence of the earth's rotation can accumulate to an important factor over a long period. Therefore, the earth's rotation has to be taken into account in many circumstances; however, when it is indeed too small to be considered, making the approximation of $f = 0$ brings many conveniences and also enhances the efficiency of scientific endeavours. This thesis will analyze near-resonance with and without the earth's rotation distinctly.

Throughout this thesis, we will be studying a near-resonant triad formed by harmonic 2 – mode 2, harmonic 1 – mode 3 and harmonic 1 – mode 1 waves[8]. The frequencies and the wavenumbers of them are

$$\text{frequency:} \qquad \omega_1 = -2\omega_{M_2}, \qquad \omega_2 = \omega_{M_2}, \qquad \omega_3 = \omega_{M_2}, \tag{2.18a}$$

$$\text{vertical wavenumber:} \qquad m_1 = \frac{2\pi}{H}, \qquad m_2 = -\frac{3\pi}{H}, \qquad m_3 = \frac{\pi}{H}, \tag{2.18b}$$

where ω_{M_2} is the M_2 tidal frequency given by (1.47), and horizontal wavenumbers of the internal waves can be computed by using the dispersion relation for internal waves, which is, in the general rotating case,

$$\omega^2 = \frac{N^2k^2 + \delta m^2}{k^2 + m^2}. \tag{2.19}$$

Notice that only waves which meet and interact are able to form resonant triads, so we need to require that all three waves have positive phase speeds.

2.2.4 Near-resonance Internal Wave Triads with the Earth's Rotation

For a model with $Ro \leq 1$ [Kundu and Cohen, 2004][9], it is necessary to include the earth's rotation. Furthermore, we want to take the full nonhydrostaticity into account and include the small amplitude of wave motion to enable a weakly-nonlinear analysis, thus obtaining resonant triad theory. In summary, the three parameters satisfy

$$\epsilon \ll 1, \quad \mu = 1, \quad Ro \leq 1. \tag{2.20}$$

[8]Harmonic number is defined as the wave frequency divided by tidal frequency ω_{M_2}, for instance, harmonic 2 wave is the wave with frequency of twice of the tidal frequency.

[9]$Ro = \frac{U^2}{f^2L^2}$. Recall $\delta = \frac{f^2L^2}{U^2}$, so $\delta = \frac{1}{Ro}$.

Eliminating b in (1.27a) and (1.27c) on the left hand side leads us to

$$\frac{\partial^2}{\partial t^2}\nabla^2\psi + N^2\psi_{xx} = \delta v_{zt} + \epsilon\frac{\partial}{\partial t}J\left(\psi, \nabla^2\psi\right) + \epsilon\frac{\partial}{\partial x}J\left(\psi, b\right) \tag{2.21a}$$

$$v_{zt} + \psi_{zz} = \epsilon\frac{\partial}{\partial z}J\left(\psi, v\right), \tag{2.21b}$$

which can be combined as

$$\frac{\partial^2}{\partial t^2}\nabla^2\psi + N^2\psi_{xx} + \delta\psi_{zz} = \epsilon\frac{\partial}{\partial t}J\left(\psi, \nabla^2\psi\right) + \epsilon\frac{\partial}{\partial x}J\left(\psi, b\right) + \epsilon\delta\frac{\partial}{\partial z}J\left(\psi, v\right), \tag{2.22}$$

where $\nabla^2 = \frac{\partial^2}{\partial x^2} + \frac{\partial^2}{\partial z^2}$. Note that because of nonlinearity, it is hard to eliminate v and b to obtain a closed system involving only ψ, hence we have the Jacobian terms of v and b.

On linearizing (2.22) and seeking solutions of the form $\psi \propto e^{-i(kx+mz-\omega t)}$, we obtain the dispersion relation

$$\omega^2 = \frac{N^2k^2 + \delta m^2}{k^2 + m^2} \tag{2.23}$$

with linear solutions

$$\psi^{(0)}(x,z,t) = \frac{1}{2}\sum_{n=1}^{3}\left\{\frac{a_n}{m_n}e^{i\theta_n} + \text{c.c.}\right\}\sin(m_n z), \tag{2.24}$$

$$v^{(0)}(x,z,t) = -\frac{i}{2}\sum_{n=1}^{3}\left\{\frac{a_n}{\omega_n}e^{i\theta_n} - \text{c.c.}\right\}\cos(m_n z), \tag{2.25}$$

$$b^{(0)}(x,z,t) = \frac{N^2}{2}\sum_{n=1}^{3}\left\{\frac{k_n}{m_n\omega_n}a_n e^{i\theta_n} + \text{c.c.}\right\}\sin(m_n z), \tag{2.26}$$

where

$$\theta_n = k_n x - \omega_n t + \phi_n, \tag{2.27}$$

and c.c. stands for complex conjugate.

Rearranging (2.23) gives

$$k = \pm m\left(\frac{\omega^2 - \delta}{N^2 - \omega^2}\right)^{\frac{1}{2}}, \tag{2.28}$$

f (s^{-1})	k_1(m^{-1})	k_2(m^{-1})	k_3 (m^{-1})	Δk (m^{-1})	Ro
0.2×10^{-4}	-0.00184	0.00133	4.42×10^{-4}	-7.0×10^{-5}	0.9
0.4×10^{-4}	-0.00182	0.00128	4.28×10^{-4}	-1.12×10^{-4}	0.45
0.5×10^{-4}	-0.00181	0.00125	4.18×10^{-4}	-1.4×10^{-4}	0.36
0.6×10^{-4}	-0.00180	0.00121	4.04×10^{-4}	-1.85×10^{-4}	0.3
0.8×10^{-4}	-0.00177	0.00110	3.67×10^{-4}	-2.97×10^{-4}	0.225
1.0×10^{-4}	-0.00172	9.4×10^{-4}	3.14×10^{-4}	-4.65×10^{-4}	0.18

Table 2.1: The wavenumbers for harmonic 2 – mode 2, harmonic 1 – mode 3, and harmonic 1 – mode 1 waves given different choices of f and constant $N = 1.0 \times 10^{-3}\mathrm{s}^{-1}$. Here, $\Delta k = k_1 + k_2 + k_3$ is the detuning of the frequency. $R_0 = \frac{U}{fL}$ is the Rossby number.

from which we obtain the horizontal wavenumbers of the aforementioned resonant triad described by (2.18a) – (2.18b)

$$k_1 = -2m_0 \left(\frac{4\omega_{M_2}^2 - \delta}{N^2 - 4\omega_{M_2}^2} \right)^{\frac{1}{2}}, \tag{2.29}$$

$$k_2 = 3m_0 \left(\frac{\omega_{M_2}^2 - \delta}{N^2 - \omega_{M_2}^2} \right)^{\frac{1}{2}}, \tag{2.30}$$

$$k_3 = m_0 \left(\frac{\omega_{M_2}^2 - \delta}{N^2 - \omega_{M_2}^2} \right)^{\frac{1}{2}}, \tag{2.31}$$

the sign's being chosen so all waves in the triad have positive phase speed.

Note that this set of wavenumbers leads to

$$k_1 + k_2 + k_3 = -\Delta k \neq 0, \tag{2.32}$$

which is the essence of near-resonant triads. We require Δk to be small compared with the k_j ($j = 1, 2, 3$) in near-resonant theory and the given resonant triad indeed satisfies this requirement (details can be found in appendix A).

Some example values of Δk in its dimensional form can be found in table 2.1, where $N(z) = 1.0 \times 10^{-3}$ s^{-1}. The non-dimensional counterparts are given by table 2.2.

δ	$\tilde{k}_1$	$\tilde{k}_2$	$\tilde{k}_3$	$\Delta\tilde{k}$
0.0039	-1.8386	1.3263	0.4421	-0.0702
0.0158	-1.8246	1.2847	0.4282	-0.1117
0.0247	-1.8140	1.2525	0.4175	-0.1440
0.0355	-1.8009	1.2121	0.4040	-0.1849
0.0632	-1.7673	1.1024	0.3675	-0.2947
0.0987	-1.7231	0.9429	0.3143	-0.4658

Table 2.2: The non-dimensional wavenumbers for harmonic 2 – mode 2, harmonic 1 – mode 3, and harmonic 1 – mode 1 waves given different choices of f and constant $N = 1.0 \times 10^{-3}\text{s}^{-1}$. Here, $\Delta k = k_1 + k_2 + k_3$. The rotation parameter δ and other variables with tilde are non-dimensionalized by $\delta = \frac{f^2\pi^2}{N^2}$ and $\tilde{k}_i = Hk_i$. Details of the non-dimensionalization will be given in section 3.1.4.

The choice of choosing the vertical profile of ψ to be a sinusoid is made due to the rigid lid boundary conditions, say $\psi(x, 0, t) = \psi(x, -1, t) = 0$, if $z = 0$ and $z = -1$ are the top and bottom boundaries, respectively. Here, ω and k are given. Without loss of generality and for convenience we let

$$\phi_1 + \phi_2 + \phi_3 = \frac{\pi}{2}, \tag{2.33}$$

thus

$$\theta_1 + \theta_2 + \theta_3 = \frac{\pi}{2} - \Delta k x. \tag{2.34}$$

If we keep the algebra without any modification, we will get unbounded amplitude functions. In fact, in the physical world, due to nonlinear interaction, none of the waves will grow unboundedly. Many previous works [Craik, 1985; Pedlosky, 1987] suggest to adjust the amplitude equations to eliminate this problem. According to multiple scale analysis [Bender and Orszag, 1999], we introduce two slowly varying variables

$$\xi = \epsilon x, \quad \tau = \epsilon t. \tag{2.35}$$

Recall that Δk defined in (2.32) is small as well and if we use this small parameter ϵ to express Δk, we will have

$$\Delta k = \epsilon\tilde{k}, \tag{2.36}$$

and naturally get

$$\Delta k x = \epsilon \tilde{k} x = \tilde{k}\xi, \tag{2.37}$$

and

$$\theta_1 + \theta_2 + \theta_3 = \frac{\pi}{2} - \tilde{k}\xi. \tag{2.38}$$

Also, the linearized stream-function $\psi^{(0)}$ becomes a function of x, ξ, t and τ

$$\psi^{(0)} = \frac{1}{2}\sum_{1}^{3}\left\{\frac{a_n(\xi,\tau)}{m_n}e^{i\theta_n} + \text{c.c.}\right\}\sin(m_n z). \tag{2.39}$$

Consequently, the linearized $v^{(0)}$ and $b^{(0)}$ are functions of x, t, ξ and τ as well. As a result, (2.22) can be written as

$$\begin{aligned}\frac{\partial^2}{\partial t^2}\nabla^2\psi + N^2\psi_{xx} + \delta\psi_{zz} &= \epsilon\left(-2\nabla^2\psi_{t\tau} - 2\psi_{x\xi tt} - 2N^2\psi_{x\xi}\right) + \epsilon\frac{\partial}{\partial t}J\left(\psi, \nabla^2\psi\right) \\ &+ \epsilon\frac{\partial}{\partial x}J\left(\psi, b\right) + \epsilon\delta\frac{\partial}{\partial z}J\left(\psi, v\right) + O\left(\epsilon^2\right), \end{aligned} \tag{2.40}$$

where

$$\nabla^2 = \frac{\partial^2}{\partial x^2} + \frac{\partial^2}{\partial z^2}. \tag{2.41}$$

Looking for asymptotic solution, we expand ψ, b and v as

$$\psi = \psi^{(0)} + \epsilon\psi^{(1)} + O\left(\epsilon^2\right), \tag{2.42}$$

$$b = b^{(0)} + \epsilon b^{(1)} + O\left(\epsilon^2\right), \tag{2.43}$$

$$v = v^{(0)} + \epsilon v^{(1)} + O\left(\epsilon^2\right). \tag{2.44}$$

The solutions of the $O(1)$ problem are the linearized solutions, which are the same as equations (2.24) – (2.26), except that the amplitudes are now functions of ξ and τ. At $O(\epsilon)$, we have

$$\begin{aligned}\frac{\partial^2}{\partial t^2}\nabla^2\psi^{(1)} + N^2\psi^{(1)}_{xx} + \delta\psi^{(1)}_{zz} &= -2\nabla^2\psi^{(0)}_{t\tau} - 2\psi^{(0)}_{x\xi tt} - 2N^2\psi^{(0)}_{x\xi} + \frac{\partial}{\partial t}J\left(\psi^{(0)}, \nabla^2\psi^{(0)}\right) \\ &+ \frac{\partial}{\partial x}J\left(\psi^{(0)}, b^{(0)}\right) + \delta\frac{\partial}{\partial z}J\left(\psi^{(0)}, v^{(0)}\right). \end{aligned} \tag{2.45}$$

Using the leading-order solutions (2.24) – (2.26)[10], we compute the three Jacobian terms.

$$\begin{aligned} J\left(\psi^{(0)}, \nabla^2\psi^{(0)}\right) &= \frac{i}{8}\sum_{n=1}^{3}\sum_{j=1}^{3}\frac{k_n}{m_n}(\kappa_n^2-\kappa_j^2)(a_n a_j e^{i(\theta_n+\theta_j)} \\ &+ a_n a_j^* e^{i(\theta_n-\theta_j)} - \text{c.c.})(\sin((m_n+m_j)z)+\sin((m_n-m_j)z)), \end{aligned} \tag{2.46}$$

where $\kappa_n^2 = k_n^2 + m_n^2$ and $\kappa_j^2 = k_j^2 + m_j^2$. To screen out the difference terms of phases $(\theta_n - \theta_j)$, we have

$$J\left(\psi^{(0)}, \nabla^2\psi^{(0)}\right) \approx F_{123} + F_{231} + F_{321}, \tag{2.47}$$

where

$$F_{pqr} = \frac{1}{8}\left(\frac{k_q}{m_q} - \frac{k_r}{m_r}\right)\left(\kappa_q^2 - \kappa_r^2\right)\left(a_q a_r e^{-i\theta_p - i\tilde{k}\xi} + \text{c.c.}\right)\sin(m_p z). \tag{2.48}$$

As a matter of fact, p, q, r can be chosen as

$$\{p,q,r\} \in \{\{1,2,3\},\{2,3,1\},\{3,2,1\}\}\,. \tag{2.49}$$

In (2.47), we use the approximation symbol[11] to denote the resonant terms composed by the three waves from the triads. To get these resonant terms, we keep the sum terms, for example, $\theta_n + \theta_j$, $m_n + m_j$ and leave out the difference terms such as $\theta_n - \theta_j$ and $m_n - m_j$. This notation has been used in [Lamb, 2007b] and is enormously effective and successful in conveying the idea. Without this notation, the algebra gets tedious, as Phillips [1981] has commented about.

Similarly, we have an expression for the Jacobian of b given by

$$J\left(\psi^{(0)}, b^{(0)}\right) = \frac{iN^2}{8}\sum_{n=1}^{3}\sum_{j=1}^{3}\frac{k_j}{m_j}\left(\frac{k_j}{m_j} - \frac{k_n}{m_n}\right)\left(a_j a_n e^{i(\theta_n+\theta_j)}\right. \tag{2.50}$$

$$\left. + a_j a_n^* e^{i(\theta_n-\theta_j)} - \text{c.c.}\right)\left(\sin((m_n+m_j)z)+\sin((m_n-m_j)z)\right) \tag{2.51}$$

and consequently we obtain

$$J\left(\psi^{(0)}, b^{(0)}\right) \approx G_{123} + G_{231} + G_{321}, \tag{2.52}$$

where

$$G_{pqr} = -\frac{N^2}{8}\left(\frac{k_q}{m_q} - \frac{k_r}{m_r}\right)\left(\frac{k_q}{\omega_r} - \frac{k_r}{\omega_r}\right)\left(a_q a_r e^{-i\theta_p - i\tilde{k}\xi} + \text{c.c.}\right)\sin(m_r z) \tag{2.53}$$

[10]Here, $a_n(\ n = 1, 2, 3)$ are functions of ξ and τ.

[11]These symbols are also used in (2.52) and (2.55) for the same purpose.

The third Jacobian is

$$J\left(\psi^{(0)},v^{(0)}\right)=\frac{1}{8}\sum_{n=1}^{3}\sum_{j=1}^{3}\left(\frac{k_n m_j}{m_n\omega_j}-\frac{k_j}{\omega_j}\right)\left(a_n a_j e^{i(\theta_i+\theta_j)}+\text{c.c.}\right)\left(\cos((m_n+m_j)z)-\cos((m_n-m_j)z)\right), \tag{2.54}$$

and so

$$\delta\frac{\partial}{\partial z}J\left(\psi^{(0)},v^{(0)}\right)\approx H_{123}+H_{231}+H_{321}, \tag{2.55}$$

where

$$H_{pqr}=\frac{\delta m_p}{8}\left(\frac{k_q m_r}{m_r\omega_r}-\frac{k_r}{\omega_q}+\frac{k_r m_q}{m_r\omega_q}-\frac{k_q}{\omega_q}\right)\left(a_q a_r e^{-i\theta_p-i\tilde{k}\tilde{x}}+\text{c.c.}\right)\sin(m_p z). \tag{2.56}$$

The three Jacobian terms then add up as

$$\begin{aligned}\frac{\partial}{\partial t}J\left(\psi^{(0)},\nabla^2\psi^{(0)}\right) &+ \frac{\partial}{\partial x}J\left(\psi^{(0)},b^{(0)}\right)+\delta\frac{\partial}{\partial z}J\left(\psi^{(0)},v^{(0)}\right)\\ &\approx i\alpha_{123}\left(a_2a_3e^{-i\tilde{k}\xi}e^{-i\theta_1}-\text{c.c.}\right)\sin(m_1z)\\ &+ i\alpha_{231}\left(a_3a_1e^{-i\tilde{k}\xi}e^{-i\theta_2}-\text{c.c.}\right)\sin(m_2z)\\ &+ i\alpha_{321}\left(a_1a_2e^{-i\tilde{k}\xi}e^{-i\theta_3}-\text{c.c.}\right)\sin(m_3z),\end{aligned} \tag{2.57}$$

where

$$\alpha_{pqr} = \frac{1}{8}N^2\left(\frac{k_q}{m_q}-\frac{k_r}{m_r}\right)\left(\frac{\omega_p}{N^2}\left(\kappa_q^2-\kappa_r^2\right)+k_p\left(\frac{k_q}{\omega_q}-\frac{k_r}{\omega_r}\right)\right) \tag{2.58}$$

$$+ \frac{\delta m_p}{8}\left(\frac{k_q}{m_q}-\frac{k_r}{m_r}\right)\left(\frac{m_r}{\omega_r}-\frac{m_q}{\omega_q}\right). \tag{2.59}$$

The sum of the first three terms on the RHS of (2.45) is

$$-2\nabla^2\psi_{t\tau}-2\psi_{x\xi tt}-2N^2\psi_{x\xi}=-\sum_{j=1}^{3}\left\{\kappa_j^2\frac{i\omega_j}{m_j}\left(\frac{\partial a_j}{\partial\tau}+C_{g_j}\frac{\partial a_j}{\partial\xi}\right)e^{i\theta_j}+\text{c.c.}\right\}\sin(m_jz), \tag{2.60}$$

where

$$C_{g_j}=\frac{k_j\left(N^2-\omega_j^2\right)}{\kappa_j^2\omega_j}, \tag{2.61}$$

and C_{g_j} is the group velocity of the j^{th} linear long internal wave.

To eliminate the secular terms and close the system, we set

$$\frac{\partial a_p}{\partial \tau} + C_{g_p}\frac{\partial a_p}{\partial \xi} = -\gamma_{pqr} a_q^* a_r^* e^{i\tilde{k}\xi}, \tag{2.62}$$

where

$$\begin{aligned}\gamma_{pqr} = \frac{\alpha_{pqr}}{\kappa_p^2 \frac{\omega_p}{m_p}} &= \frac{1}{8}\frac{m_p N^2}{\kappa_p^2}\left(\frac{k_q}{m_q} - \frac{k_r}{m_r}\right)\left(\left(\frac{k_q}{\omega_q} - \frac{k_r}{\omega_r}\right)\left(\frac{k_1}{\omega_1} + \frac{k_2}{\omega_2} + \frac{k_3}{\omega_3}\right)\right. \\ &+ \left.\delta\left(\frac{m_q}{\omega_q} - \frac{m_r}{\omega_r}\right)\left(\frac{m_1}{\omega_1} + \frac{m_2}{\omega_2} + \frac{m_3}{\omega_3}\right)\right),\end{aligned} \tag{2.63}$$

for $\{p,q,r\} = \{1,2,3\}, \{2,3,1\}$ or $\{3,2,1\}$.

To work on the complex amplitude function in a convenient way, we separate a complex function into its real and complex part. Here, we write $a_p = c_p - is_p$ and hence obtain

$$\psi^{(0)}(x,z,t) = \sum_{n=1}^{3}\left\{\frac{c_n}{m_n}\cos\theta_n + \frac{s_n}{m_n}\sin\theta_n\right\}\sin(m_n z) \tag{2.64a}$$

$$b^{(0)}(x,z,t) = N^2\sum_{n=1}^{3}\left\{c_n\frac{k_n}{m_n\omega_n}\cos\theta_n + s_n\frac{k_n}{m_n\omega_n}\sin\theta_n\right\}\sin(m_n z) \tag{2.64b}$$

$$v_{(0)}(x,z,t) = -\sum_{n=1}^{3}\left\{\frac{s_n}{\omega_n}\cos\theta_n - \frac{c_n}{\omega_n}\sin\theta_n\right\}\sin(m_n z). \tag{2.64c}$$

Then (2.62) becomes

$$\frac{\partial c_p}{\partial \tau} + C_{g_p}\frac{\partial c_p}{\partial \xi} = -\gamma_{pqr}\left((c_q c_r - s_q s_r)\cos(\tilde{k}\xi) - (s_q c_r + c_q s_r)\sin(\tilde{k}\xi)\right), \tag{2.65a}$$

$$\frac{\partial s_p}{\partial \tau} + C_{g_p}\frac{\partial s_p}{\partial \xi} = \gamma_{pqr}\left((c_q c_r - s_q s_r)\sin(\tilde{k}\xi) + (s_q c_r + c_q s_r)\cos(\tilde{k}\xi)\right). \tag{2.65b}$$

2.2.5 Near-resonant Internal Wave Triads without the Earth's Rotation

If we have negligible rotational effects and keep the other assumptions in the model, we set the parameters as

$$\epsilon \ll 1, \qquad \mu = 1, \qquad R_0 \gg 1. \tag{2.66}$$

$N(\mathrm{s}^{-1})$	$k_1(\mathrm{m}^{-1})$	$k_2(\mathrm{m}^{-1})$	$k_3(\mathrm{m}^{-1})$	$\Delta k(\mathrm{m}^{-1})$
0.0006	-0.0033	0.0023	7.6×10^{-4}	-3.1×10^{-4}
0.0008	-0.0024	0.0017	5.6×10^{-4}	-1.2×10^{-4}
0.001	-0.0018	0.0013	4.5×10^{-4}	-5.7×10^{-5}
0.0015	-0.0012	8.9×10^{-4}	3.0×10^{-4}	-1.6×10^{-5}
0.002	-8.9×10^{-4}	6.6×10^{-4}	2.2×10^{-4}	-6.7×10^{-6}
0.0025	-7.1×10^{-4}	5.3×10^{-4}	1.8×10^{-4}	-3.4×10^{-6}

Table 2.3: The dimensional wavenumbers for harmonic 2 – mode 2, harmonic 1 – mode 3, and harmonic 1-mode 1 waves given different choices of N when no earth's rotation is considered. Here, $\Delta k = k_1 + k_2 + k_3$.

The assumption $R_0 \gg 1$ amounts to setting $\delta = 0$. The three waves discussed earlier (2.18a) – (2.18b) also form a near-resonant triad. Now, the dispersion relation (2.23) for internal waves becomes

$$\omega^2 = \frac{N^2 k^2}{k^2 + m^2}. \tag{2.67}$$

With the same choice of waves as in (2.18a) – (2.18b), we now obtain a different set of horizontal wavenumbers

$$k_1 = -\frac{4m_0\omega_{M_2}}{\sqrt{N^2 - 4\omega_{M_2}^2}}, \tag{2.68a}$$

$$k_2 = \frac{3m_0\omega_{M_2}}{\sqrt{N^2 - \omega_{M_2}^2}}, \tag{2.68b}$$

$$k_3 = \frac{m_0\omega_{M_2}}{\sqrt{N^2 - \omega_{M_2}^2}}, \tag{2.68c}$$

with the requirement of positive phase speed.

With the same definition of Δk as in (2.32), we still have the property that Δk is very small. The detail of the proof can be found in section 3.1.5. An example of the dimensional counterparts of these Δk and k can be found in table 2.3.

When $\delta = 0$ the governing equation (2.22) simplifies to

$$\frac{\partial^2}{\partial t^2}\nabla^2\psi + N^2\psi_{xx} = \epsilon\frac{\partial}{\partial t}J\left(\psi, \nabla^2\psi\right) + \epsilon\frac{\partial}{\partial x}J\left(\psi, b\right), \tag{2.69}$$

with the perturbation series ψ and b given by

$$\psi = \psi^{(0)} + \epsilon\psi^{(1)} + O(\epsilon^2) \tag{2.70a}$$

$$b = b^{(0)} + \epsilon b^{(1)} + O(\epsilon^2). \tag{2.70b}$$

This governing equation is different than (2.22) and the amplitude equations are obtained from setting $\delta = 0$ in (2.65a)-(2.65b), which are

$$\frac{\partial c_p}{\partial \tau} + C_{g_p}\frac{\partial c_p}{\partial \xi} = -\gamma_{pqr}\left((c_q c_r - s_q s_r)\cos(\tilde{k}\xi) - (s_q c_r + c_q s_r)\sin(\tilde{k}\xi)\right) \tag{2.71a}$$

$$\frac{\partial s_p}{\partial \tau} + C_{g_p}\frac{\partial s_p}{\partial \xi} = \gamma_{pqr}\left((c_q c_r - s_q s_r)\sin(\tilde{k}\xi) + (s_q c_r + c_q s_r)\cos(\tilde{k}\xi)\right), \tag{2.71b}$$

where

$$\gamma_{pqr} = \frac{\alpha_{pqr}}{\kappa_p^2\frac{\omega_p}{m_p}} = \frac{1}{8}\frac{m_p N^2}{\kappa_p^2}\left(\frac{k_q}{m_q} - \frac{k_r}{m_r}\right)\left(\frac{k_q}{\omega_q} - \frac{k_r}{\omega_r}\right)\left(\frac{k_1}{\omega_1} + \frac{k_2}{\omega_2} + \frac{k_3}{\omega_3}\right), \tag{2.72}$$

for $\{p, q, r\} = \{1, 2, 3\}, \{2, 3, 1\}$ or $\{3, 2, 1\}$.

The amplitude equations of near-resonant internal waves without the earth's rotation is given by (2.71a) and (2.71b), which differ from their counterparts with rotational effect in how γ_{pqr} and $\tilde{k}$ are computed.

2.2.6 Resonant Internal Wave Triads

Near-resonance without the earth's rotation is obtained on taking $\delta = 0$ in the model (2.22), describing near-resonant internal waves. If we further assume the model to be hydrostatic ($\mu = 0$), where the vertical length scale is much smaller than the horizontal length scale, then we can make the approximation

$$\kappa^2 = k^2 + m^2 \approx m^2. \tag{2.73}$$

This approximation turns the dispersion relation (2.67) into

$$\omega^2 = \frac{N^2 k^2}{m^2}, \tag{2.74}$$

where we can also write

$$k = \pm\frac{\omega m}{N}. \tag{2.75}$$

For the internal wave triad whose frequencies and vertical wavenumbers are depicted by (2.18a) – (2.18b), we now have another set of horizontal wavenumbers

$$k_1 = -\frac{4m_0\omega_{M_2}}{N}, \tag{2.76a}$$

$$k_2 = \frac{3m_0\omega_{M_2}}{N}, \tag{2.76b}$$

$$k_3 = \frac{m_0\omega_{M_2}}{N}. \tag{2.76c}$$

Here,

$$\Delta k = k_1 + k_2 + k_3 = 0, \tag{2.77}$$

together with (2.18a) – (2.18b), gives an exact resonant internal wave triad.

In order to get the amplitude equations, we only need to substitute (2.73) in to (2.71a)–(2.71b) and hence get

$$\frac{\partial c_p}{\partial \tau} + C_{g_p}\frac{\partial c_p}{\partial \xi} = -\gamma_{pqr}(c_q c_r - s_q s_r) \tag{2.78a}$$

$$\frac{\partial s_p}{\partial \tau} + C_{g_p}\frac{\partial s_p}{\partial \xi} = \gamma_{pqr}(s_q c_r + c_q s_r), \tag{2.78b}$$

where γ_{pqr} is the same as that given by (2.63). Here, with the fluid being hydrostatic, we have $\kappa_p^2 = m_p^2$, and hence

$$\gamma_{pqr} = \frac{1}{8}\frac{N^2}{m_p}\left(\frac{k_q}{m_q} - \frac{k_r}{m_r}\right)\left(\frac{k_q}{\omega_q} - \frac{k_r}{\omega_r}\right)\left(\frac{k_1}{\omega_1} + \frac{k_2}{\omega_2} + \frac{k_3}{\omega_3}\right), \tag{2.79}$$

for $\{p, q, r\} = \{1, 2, 3\}, \{2, 3, 1\}$ or $\{3, 2, 1\}$.

In fact, (2.78a) – (2.78b) can be reduced to a much simpler canonical form for characterizing resonant triads [Craik, 1985; Martin et al., 1972]

$$\frac{\partial \tilde{c}_p}{\partial \tau} + C_{g_p}\frac{\partial \tilde{c}_p}{\partial \xi} = -\tilde{\gamma}_{pqr}\tilde{c}_q\tilde{c}_r, \tag{2.80}$$

where $\tilde{c}_p$ ($p = 1, 2, 3$) are all real functions.

To understand the relationship between c_p and $\tilde{c}_p$, recall the first appearance of the amplitude a_p in (2.24) – (2.26), where we chose a_p to be complex and slowly varying with space and time. Actually, if we write

$$a_p = c_p - is_p = \sqrt{c_p^2 + s_p^2}\left(\cos\underline{\theta}_p + i\sin\underline{\theta}_p\right) = \tilde{a}_p e^{i\underline{\theta}_p}, \tag{2.81}$$

where $\underline{\theta}_p = -\arctan\frac{s_n}{c_n}$ and $\tilde{a}_p = |a_p|$ are real, then we will have the expression for ψ from (2.24) as

$$\psi^{(0)}(x,z,t) = \frac{1}{2}\sum_{n=1}^{3}\left\{\frac{\tilde{a}_n}{m_n}e^{i(\theta_n+\underline{\theta}_n)} + \text{c.c.}\right\}\sin\left(m_n z\right). \tag{2.82}$$

If we carry out the algebra as we did in section 2.2.4 and choose an appropriate value for $\phi_1+\phi_2+\phi_3$ similar to (2.33)[12] , we will get the governing amplitude equation for resonant triads in the form (2.80). This canonical form facilitates the stability analysis of resonance.

Craik [1985] has even suggested a heuristic shortcut to obtain an amplitude equation of the form (2.78a) – (2.78b). If the linear dispersion relation is represented by

$$D\left(\omega, \vec{k}\right) = 0, \tag{2.83}$$

then the Taylor expansion of slow modulation denoted by the small parameter ϵ of each complex amplitude a_j is given by

$$D\left(\omega_p + \epsilon\frac{\partial}{\partial t}, \vec{k}_p - \epsilon\vec{\nabla}\right)a_p = \epsilon\left(\frac{\partial D}{\partial\omega_p}\frac{\partial}{\partial t} - \frac{\partial D}{\partial k_p}\cdot\vec{\nabla}\right)a_p + \text{O}\left(\epsilon^2\right). \tag{2.84}$$

Energy transformation between resonant triads indicates that the slow modulation of each amplitude is from the nonlinear interaction, so we claim

$$D\left(\omega_p + \frac{\partial}{\partial t}, \vec{k}_p - \vec{\nabla}\right)a_p = \gamma_p a_q^* a_r^* + \text{higher order interactions}. \tag{2.85}$$

Therefore, we have

$$\left(\frac{\partial D}{\partial\omega_p}\frac{\partial}{\partial t} - \frac{\partial D}{\partial\vec{k_p}}\cdot\vec{\nabla}\right)a_p = \gamma_p a_q^* a_r^*. \tag{2.86}$$

[12]We will have to assume ϕ_j $(j = 1, 2, 3)$ to be slowly varying since the θ-relation will involve the sum of $\underline{\theta}_j$ $(j = 1, 2, 3)$, which are indicated as slowly varying functions by its definition.

To leading order, a small perturbation δk and $\delta\omega$ of wavenumber and frequency satisfy

$$\delta\omega(\frac{\partial D}{\partial \omega}) + \delta\vec{k}\cdot(\frac{\partial D}{\partial \vec{k}}) = 0, \tag{2.87}$$

and hence

$$\frac{\frac{\partial D}{\partial \vec{k}_p}}{\frac{\partial D}{\partial \omega_p}} = -\frac{\partial \omega_p}{\partial \vec{k}_p} = -\vec{C}_{g_p}. \tag{2.88}$$

Using (2.88), (2.86) turns into

$$(\frac{\partial}{\partial t} + \vec{C}_{g_p}\cdot\vec{\nabla})a_p = \frac{\gamma_p}{\frac{\partial D}{\partial \omega_p}} a_q^* a_r^*, \tag{2.89}$$

which is in the same form of (2.78a) – (2.78b).

2.2.7 Temporal and Spatial Near-resonance

The results from the analysis of previous sections are first-order PDEs: (2.65a) – (2.65b), (2.71a) –(2.71b) and (2.78a) – (2.78b). In fact, (2.71a) –(2.71b) and (2.78a) – (2.78b) are special cases of (2.65a) – (2.65b), since on setting $\delta = 0$ in (2.65a) – (2.65b), we have (2.71a) – (2.71b) and by further setting $\kappa^2 \approx m^2$ and $\tilde{k} = 0$, we have (2.78a) – (2.78b). If, on one hand, the spatial derivatives are negligible, we obtain from (2.65a) – (2.65b) the governing equation for wave amplitude of temporal near-resonance, namely

$$\frac{\partial c_p}{\partial \tau} = -\gamma_{pqr}\left((c_q c_r - s_q s_r)\cos(\tilde{k}\xi) - (s_q c_r + c_q s_r)\sin(\tilde{k}\xi)\right), \tag{2.90a}$$

$$\frac{\partial s_p}{\partial \tau} = \gamma_{pqr}\left((c_q c_r - s_q s_r)\sin(\tilde{k}\xi) + (s_q c_r + c_q s_r)\cos(\tilde{k}\xi)\right). \tag{2.90b}$$

On the other hand, if the amplitudes actually do not change with time, we obtain spatial near-resonance and its governing equations

$$\frac{\partial c_p}{\partial \xi} = -\frac{\gamma_{pqr}}{C_{g_p}}\left((c_q c_r - s_q s_r)\cos(\tilde{k}\xi) - (s_q c_r + c_q s_r)\sin(\tilde{k}\xi)\right), \tag{2.91a}$$

$$\frac{\partial s_p}{\partial \xi} = \frac{\gamma_{pqr}}{C_{g_p}}\left((c_q c_r - s_q s_r)\sin(\tilde{k}\xi) + (s_q c_r + c_q s_r)\cos(\tilde{k}\xi)\right). \tag{2.91b}$$

Since it is not likely that we can solve (2.65a) – (2.65b) analytically, we will solve these equations numerically. The merit of dividing up the temporal and spatial near-resonance is that if we

know the type of near-resonance, we can turn the system of PDEs (2.65a) – (2.65b) into a set of ODEs (2.90a) – (2.90b) or (2.91a) – (2.91b), which are much easier to solve numerically [Neef, 2004; Press et al., 1992]. Certainly, in many cases, the temporal and spatial variations are both important and we have to solve the system of PDEs (2.65a) – (2.65b).

2.3 Stability Analysis of the Resonant Amplitude Equations

This section focuses on the stability of temporal resonance[13], which gives us a glimpse of the stability of this model. If we choose appropriate θ_j ($j = 1, 2, 3$) similar to (2.34), the real amplitude equations[14] depicting a temporally resonant internal wave triad will adopt the form (2.80) and hence be described by

$$\frac{\partial a_p}{\partial \tau} = -\gamma_{pqr} a_q a_r, \tag{2.92}$$

where

$$\gamma_{pqr} = \frac{\alpha_{pqr}}{\kappa_p^2 \frac{\omega_p}{m_p}} = \frac{1}{8}\frac{N^2}{m_p}\left(\frac{k_q}{m_q} - \frac{k_r}{m_r}\right)\left(\frac{k_q}{\omega_q} - \frac{k_r}{\omega_r}\right)\left(\frac{k_1}{\omega_1} + \frac{k_2}{\omega_2} + \frac{k_3}{\omega_3}\right), \tag{2.93}$$

and a_p ($\{p, q, r\} \in \{\{1, 2, 3\}, \{2, 3, 1\}, \{3, 2, 1\}\}$) is the amplitude of different waves in the internal wave triad.

From (2.93), for the resonant wave triads defined by (2.18a) – (2.18b), we have

$$\gamma_{123} = \frac{N^2}{8m_1}\left(\frac{k_1}{m_1} + \frac{k_2}{m_2} + \frac{k_3}{m_3}\right)\left(\frac{k_2}{m_2} - \frac{k_1 + k_2}{m_1 + m_2}\right)\left(\frac{k_2}{\omega_2} - \frac{k_1 + k_2}{\omega_1 + \omega_2}\right) \tag{2.94}$$

$$= \frac{N^2}{8m_p}\left(\frac{k_1}{m_1} + \frac{k_2}{m_2} + \frac{k_3}{m_3}\right)\frac{(k_2 m_1 - k_1 m_2)}{m_2(-m_3)}\frac{(k_2\omega_1 - k_1\omega_2)}{\omega_2(-\omega_3)}, \tag{2.95}$$

where we used the resonant triad condition (2.11a) – (2.11b) to express k_3, m_3 and ω_3.

Given $\omega_1 = -2\omega_{M_2}$ and $\omega_3 = \omega_{M_2}$, we obtain

$$\gamma_{123}\gamma_{231} = -\frac{N^4}{64}\left(\frac{k_1}{m_1} + \frac{k_2}{m_2} + \frac{k_3}{m_3}\right)^2 \frac{(k_1 m_2 - k_2 m_1)^2}{m_1^2 m_2^2 m_3^2}\frac{(k_1\omega_2 - k_2\omega_1)^2}{\omega_1{\omega_2}^2\omega_3} > 0. \tag{2.96}$$

By using the same technique, we get $\gamma_{123}\gamma_{312} < 0$.

[13] $\frac{\partial a_p}{\partial \xi} = 0$, for $p = 1, 2, 3$

[14] More on getting the real amplitude equation should be referred back to (2.2.6).

Since

$$\gamma_{123}\gamma_{321} > 0, \tag{2.97a}$$

$$\gamma_{123}\gamma_{231} < 0, \tag{2.97b}$$

then if a_n are functions of ξ only, an appropriate choice of $\tilde{A}_i$ allows us to rescale the a_i as

$$a_1 = \tilde{A}_1 A_1, \tag{2.98}$$

$$a_2 = \tilde{A}_2 A_2, \tag{2.99}$$

$$a_3 = \tilde{A}_3 A_3, \tag{2.100}$$

and hence we can transform (2.92) into the simplified form [Lamb, 2007a]

$$\frac{\partial}{\partial\hat{\tau}} A_1 = A_2 A_3, \tag{2.101a}$$

$$\frac{\partial}{\partial\hat{\tau}} A_2 = -2A_3 A_1, \tag{2.101b}$$

$$\frac{\partial}{\partial\hat{\tau}} A_3 = A_1 A_2. \tag{2.101c}$$

We note that (2.101a) – (2.101c) can be combined[15] to give

$$\frac{\partial}{\partial\hat{\tau}} \left(A_1^2 + A_2^2 + A_3^2\right) = 0, \tag{2.102}$$

which allows us to define

$$E = A_1^2 + A_2^2 + A_3^2 = \text{constant}, \tag{2.103}$$

from which, we roughly see conservation of energy since energy is proportional to the square of the amplitude. Craik [1985], in fact, had described the energy conservation of resonant triads in a more exact way with his energy expressed by Cairns as

$$\mathcal{E} = \tfrac{1}{4}\omega \left(\frac{\partial D}{\partial \omega}\right) |A|^2, \tag{2.104}$$

where A is the amplitude of the fluid particles and the 2-D dispersion relationship is given by $D(\omega, k) = 0$ with ω being the frequency and k being the wavenumber. Martin et al. [1972] also briefly discussed energy conservation of internal wave triads in appendix B of their 1971 paper.

[15] We take (2.101a)$\times A_1$ +(2.101b) $\times A_2$ + (2.101c) $\times A_3$.

Also, (2.101a) and (2.101c) can be combined to give

$$\frac{\partial}{\partial \tau}(A_1^2 - A_3^2) = 0, \tag{2.105}$$

and hence

$$F = A_1^2 - A_3^2 = \text{constant}. \tag{2.106}$$

We now use the constants E and F to analyze the stability of $\hat{a}_p$ $(p = 1, 2, 3)$[Lamb, 2007a]. In a three dimensional coordinate system given by A_1, A_2 and A_3, (2.103) represents a family of spheres and (2.106) a family of hyperbolae. This result is shown in figure 2.2, where a sphere and a hyperbolae surface are drawn together in the Cartesian coordinates (A_1, A_2, A_3).

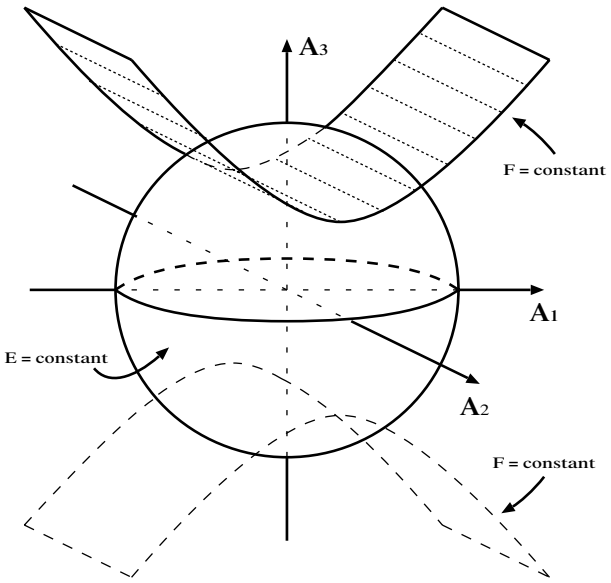

Figure 2.2: The plot of a sphere given by (2.103) and a hyperbole in accord with (2.106). The solution of the system (A_1, A_2, A_3) will travel along the trajectory given by the hyperbole on the sphere surface.

To understand how the solution of (2.101a) – (2.101c) travels subject to the constraints (2.103) and (2.106), we choose initial conditions $(\pm E^{\frac{1}{2}}, 0, 0)$, $(0, \pm E^{\frac{1}{2}}, 0)$ and $(0, 0, \pm E^{\frac{1}{2}})$ on the sphere. If the variables start off at those points, according to (2.101a) - (2.101c), the RHS of the ODE system will all be zero and hence those points are the equilibrium points of the system. If the solution is initially at those points, it will remain at those points over time.

When the solution is initially near these equilibrium points, for example, $(E^{\frac{1}{2}}, 0, 0)$, we can assume it to be $A_0 = (E^{\frac{1}{2}} + \epsilon_1, \epsilon_2, \epsilon_3)$, where ϵ_j $(j = 1, 2, 3)$ satisfy the equation

$$\left(E^{\frac{1}{2}} + \epsilon_1\right)^2 + \epsilon_2^2 + \epsilon_3^2 = E, \tag{2.107}$$

which guarantees A_0 to be on the sphere surface. We also know that ϵ_j $(j = 1, 2, 3)$ have to be small, so that F defined in (2.106) is close to $-E$ and the hyperbole given by (2.106) is very close to the plane given by $A_3 = 0$. The trajectory given by this hyperbole enables the variables to stay near the fixed points of the system $(E^{\frac{1}{2}}, 0, 0)$. The same idea can be applied near $(-E^{\frac{1}{2}}, 0, 0)$ and $(0, 0, \pm E^{\frac{1}{2}})$ to show that it stays near this fixed point.

However, for the other equilibrium point $(0, E^{\frac{1}{2}}, 0)$, if we choose a nearby point $P_0 = (\epsilon_1, E^{\frac{1}{2}} + \epsilon_2, \epsilon_3)$ with small ϵ_j (j = 1,2,3) and enforce the condition that this point is on the sphere surface, we then will have a very small value of F given by (2.106), leading to (2.106) representing a hyperbola close to $(0, 0, E^{\frac{1}{2}})$. As a consequence, we know that an orbit that passes near P_0 will travel a long distance along the surface of the sphere.

Therefore, we claim that the equilibrium points along axis A_2 will be unstable whereas that along axis A_1 and A_3 will be stable. Hence we conclude that the wave mode whose coefficient is different from the other two is unstable and the other two modes are stable. This result can also be shown in figure 3.9, where we will witness that the amplitudes of harmonic 1 – mode 1 wave and harmonic 1 – mode 3 wave vary in a small range, while that of harmonic 2 – mode 2 waves fluctuates much more and passes through the horizontal axis periodically.

2.4 Other Sets of Resonant Internal Wave Triad

This thesis has so far been focused on the specific wave triad given by (2.18a) – (2.18b) to demonstrate the near-resonant and resonant theory. In fact, resonance is not confined to these three waves of the specific wave triad but occurs to a series of other three waves. The general mathematical expression of the possible resonant triad components can be sought by combining the resonance condition (2.11a) – (2.11b) as well as the dispersion relation of internal waves (2.74) in the hydrostatic limit.

For a triad with first harmonic, second harmonic and first harmonic waves[16], we have

$$\omega_1 = \omega_{M_2}, \tag{2.108a}$$
$$\omega_2 = -2\omega_{M_2}, \tag{2.108b}$$
$$\omega_3 = \omega_{M_2}, \tag{2.108c}$$

with associated wavenumbers $\vec{k}_1, \vec{k}_2$, and $\vec{k}_3$ respectively, where $\vec{k}_i = \{k_i, m_i\}$. On using (2.18b) and (2.74), we have

$$k_1 = \mp\frac{\omega_{M_2}(m_2 + m_3)}{N}, \tag{2.109a}$$
$$k_2 = \mp\frac{2\omega_{M_2} m_2}{N}, \tag{2.109b}$$
$$k_3 = \pm\frac{\omega_{M_2} m_3}{N}. \tag{2.109c}$$

Substituting (2.109a) – (2.109c) into (2.11a) then gives

$$\mp\frac{\omega_{M_2}(m_2 + m_3)}{N} \mp \frac{2\omega_{M_2} m_2}{N} \pm \frac{\omega_{M_2} m_3}{N} = 0, \tag{2.110}$$

which can be expanded as four independent expressions, namely

$$\frac{\omega_{M_2}(m_2 + m_3)}{N} + \frac{2\omega_{M_2} m_2}{N} + \frac{\omega_{M_2} m_3}{N} = 0, \tag{2.111a}$$
$$\frac{\omega_{M_2}(m_2 + m_3)}{N} + \frac{2\omega_{M_2} m_2}{N} - \frac{\omega_{M_2} m_3}{N} = 0, \tag{2.111b}$$
$$\frac{\omega_{M_2}(m_2 + m_3)}{N} - \frac{2\omega_{M_2} m_2}{N} + \frac{\omega_{M_2} m_3}{N} = 0, \tag{2.111c}$$
$$\frac{\omega_{M_2}(m_2 + m_3)}{N} - \frac{2\omega_{M_2} m_2}{N} - \frac{\omega_{M_2} m_3}{N} = 0, \tag{2.111d}$$

The above four equations (2.111a) – (2.111d) can be solved as

$$3m_2 + 2m_3 = 0, \tag{2.112a}$$
$$m_2 = 0, \tag{2.112b}$$
$$m_3 = 0, \tag{2.112c}$$
$$0 = 0. \tag{2.112d}$$

[16]The subindex labels different waves.

Only (2.112a) is a physically meaningful expression and when combined with (2.18b), it gives

$$m_1 = -\frac{1}{3}m_3, \tag{2.113a}$$

$$m_2 = -\frac{2}{3}m_3, \tag{2.113b}$$

$$m_3 = m_3. \tag{2.113c}$$

Therefore, given harmonics as in (2.108a) – (2.108c), the possible modes for internal wave triads are mode n, mode $2n$ and mode $3n$ correspondingly, where $n \in \mathbb{N}$. In this thesis, we choose to study the simplest case, i.e. when $n = 1$.

2.5 Parametric Subharmonic Instability

As a consequence of studies on resonant triads, parametric subharmonic instability (PSI), as a branch and a special case of resonant triad interaction, emerged in the 1970s. With its potential of explaining the energy evolvement, PSI has drawn many researchers' attention [McEwan and Robinson, 1975; Koudella and Staquet, 2005; Williams et al., 2007], especially in explaining breaking and the energy cascade of internal gravity waves. We now briefly introduce PSI.

In the resonant triad condition (2.11a) – (2.11b), if we have

$$\left|\frac{\omega_2}{\omega_1}\right| = \beta, \left|\frac{\omega_3}{\omega_1}\right| = 1 - \beta, \tag{2.114}$$

where $\beta < 1$, then, this triad resonance is PSI. In fact, we can write (2.114) as

$$|\omega_1| = |\omega_2| + |\omega_3|, \tag{2.115}$$

We define the wave with the largest frequency ω_1 is the parent wave, while the other two are child waves. The interaction of the parent wave and the child waves is called *parametric subharmonic instability*. Notice that we have defined PSI in the context of frequency. Actually, similar definitions of PSI can be applied in terms of wavenumbers.

CHAPTER 3

NUMERICAL SIMULATION

3.1 Development of the Numerical Strategies

Our resonance-like phenomenon was first discovered in a fully nonlinear numerical simulation of tidal flow over a shelf step. We have taken the essential elements of this phenomenon and have duplicated it in a simpler boundary forced problem, which produces the same result.

To explain the result, we have developed an exact resonant internal wave triad theory in section 2.2.6 concordant with the theory used by Martin et al. [1972] to explain their experimental results. However, this theory leads to a discrepancy in the wave form of the horizontal velocity when applied to explain the numerical results; consequently, we developed the near-resonant internal wave triad theory and obtained excellent agreement. These numerical simulations were originally run under the assumption of $f = 0$ and later, we included the earth's rotation and take various f values into account.

3.1.1 IGW: a Fully Nonlinear Numerical Model

IGW, short for internal gravity waves, is a numerical code developed by Kevin Lamb [Lamb, 1994]. The original code was used to simulate flow over topography and has been polished over time and used for various projects [Lamb and Yan, 1996; Lamb, 2002, 2007b].

This code uses a finite volume method combined with a second order projection technique [Bell and Marcus, 1989] to solve the Navier Stokes equation or Euler equations [Kundu and

Cohen, 2004] under the assumption of an incompressible Boussinesq[1] fluid.

In this thesis, we use IGW code to solve the inviscid, non-diffusive Euler equations to simulate internal waves generated by tide topography interaction as well as boundary forced internal waves.

3.1.2 Internal Wave Generation by Tide-topography Interaction

As shown in figure 3.1, the barotropic current interacts with the topography and generates internal waves over the slope region. Waves of different harmonics and different modes are generated at the same time. The data we obtain from the numerical output are the result of the composition of different waves. To study the properties of different elements, we run the model for a long enough time[2] and collect the horizontal velocity $u(\tilde{\xi}, z, t)$[3]. To simplify this problem, we choose to work on the horizontal velocity at the surface ($z = 0$ km) and decompose $u(\tilde{\xi}, 0, t)$ into its various Fourier components. The easiest and most convenient way to decompose one wave is to approximate $u(\tilde{\xi}, z, t)$ by its Fourier series

$$u(\tilde{\xi}, z, t) = \sum_n \left\{ a_n(\tilde{\xi}, z)\cos(n\omega_{M_2}t) + b_n(\tilde{\xi}, z)\sin(n\omega_{M_2}t) \right\}, \tag{3.1}$$

with the Fourier coefficients[4] given by

$$a_n(\tilde{\xi}, z) = \frac{1}{T_0}\int_{22T_0}^{24T_0} u(\tilde{\xi}, z, \tau)\cos(n\omega_{M_2}\tau)d\tau, \tag{3.2}$$

$$b_n(\tilde{\xi}, z) = \frac{1}{T_0}\int_{22T_0}^{24T_0} u(\tilde{\xi}, z, \tau)\sin(n\omega_{M_2}\tau)d\tau. \tag{3.3}$$

After the harmonic decomposition of the horizontal velocity according to (3.1), we are also interested in the modal components of different harmonics, and thus we separate a_n and b_n into

[1] A Boussinesq fluid is a fluid to which the Boussinesq approximation has been applied.

[2] In this thesis, we typically run the model for 24 tidal periods.

[3] We choose a reference frame which is moving with the barotropic tide, where $\tilde{\xi}$ is the horizontal coordinate and z is the vertical coordinate. Note that this $\tilde{\xi}$ is not related to the ξ defined by ϵx in chapter 2.

[4] T_0 is the tidal period.

vertical modes via

$$a_n(\tilde{\xi}, z) = \sum_j a_{nj}(\tilde{\xi}) \cos(\frac{j\pi z}{H}), \tag{3.4}$$

$$b_n(\tilde{\xi}, z) = \sum_j b_{nj}(\tilde{\xi}) \cos(\frac{j\pi z}{H}). \tag{3.5}$$

Note that because of the use of a rigid lid and constant N, the streamfunction satisfies $\psi \propto \sin(\frac{n\pi}{H})$ and hence u can be expanded in a cosine series in the vertical coordinate.

Figure 3.2 displays the first ten modes of the horizontal velocity u of the first harmonic internal waves generated by tidal topography interaction, while figure 3.3 shows their counterparts of the second harmonic internal waves. In these figures, for most of the cases, the higher the mode, the weaker the amplitudes of the decomposed waves. However, in figure 3.3 - (b), we witness an exception where the amplitude of mode 2 wave is greater than that of mode 1 wave and basically is the dominant wave amplitude among all the ten modes. What else stands out the most in these two figures, and can be seen in figure 3.5 is that (a), (c) in figure 3.2 and (b) in figure 3.3 form a resonant-triad-like physical phenomenon, with the amplitude shapes very similar to that of the resonant Rossby wave triad in Pedlosky [1987]. Before investigating the mathematical theory behind this phenomenon, we introduce boundary forced internal waves, where the mechanism with regard to wave interaction is the same as tide topography generated internal waves.

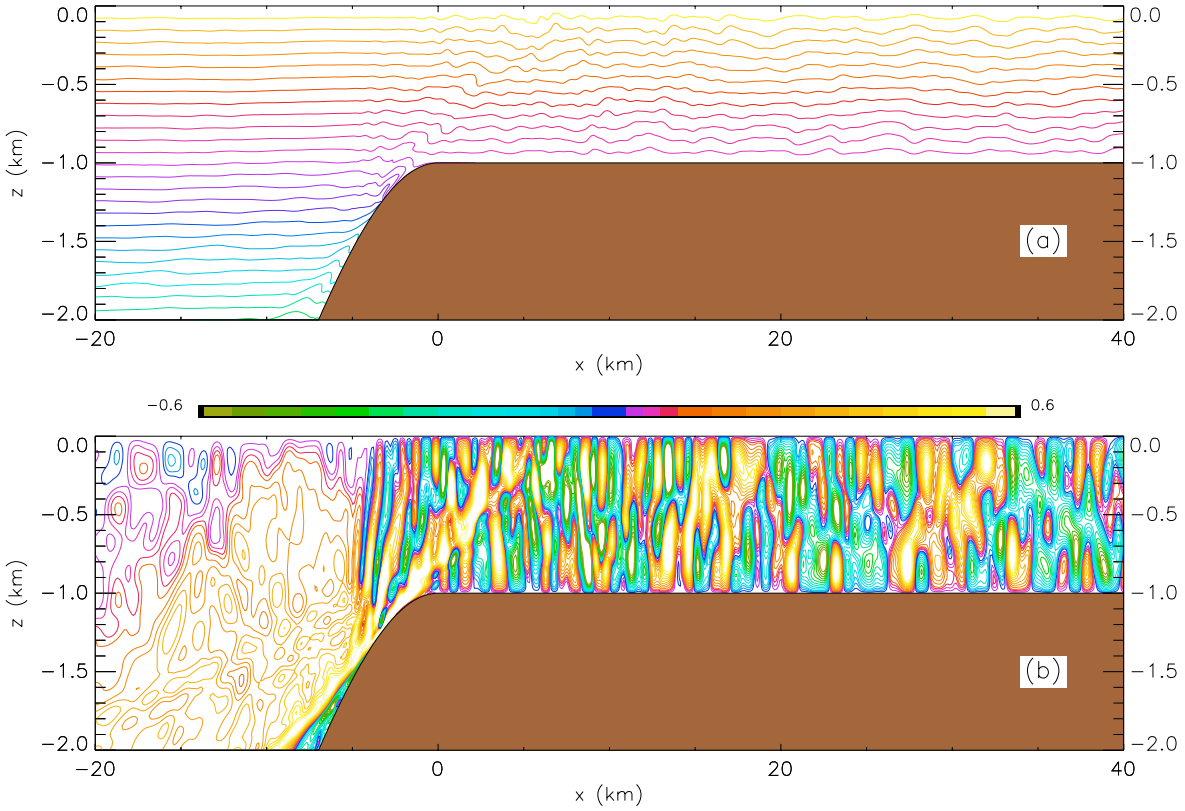

Figure 3.1: Density and vertical velocity fields after 20 tidal periods. (a) Density. (b) Vertical velocity in cm/s. Deep water region, from $z = 0$ km to $z = -5$ km is not fully displayed.

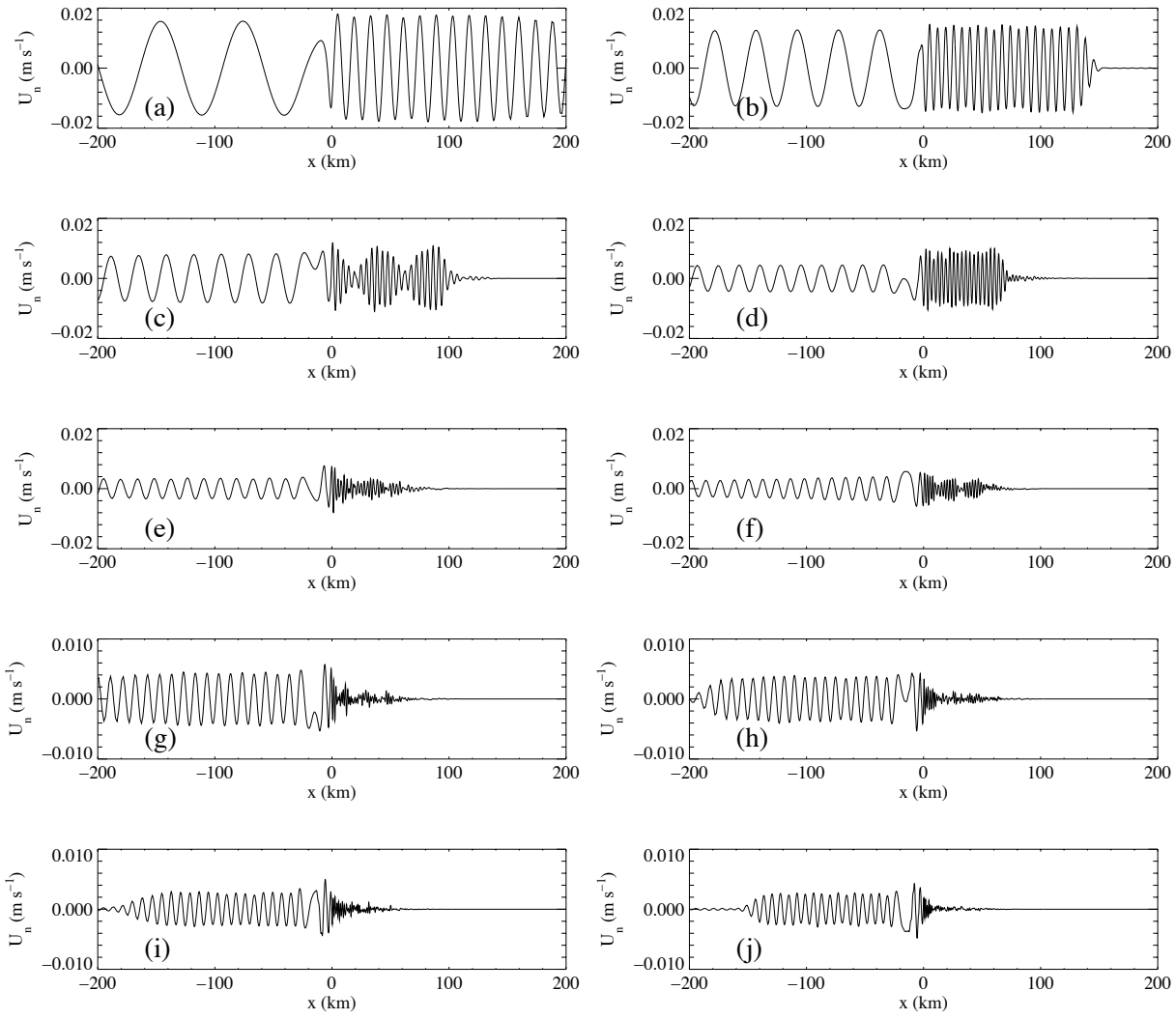

Figure 3.2: The decomposition of horizontal velocity at the surface $z = 0$ km in different modes for harmonic 1 wave. (a) Mode 1. (b) Mode 2. (c) Mode 3. (d) Mode 4. (e) Mode 5. (f) Mode 6. (g) Mode 7. (h) Mode 8. (i) Mode 9. (j) Mode 10.

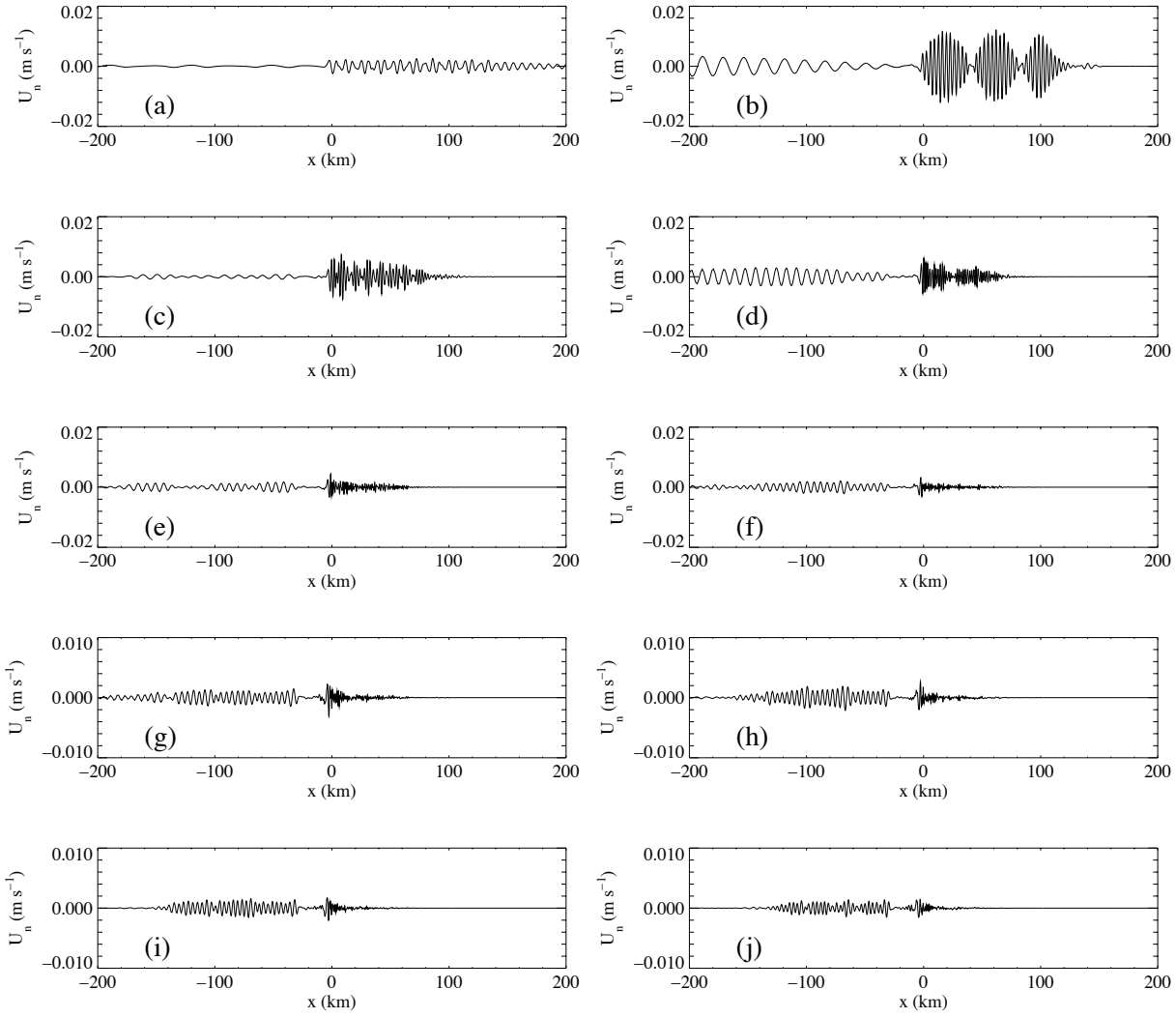

Figure 3.3: The decomposition of horizontal velocity at the surface $z = 0$ km in different modes for harmonic 2 wave. (a) Mode 1. (b) Mode 2. (c) Mode 3. (d) Mode 4. (e) Mode 5. (f) Mode 6. (g) Mode 7. (h) Mode 8. (i) Mode 9. (j) Mode 10.

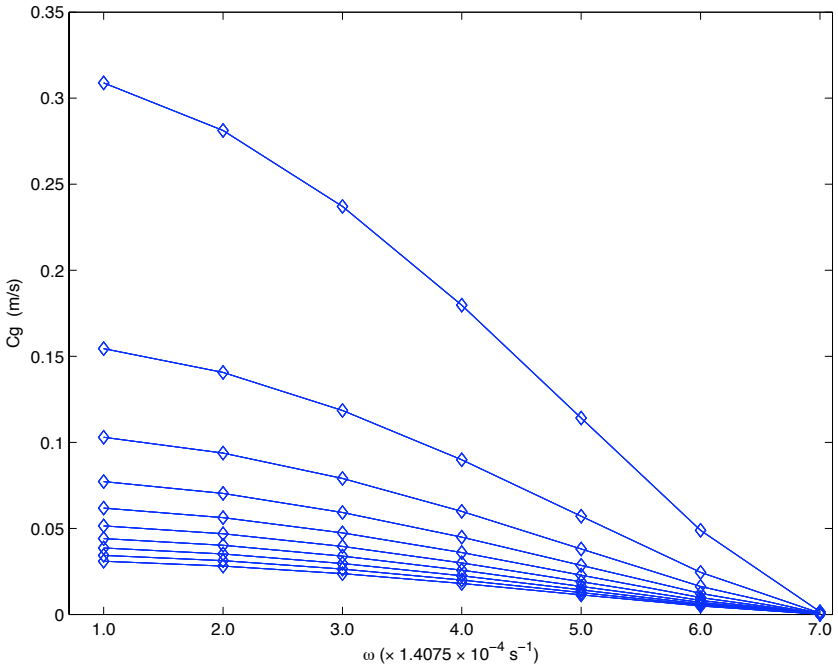

Figure 3.4: Plot of group velocity for different harmonics when $f = 0$. The diamond symbols represent the group velocity of the time-harmonics from harmonic 1 wave to harmonic 7 wave. The uppermost and lowermost curves correspond to mode 1 and mode 10 wave respectively. Lines of mode n ($2 \leq n \leq 9$) are subsequently placed in-between, leading us to the conclusion that group velocity is inversely proportional to mode number.

3.1.3 Internal Waves Generation by Boundary Forcing

After the generation of internal waves by tide topography interaction, waves propagate rightward with different velocities. Among all the time-harmonics[5], the harmonic 1 – mode 1 wave is the one that travels the fastest, as can be seen in figure 3.4. For the harmonic 1 – mode 3 wave, we plug $\omega = \omega_{M_2}$ and $m = 3m_0$ into (2.61) and find its group velocity 0.1030 m/s. Similarly, we find that the group velocity of harmonic 2 – mode 2 wave is 0.1406 m/s.

Therefore, the harmonic 2 – mode 2 wave can travel faster than the harmonic 1 – mode 3 wave; however, in figure 3.5, we see that the harmonic 2 – mode 2 wave has spread no farther

[5]Time-harmonic was firstly used in Tabei et al. [2004] to denote the harmonic n waves, where $n = 2, 3, 4, \cdots$.

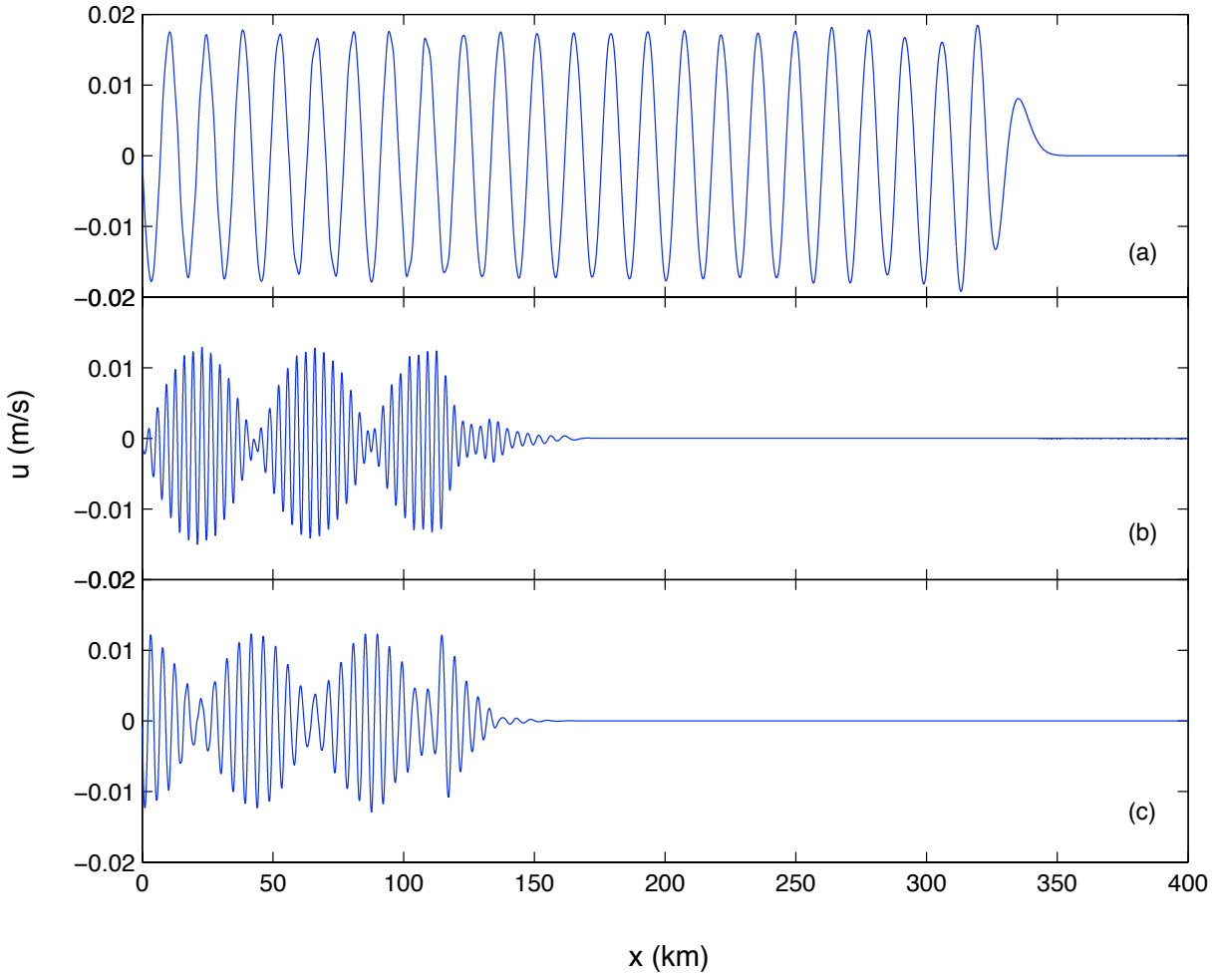

Figure 3.5: The resonant-like phenomenon in the tidal shoaling model after Fourier decomposition. (a) Harmonic 1 – mode 1. (b) Harmonic 2 – mode 2. (c) Harmonic 1 – mode 3.

than the harmonic 1 – mode 3 wave and the envelopes/amplitudes of these two waves are just out of phase. This wave envelope placement shows energy transfer between these two waves. Among the harmonic 1 waves shown in figure 3.2, the amplitude of mode 1, mode 2 and mode 3 waves are the largest; while for harmonic 2 waves demonstrated by figure 3.3, the amplitude of mode 2 waves are most prominent. With the fact that harmonic 2 – mode 2 is not among the

forced waves, we would guess this new prominent wave is the product of wave interaction. The equal propagating distance of harmonic 2 – mode 2 and harmonic 1 – mode 3 wave and their energy transfer demonstrated by their envelope phases further drives us to wonder if it is just the interaction of harmonic 1– mode 1 and harmonic 1 – mode 3 that transfers energy to this strong wave: harmonic 2 – mode 2 wave. Bearing this thought in mind, as demonstrated in figure 3.6, we tried out a simpler model, where harmonic 1 – mode 1 and harmonic 1 – mode 3 waves are forced at the left boundary and the fluid depth is a constant. The mathematical equation for this forcing mechanism is

$$u_t = F_1 \cos(\omega t) \cos(\frac{\pi}{H} z) + F_2 \cos(\omega t) \cos(\frac{3\pi}{H} z) \tag{3.6}$$

at the left boundary.

Two internal waves are generated at the boundary and interact in the same fashion as the internal waves generated by tide topography interaction. In understanding the resonant-like phenomenon, one generation mechanism is as good as the other. However, since the tide topography interaction is numerically much more expensive than the boundary forcing, we will study near-resonant triads for different parameter values using the boundary forcing method.

Later on, instead of using harmonic 1 – mode 1 and harmonic 1 – mode 3 as the forced wave, we force harmonic 1 – mode 1 and harmonic 2 – mode 2 and as expected, get the resonant-like phenomenon demonstrated in figure 3.7. Notice that in figure 3.7, when the harmonic 2 – mode 2 wave is the forced wave, its initial amplitude is nonzero, whereas in figure 3.5, as the forced wave, harmonic 1 – mode 3 wave has a nonzero initial amplitude. The mathematical equation for this forcing is

$$u_t = F_1' \cos(\omega t) \cos(\frac{\pi}{H} z) + 2F_2' \cos(2\omega t) \cos(\frac{2\pi}{H} z). \tag{3.7}$$

In fact, in order to inspect the sensitivity of our near-resonant theory to the nonlinearity of the models, we will also need to change the forcing amplitudes (F_1 and F_2) in order to adjust the nonlinearity. The related analysis will be presented later.

3.1.4 The Scaling Details that Link Theories and Numerics

Numerical models tend to present vivid and sensible results, particularly in the way of figures. In many numerical models, we tend to solve dimensional equations and plot figures in their physical

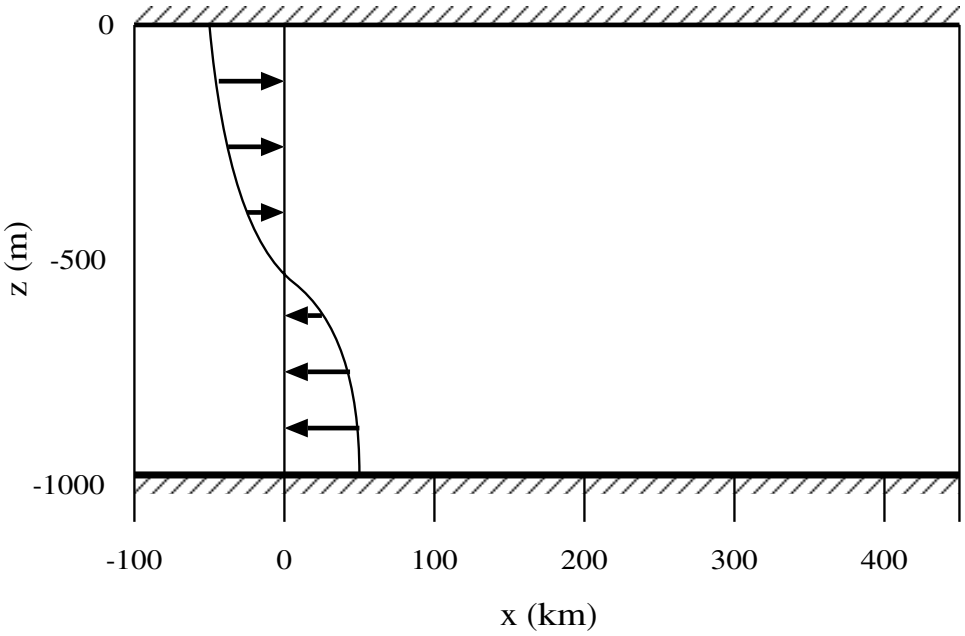

Figure 3.6: Forcing of harmonic 1 – mode 1, harmonic 1 – mode 3 waves on the left boundary at $x = 0$ km. The water depth is 1 km and the length of the domain is sufficiently large (we take 450 km here), so that the waves will not reflect off the right boundary and return to the region of interest.

scales. This idea is different from that of theoretical analysis, where non-dimensional equations and dimensionless variables give us a clear grasp and understanding of the physical problems.

In the two numerical models discussed in section 3.1.2 and section 3.1.3, we deal with all the variables in their original dimensional form and results are presented correspondingly. However, in the theoretical part investigating the amplitude equations of resonance and near-resonance, we analyze the governing equations in non-dimensional form. To allow the comparability of the theoretical and numerical results, we need some work devoted on quantifying the scales involved in non-dimensionalization of the governing equations of internal waves from section 1.6.2.

Certainly, we find the theoretical scales (1.24) – (1.26) without actual values not particularly useful in the numerical calculation and hence they must be quantified. In this section, we present the scales of the system in terms of standard quantities. The basic units in SI (Système International d'unités) are given in table 3.1.

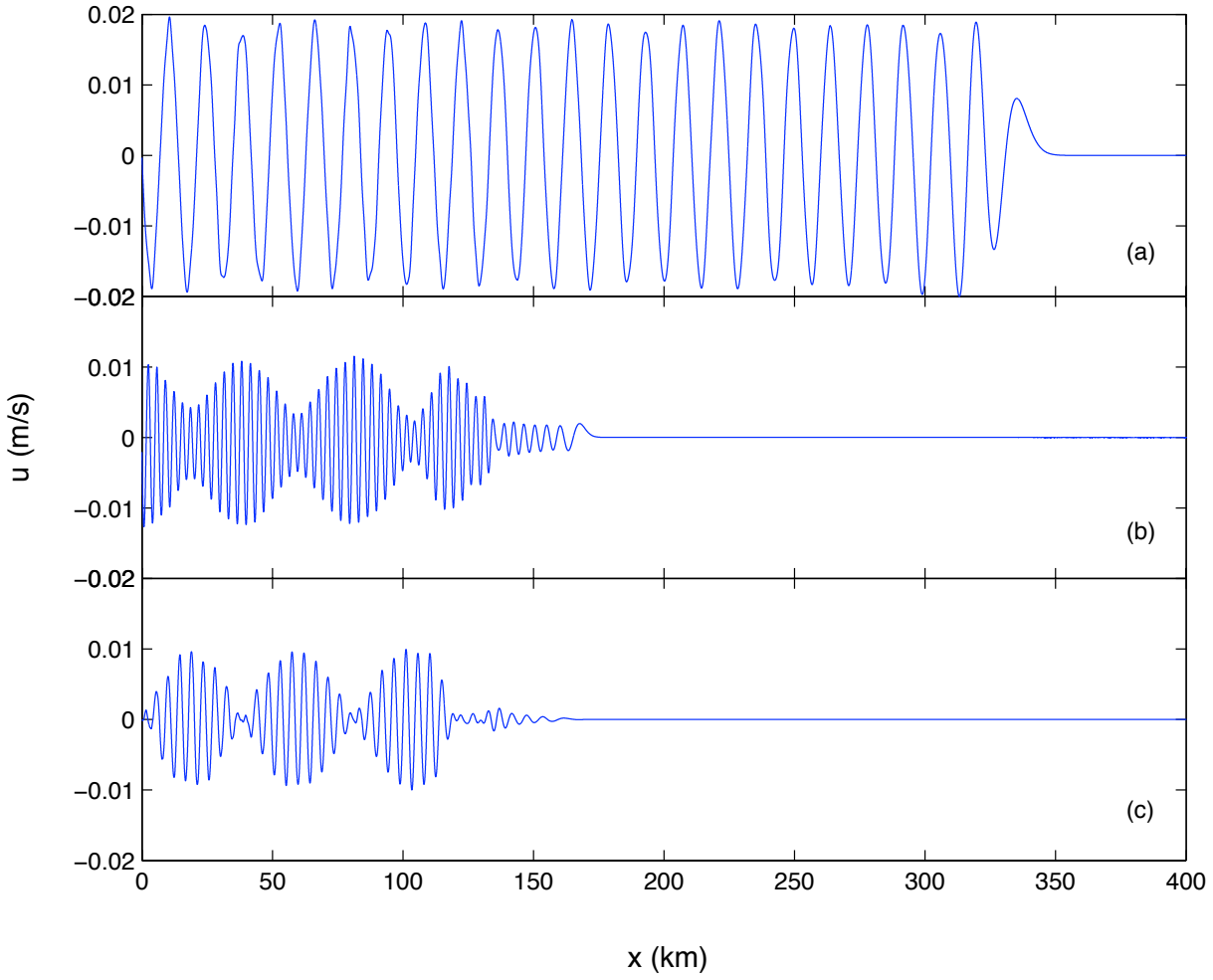

Figure 3.7: resonant-like phenomenon when harmonic 1 – mode 1, harmonic 2 – mode 2 waves are forced at the boundary. (a) Harmonic 1 – mode 1. (b) Harmonic 2 – mode 2. (c) Harmonic 1 – mode 3.

In the near-resonant internal wave triads problem, we require basic dimensions. Since here we have no variables related to mass, temporal and spatial scales are sufficient.

For the nonhydrostatic case, from (1.28) we have $\mu = 1$, leading to

$$L = H, \tag{3.8}$$

so we use H as the horizontal and vertical length scale. Looking at (1.24) – (1.26), we find one

Variable	Description	Unit (short form)
M	Mass	Kilograms (kg)
L/H	Length/Height	Meters (m)
T	Time	Seconds (s)

Table 3.1: The basic dimensions.

of the time related variables is N, which yields the buoyancy period

$$T_1 = \frac{2\pi}{N}. \tag{3.9}$$

Another way to obtain the temporal dimension is to use velocity scale U as the intermediate variable as in

$$T_2 = \frac{L}{U}. \tag{3.10}$$

From (3.8), L has the same length scale as H. To get U, we choose it to be the velocity c_1 of the mode 1 waves. From the eigenvalue problem[6] with a constant N under a non-rotating hydrostatic assumption

$$\phi'' + \frac{N^2}{c^2}\phi = 0, \tag{3.11}$$

$$\phi(0) = \phi(-H) = 0, \tag{3.12}$$

where (3.12) is from the rigid lid boundary condition and $z = 0$, $z = -H$ are the top and bottom boundary respectively, we have the solution for a mode n wave

$$\phi = \sin(\frac{n\pi}{H}z), \qquad n = 1, 2, 3, \cdots . \tag{3.13}$$

From (3.11), we have a general expression for the phase speed of a non-rotating ($f = 0$) hydrostatic wave of mode n, namely

$$c_n = \frac{NH}{n\pi}, \tag{3.14}$$

[6]See the next chapter for the detailed derivation and explanation of this equation.

so that for a mode 1 wave[7],

$$c_1 = \frac{NH}{\pi}, \tag{3.15}$$

and hence

$$T_2 = \frac{H}{c} = \frac{H}{\frac{NH}{\pi}} = \frac{\pi}{N}. \tag{3.16}$$

Since we can choose either T_1 or T_2 for this problem, without loss of generality we choose the time scale to be T_2.

We refer back to (1.28) so as to write δ as

$$\delta = \frac{f^2L^2}{U^2} = \frac{f^2H^2}{(\frac{H}{T})^2} \tag{3.17}$$

$$= f^2\frac{\pi^2}{N^2}, \tag{3.18}$$

where (3.17) follows from (3.8) and (3.18) follows from (3.9).

With the obtained dimensions here, we go back to quantify (1.24) - (1.26) as

$$(x, z, t) = \left(H\tilde{x}, H\tilde{z}, \frac{\pi}{N}\tilde{t}\right) \tag{3.19}$$

$$(\psi, b, v) = \epsilon\left(\frac{NH^2}{\pi}\tilde{\psi}, \frac{N^2H}{\pi}\tilde{b}, fH\tilde{v}\right) \tag{3.20}$$

$$N^2 = \frac{N^2}{\pi^2}\tilde{N}^2 \quad \Rightarrow \tilde{N} = \pi. \tag{3.21}$$

3.1.5 A Note on Investigating a Numerical Model by Scaling

In the boundary forced model, we have the following fundamental variables

$$\text{time related :} \quad \omega, N \text{ and } f, \tag{3.22}$$

$$\text{length related :} \quad H, \tag{3.23}$$

$$\text{others :} \quad F_a, \tag{3.24}$$

where F_a is a typical forcing amplitude with dimension

$$\frac{U}{T} = \frac{L}{T^2}. \tag{3.25}$$

[7](3.14) indicates that phase speed is inversely proportional to mode number. Recall that a similar conclusion was drawn in figure 3.4

The three temporal variables supply two non-dimensional variables: $\frac{f}{\omega}$ and $\frac{\omega}{N}$. F_a can then be combined with time and length variables to form the other non-dimensional variables via $\frac{F_a}{H\omega N}$.

The ratio $\frac{f}{\omega}$ indicates the significance of the earth's rotation. The full dispersion relation for internal gravity waves is (2.23), whose dimensional counterpart is

$$\omega^2 = \frac{k^2N^2 + m^2f^2}{k^2 + m^2}. \tag{3.26}$$

Solving (3.26) for $\frac{f^2}{\omega^2}$ yields

$$\frac{f^2}{\omega^2} = \frac{k^2 + m^2}{m^2} - \frac{k^2N^2}{m^2\omega^2}. \tag{3.27}$$

If $\frac{f^2}{\omega^2} \ll 1$, then (3.27) can be approximated by

$$0 = \frac{k^2 + m^2}{m^2} - \frac{k^2N^2}{m^2\omega^2}, \tag{3.28}$$

which can be rearranged to read

$$\omega^2 = \frac{k^2N^2}{k^2 + m^2} \qquad \text{and} \qquad \frac{\omega^2}{N^2} = \frac{k^2}{k^2 + m^2}. \tag{3.29}$$

Then (3.29) is the dimensional dispersion relation with negligible rotational effects[8].

When $\frac{\omega^2}{N^2}$ itself is also small, then in (3.29), we have $m^2 \gg k^2$ and hence

$$\frac{\omega^2}{N^2} = \frac{k^2}{m^2}. \tag{3.30}$$

It follows that the dispersion relation is

$$\omega^2 = \frac{k^2N^2}{m^2}, \tag{3.31}$$

which is the dispersion relation of hydrostatic internal waves without the earth's rotation.

Similar to (3.6), the equation of a typical forcing mechanism is presented as

$$u_t = F_a \cos(\omega t). \tag{3.32}$$

As we see from (3.32), u, the horizontal velocity of the current is proportional to $\frac{F_a}{\omega}$. The requirement for the validity of linearization in Leblond and Mysak [1978] is given by the condition

[8]We note that (3.29) can also be directly obtained by setting $f = 0$ in (3.26).

$\frac{f}{\omega}$	Importance of the Coriolis force
$\frac{\omega}{N}$	Hydrostaticity
$\frac{F_a}{H\omega N}$	Nonlinearity

Table 3.2: Property of the three nondimensional variables.

that the ratio of the fluid velocity (U) to phase speed (C) is much small than 1. This conclusion provides us a way to evaluate the nonlinear parameter in this model. The phase speed under constant N, the non-rotating assumption and the hydrostatic assumption is given by (3.15), so the nonlinearity parameter is

$$\frac{U}{C} = \frac{\frac{F_a}{\omega}}{\frac{NH}{\pi}}. \tag{3.33}$$

Ignoring the factor of π, we claim that $\frac{F_a}{H\omega N}$ describes the nonlinearity of the model.

A summary of the parameters is given by table 3.2. These three non-dimensional variables depict the gist of the model and become the indicators of a variety of aspects of the numerical model. In the numerical simulation, based on the three non-dimensional parameters, we choose different parameters for the model set-up. And the numerical results can be classified into three categories divided according to the three non-dimensional parameters given by table 3.2.

We now can also refer to appendix A where we have given a full account of the smallness of Δk defined by (2.32) based on these three nondimensional parameters governing the boundary forced model.

3.2 Results

In this section, we present the results of solving the amplitude equations (2.91a) – (2.91b) numerically and compare the theoretical solution with the numerical output. First, we verify the equality of internal waves generated by tidal topography interaction and by boundary forcing[9] in terms of the resonant interaction mechanism; then, we try to use resonant theory to explain the model output but find disagreement; at last, we find the near-resonant theory helps understand

[9] At this step, based on the obtained result, we claim this resonance to be purely spatially.

the resonant-like phenomenon and gives satisfactory match to the numerical output.

3.2.1 Equality of the Two Numerical Runs

As we have explained in sections 3.1.2 and 3.1.3, these two methods of internal waves generation have the same mechanism with regard to what we are interested in – near-resonant wave-wave interaction. This can be demonstrated by figure 3.8, where the result of the decomposition of these three waves matches well. The phases of these three waves from these two models agree well, while the amplitudes are the same up to a negligible numerical error. We might have noticed that at the wave front, we do not see the exact same wave form of the two set of waves. This difference is from the fact that the time domain has a minor disagreement due to the mechanics of our Fourier decomposition. The amplitudes of harmonic 1 – mode 1 wave in the two cases oscillate equally mildly compared to the other two waves from the triad, and so is stable. We further witness that the amplitudes of harmonic 2 – mode 2 wave of the two simulation are both unstable.

3.2.2 Near-resonance or Resonance

Since figure 3.5 is resonant-like, we certainly could try to use the resonant theory to explain it. To apply resonant theory on internal waves, we assume that the fluid is hydrostatic ($\mu = 0$), so that the dispersion relation is (2.74) and we will get exact resonant triad with the given three waves. We can then carry on to derive the amplitude equation (2.78a) – (2.78b). Martin et al. [1972] has worked this theory out and used it to explain an experimental result.

In running the model with different time ranges, we find the resonant-like phenomenon is not time sensitive, and so we take it as being spatial resonance. In solving (2.91a) – (2.91b), we compare the results in figure 3.9, where the solid red line represents the result of model output, while the red dotted line depicts the theoretical result. Notice that the model output captures the motion of the wave, so we can see from the figure that the harmonic 1 – mode 1 wave travels the fastest. The model does not take wave propagation into account and thus we can see the red dotted wave in front of harmonic 2 – mode 2 wave and harmonic 1 – mode 3 wave in (b) and (c) respectively[10]. Comparison of these two lines indicates that the wave amplitude is well predicted

[10]In most of the following figures, we all see the red dotted line surpass the blue solid line. This surpass is from

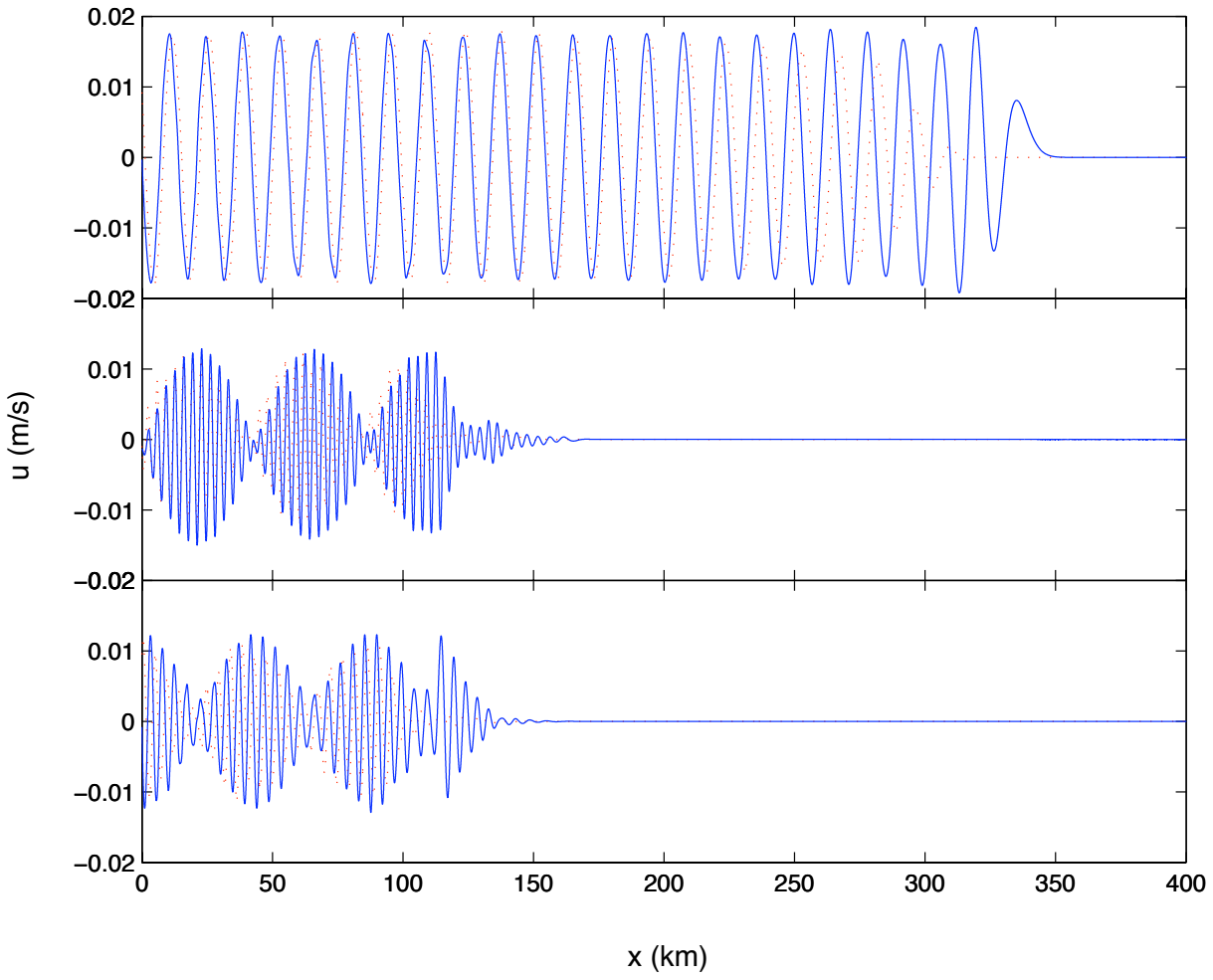

Figure 3.8: Plot of $u(x, 0, t)$ at 24 tidal period of the two numerical models. $f = 0$, $N = 0.001$ s^{-1}, $H = 1$ km. Blue solid: internal waves from forced boundary. Red dotted: internal waves generated by tide topography interaction. (a) Harmonic 1 – mode 1 wave. (b) Harmonic 2 – mode 2. (c) Harmonic 1 – mode 3 wave.

by the resonant internal wave triads theory. This comparison also leads to the discrepancy: in (b), the half-wavelength of the wave envelope in of the model output is 40 km, however, the resonant

the fact that we have not captured the propagating motion of the waves and treat them as static.

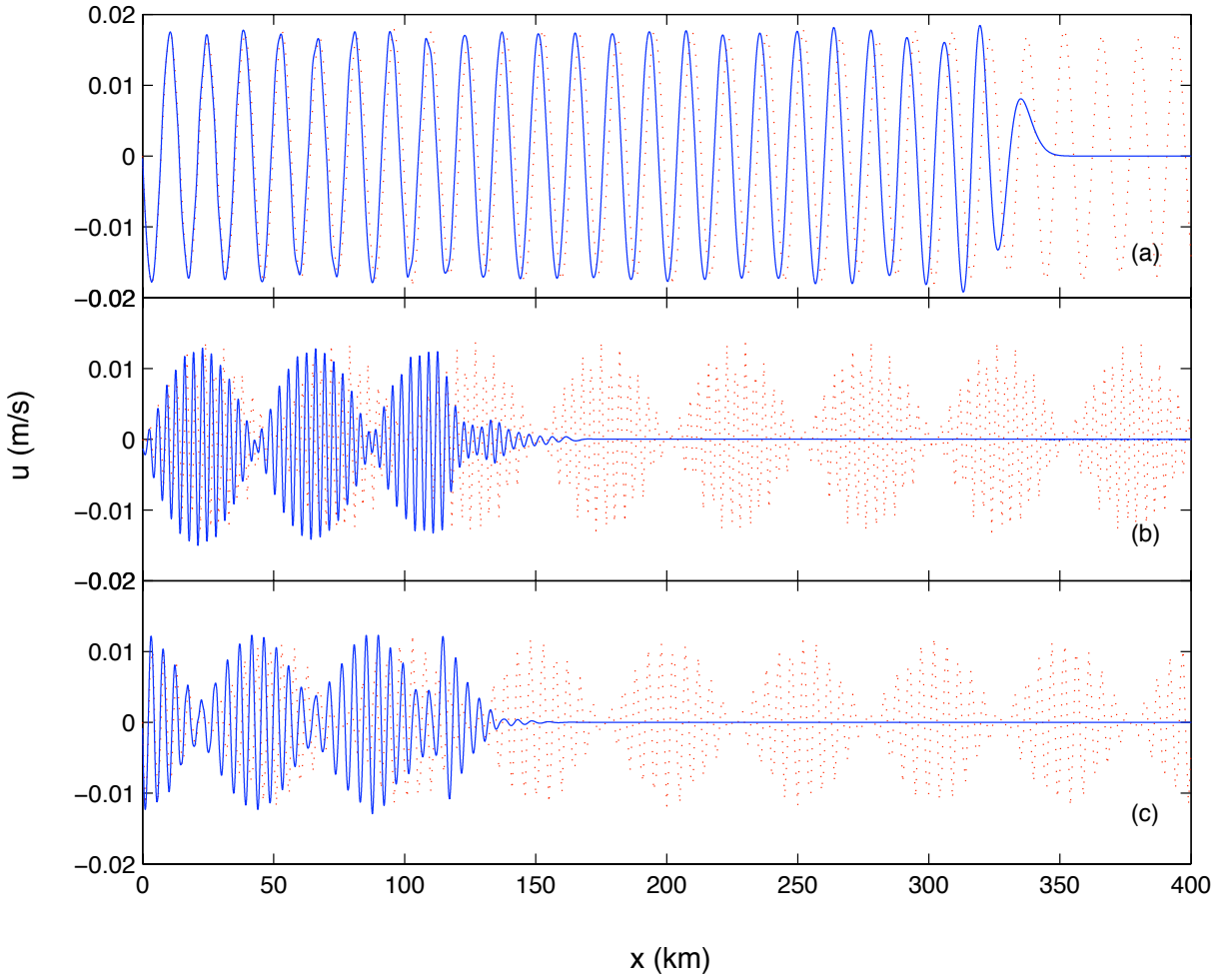

Figure 3.9: $f = 0$, $N = 0.001$ s^{-1}, $H = 1$ km. Blue solid: amplitude DE solution for resonant theory. Red dotted: tidal shoaling model output. (a) Harmonic 1 – mode 1 wave. (b) Harmonic 2 – mode 2. (c) Harmonic 1 – mode 3 wave.

theory predicts the half-wavelength to be 50 km. This discrepancy represents a 25% error, so we could start to wonder if there is a better theory which explains the resonant-like phenomenon with less error.

Remember that to apply the exact resonant theory to explain the numerical result, we as-

sumed that the three waves are hydrostatic. In fact, we can use $\mu = (\frac{k}{m})^2$ to evaluate the non-hydrostaticity and get

$$\mu_1 = 0.0752, \quad \mu_2 = 0.01, \quad \mu_3 = 0.01, \tag{3.34}$$

where μ_1, μ_2 and μ_3 are the nonhydrostatic parameters of harmonic 2 – mode 2, harmonic 1 – mode 3 and harmonic 1 – mode 1 wave respectively. We notice that the values of the nonhydrostatic parameter might not be small enough for us to assume the waves to be hydrostatic.

3.2.3 Near-resonance without the Earth's Rotation

Since the resonant theory does not well predict the observed resonant-like phenomenon, we tried to modify the assumptions such as non-hydrostaticity and negligible earth's rotation ($f = 0$), so as to come up with near-resonant theory in section 2.2.5. Figure 3.10 displays the result of the amplitude equations and the model output, showing that the near-resonant theory is significantly more accurate in explaining the numerical model result. Also, unlike in figure 3.10, when $N = 0.001\ s^{-1}$, figure 3.11 demonstrates the merits of the near-resonant theory when $N = 0.002\ s^{-1}$. Note that the x limits of the two figures are different. In these two cases ($N = 0.001\ s^{-1}$ and $N = 0.002\ s^{-1}$), Δk is comparatively small (see table (2.3)). In these two runs of different N, we have kept the nonlinearity to be the same by increase the forcing amplitude as we choose a larger N. We can see that in figure 3.10, the amplitude of harmonic 1 – mode 1 wave is 0.018 m, whereas it is 0.036 m in figure 3.11.

Setting different N in the numerical models, we find that in the range of N producing the resonant-like phenomenon, the greater N is, the larger the wavelengths of the waves are. To be more specific, for (3.10) - (a), we see that there are 7 wave crests in the domain of $[0, 100]$ km, whereas in (3.11) - (b), we find only 3 wave crests in the same domain. This fact can be explained by its dispersion relation (2.67), which is also

$$k^2 = \frac{m^2\omega^2}{N^2 - \omega^2}. \tag{3.35}$$

In (3.35), as N increases, k decreases, and since the wavelength follows $\lambda = \frac{2\pi}{k}$, λ grows with N.

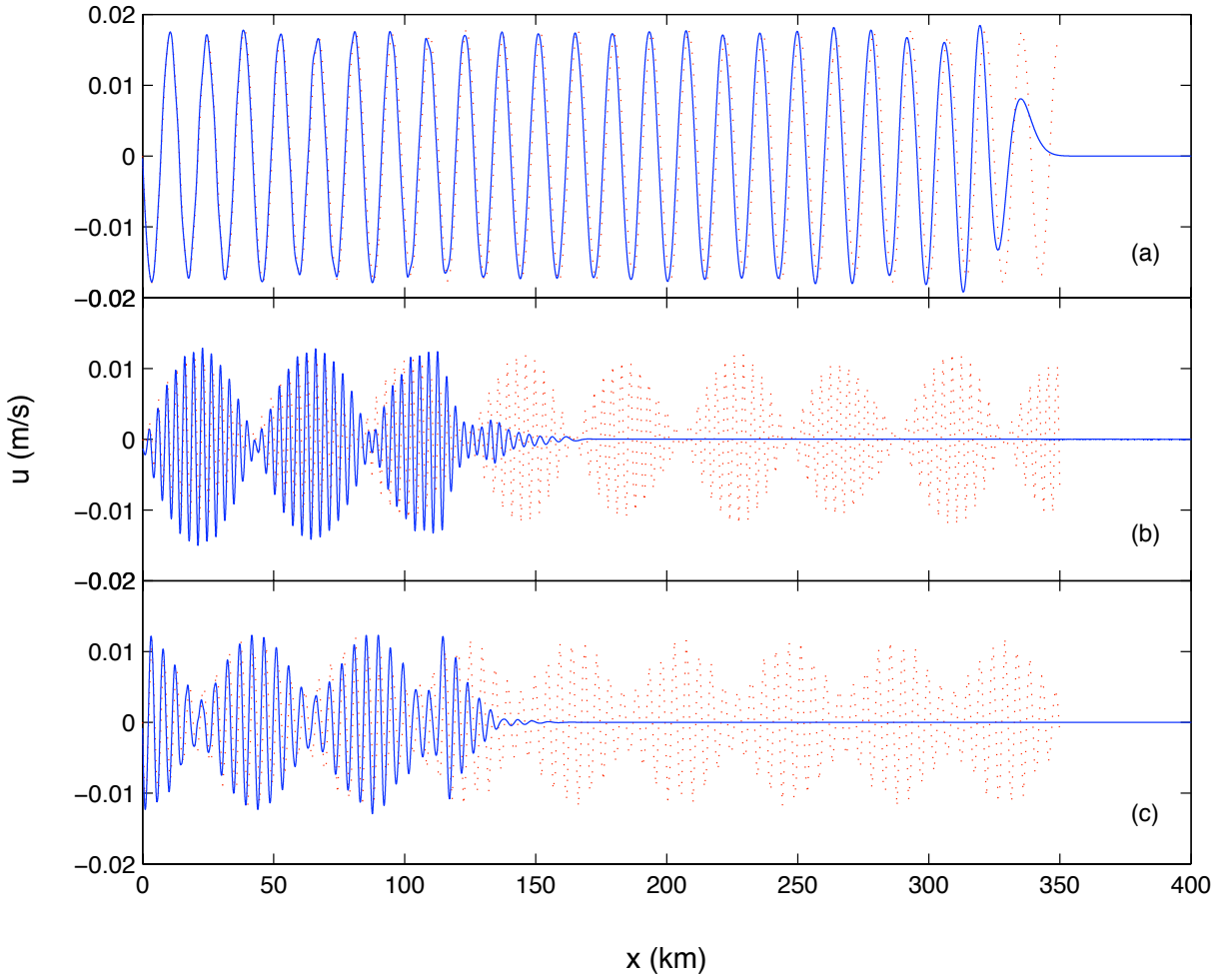

Figure 3.10: $f = 0$, $N = 0.001$ s^{-1}, $H = 1$ km. Blue solid: output of boundary forced model at 24 T_0 . Red dotted: amplitude DE solution for near-resonant theory. (a) Harmonic 1 – mode 1. (b) Harmonic 2 – mode 2. (c) Harmonic 1 – mode 3.

3.2.4 Near-resonance with the Earth's Rotation

In dealing with the earth's rotation, we have a switch in the numerical code. If we set it to be 0, the earth's rotation will not be taken into account. This set-up is what we choose in section 3.2.3. Alternatively, if the switch is 1, the earth's rotation can be included and specified by further

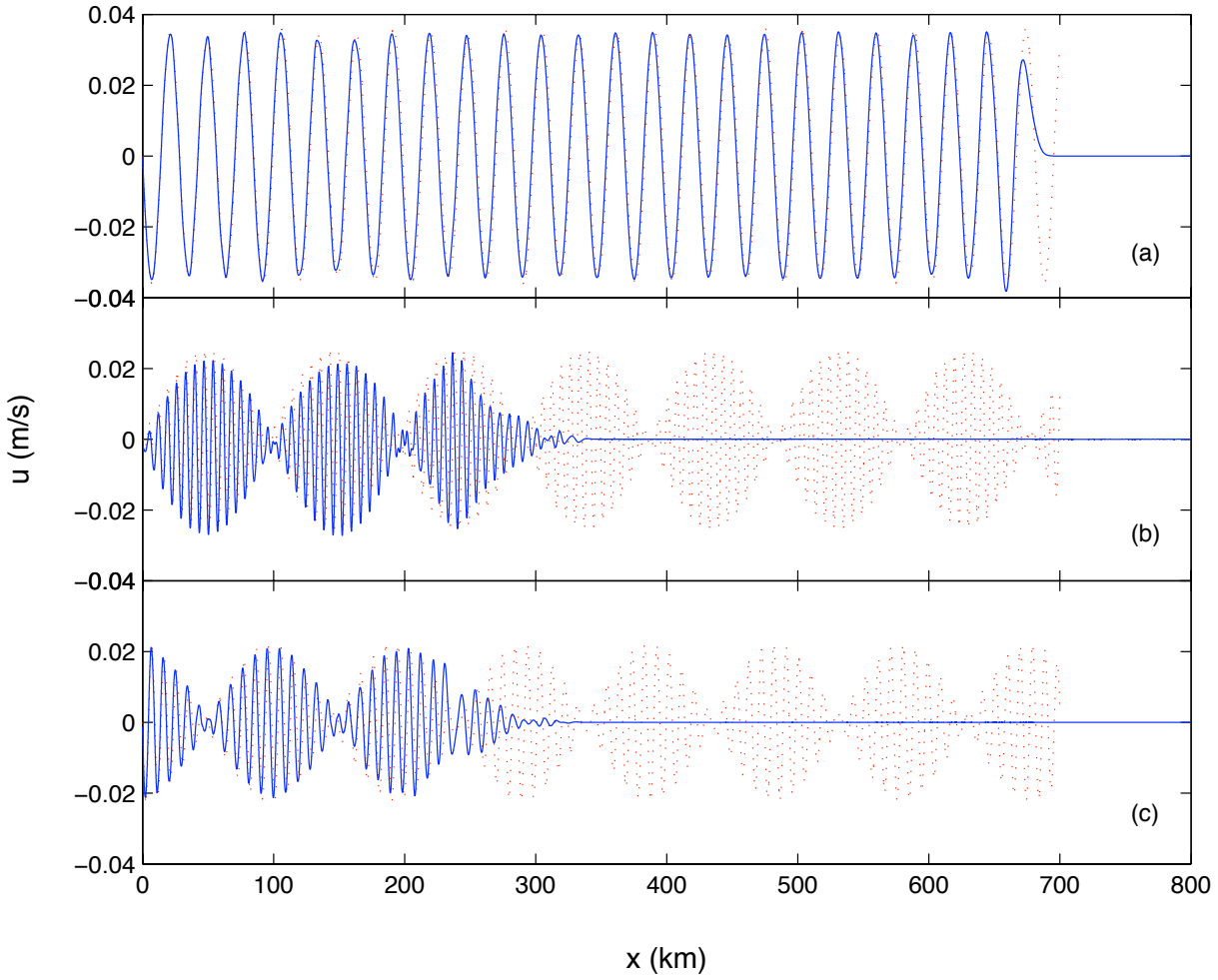

Figure 3.11: $f = 0$, $N = 0.002$ s^{-1}, $H = 1$ km. Blue solid: output of boundary forced model at 24 T_0. Red dotted: amplitude DE solution for near-resonance theory without the earth's rotation. (a) Harmonic 1 – mode 1 wave. (b) Harmonic 2 – mode 2 wave. (c) Harmonic 1 – mode 3 wave.

setting the value of f. Results for non-zero f are shown in figure 3.12 – 3.15. Comparing the theoretical result and numerical output in these listed figures, these results agree very well in a certain range of f. In this range, as f increases, the wavelengths decline. This trend can be seen by comparing subplots (a) of figure 3.12 and figure 3.14, where in (3.12), the wavelength

of harmonic 1 – mode 1 is smaller than that in (3.14). To explore the theoretical explanation, we refer to the dimensional dispersion relation corresponding to (2.23),

$$\omega^2 = \frac{N^2k^2 + f^2m^2}{k^2 + m^2},$$

which leads to

$$k^2 = m^2\frac{\omega^2 - f^2}{N^2 - \omega^2}. \tag{3.36}$$

When ω, N and m do not change but f increases, k decreases[11], and hence the wavelength increases.

In figure 3.15 where $f = 1.0 \times 10^{-2}$ s^{-1}, near-resonant theory still does a pretty good job at predicting the trend of the three waves, however it slightly underestimates the amplitude of the horizontal velocity of the harmonic 2 – mode 2 wave. Because

$$\Delta k = -4.65 \times 10^{-4}, \tag{3.37}$$

the relative detuning to that of each wavenumber. for the three wavs is

$$\frac{\Delta k}{k_1} = 0.2703, \tag{3.38}$$

$$\frac{\Delta k}{k_2} = -0.4940, \tag{3.39}$$

$$\frac{\Delta k}{k_3} = -1.4821, \tag{3.40}$$

whose maximum $|\frac{\Delta k}{k_3}|$ is obviously too large for us to assume Δk is small and hence apply the near-resonant theory. The failure of near resonant theory can be demonstrated in figure 3.16, where the theoretical result of the harmonic 2 – mode 2 wave under-predict the wave amplitude of the numerical output. However, as we can see from figure 3.15 this theory still predict the shapes and the wavelengths very well.

3.2.5 Near-Resonance with Different Nonlinearity

Figures 3.5, 3.10, and 3.15 – 3.16 describe near-resonant internal wave triads resulting from models with the same value of the nonlinear parameter $\frac{F_a}{H\omega_{M_2}N}$ (see table 3.2). From these figures,

[11] According to the choice of parameters of the numerical models, $f < \omega < N$.

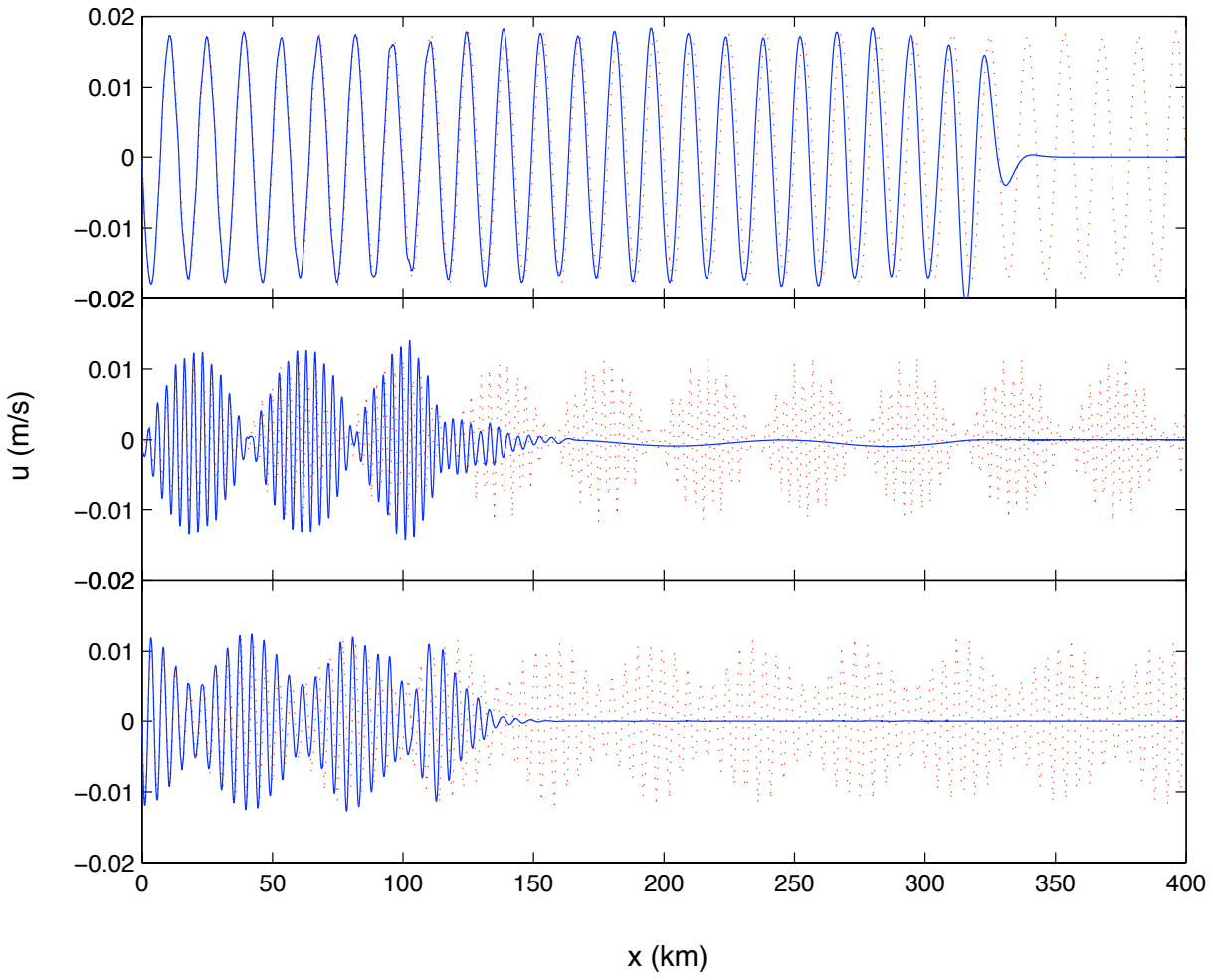

Figure 3.12: $f = 0.2 \times 10^{-4}$ s^{-1}, $N = 0.001$ s^{-1}, $H = 1$ km. Blue solid: output of boundary forced model at 24 T_0. Red dotted: amplitude DE solution for near-resonance theory with the earth's rotation. (a) Harmonic 1 – mode 1. (b) Harmonic 2 – mode 2. (c) Harmonic 1 – mode 3.

we are not able to analyse if our theory is still valid when the model becomes very nonlinear. This section is intended to investigate two other runs with different nonlinearity parameters. The result will be able to inform us how important weakly nonlinearity is when apply near-resonant theory to explain model result.

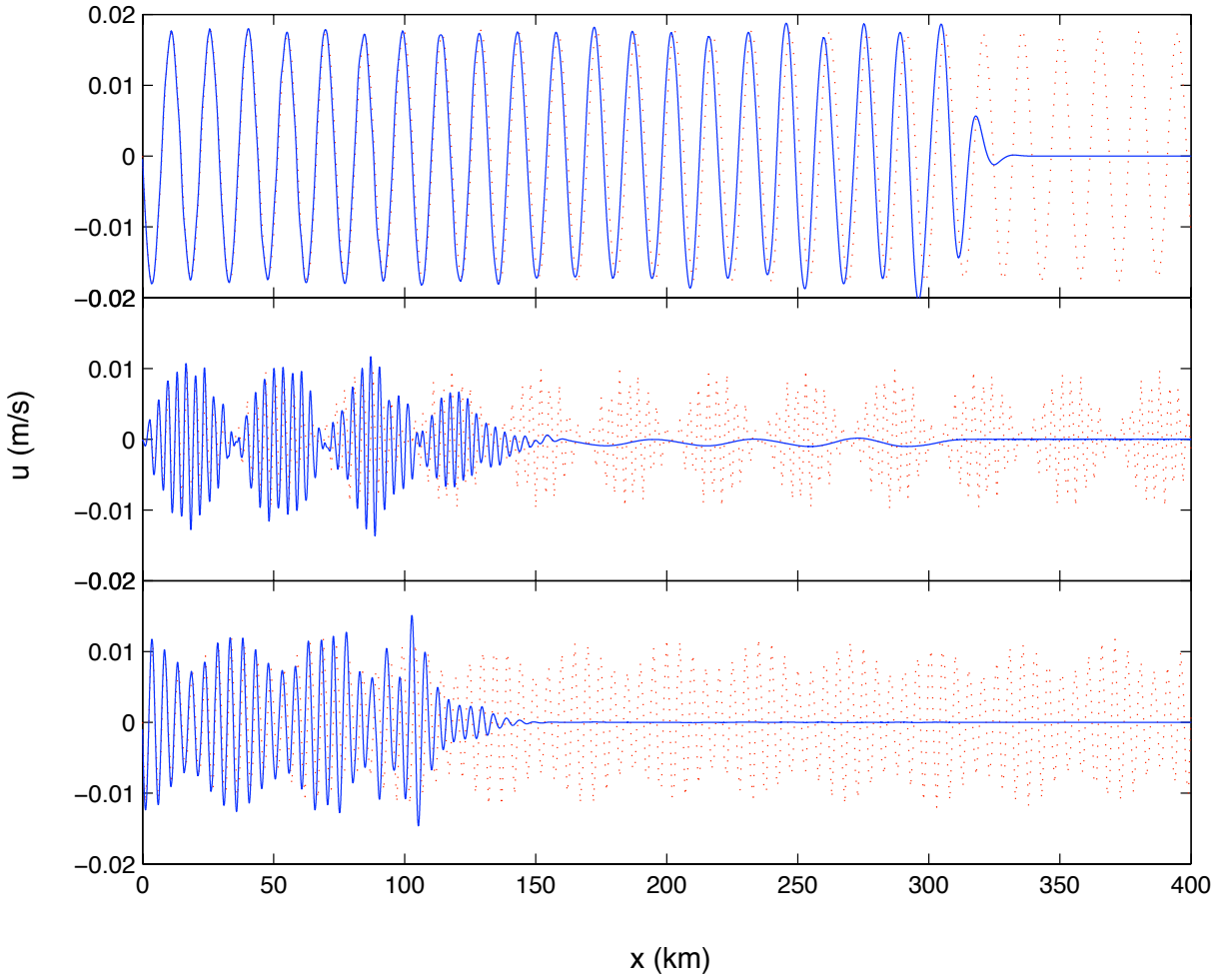

Figure 3.13: $f = 0.4 \times 10^{-4}$ s^{-1}, $N = 0.001$ s^{-1}, $H = 1$ km. Blue solid: output of boundary forced model at 24 T_0. Red dotted: amplitude DE solution for near-resonance theory with the earth's rotation. (a) Harmonic 1 – mode 1. (b) Harmonic 2 – mode 2. (c) Harmonic 1 – mode 3.

Figure 3.17 shows the result of the run with a forcing amplitude which is half of what have been used in the previous runs. The forcing mechanism is described by this mathematical equation

$$u_t = 0.009\omega_{M_2} \cos(\omega t) \cos(\frac{\pi}{H} z) + 0.0065\omega_{M_2} \cos(\omega t) \cos(\frac{3\pi}{H} z). \tag{3.41}$$

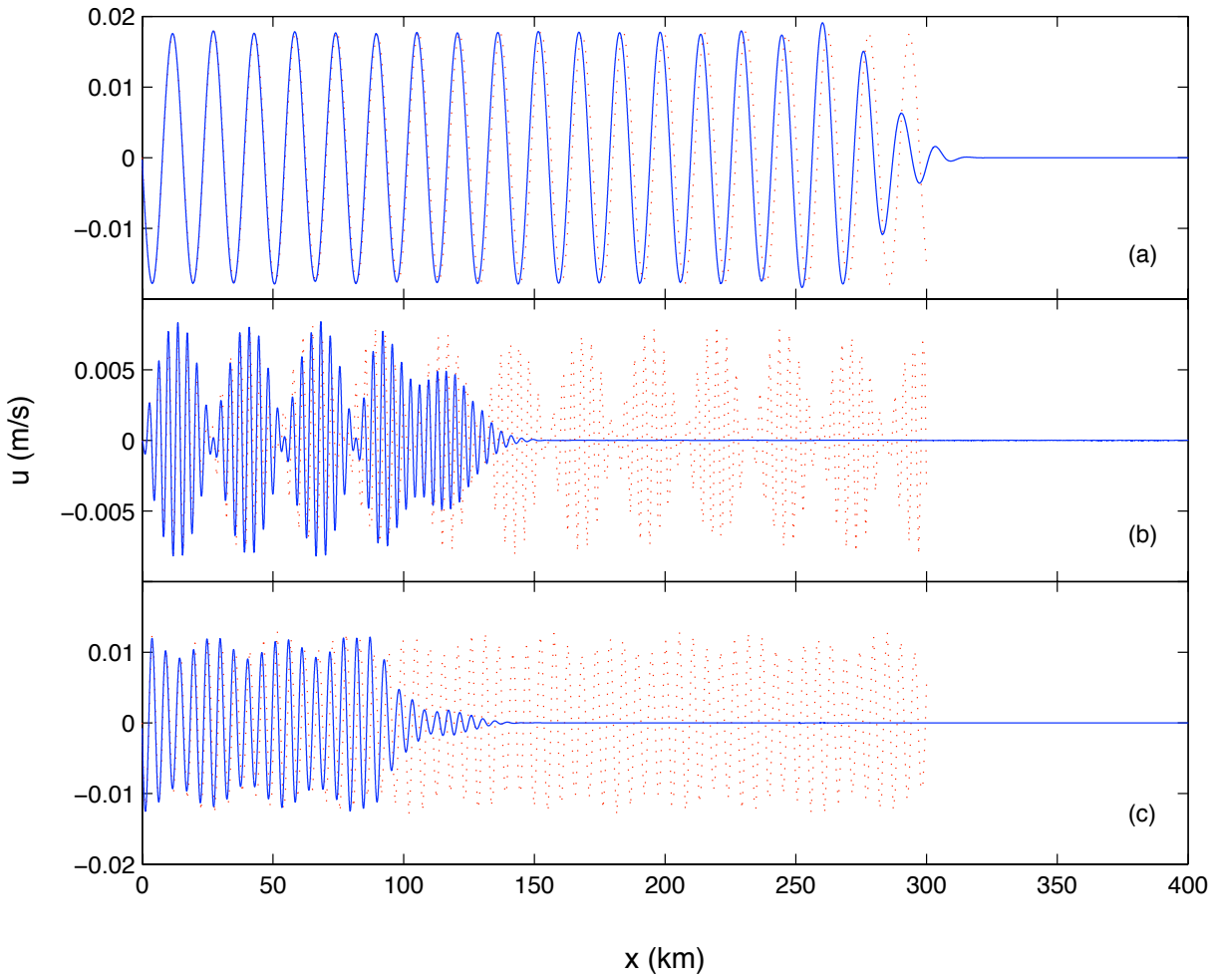

Figure 3.14: $f = 0.6 \times 10^{-4}$ s^{-1}, $N = 0.001$ s^{-1}, $H = 1$ km. Blue solid: output of boundary forced model at 24 T_0. Red dotted: amplitude DE solution for near-resonance theory with the earth's rotation. (a) Harmonic 1 – mode 1. (b) Harmonic 2 – mode 2. (c) Harmonic 1 – mode 3.

In this figure, we can see the incredible overlap between the dotted line and the sold line. For example, in (b), which shows the harmonic 2 – mode 2 wave generated by near-resonant interaction, the numerical result represented by the solid line can be very well predicted by the theoretical result depicted by the dotted line.

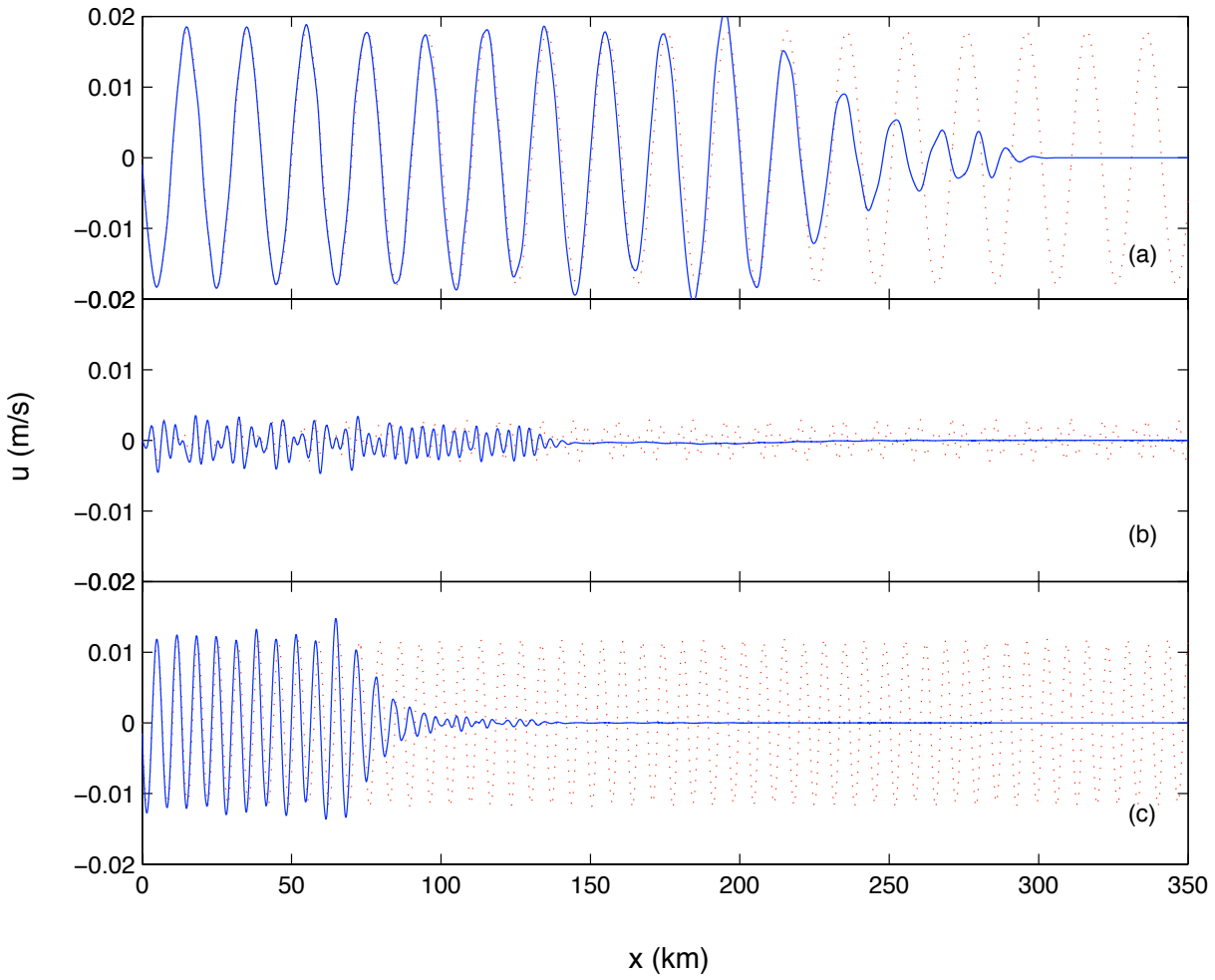

Figure 3.15: $f = 1.0 \times 10^{-4}$ s^{-1}, $N = 0.001$ s^{-1}, $H = 1$ km. Blue solid: output of boundary forced model at 24 T_0. Red dotted: amplitude DE solution for near-resonance theory with the earth's rotation. (a) Harmonic 1 – mode 1. (b) Harmonic 2 – mode 2. (c) Harmonic 1 – mode 3.

Figure 3.18 presents the result with a forcing by this equation

$$u_t = 0.036\omega_{M_2}\cos(\omega t)\cos(\frac{\pi}{H}z) + 0.026\omega_{M_2}\cos(\omega t)\cos(\frac{3\pi}{H}z). \tag{3.42}$$

Unlike figure 3.17, the overlap between the two lines is not as good. As we can see that in the plot of harmonic 1 – mode 1 wave shown in (a), the two types of lines match very well for

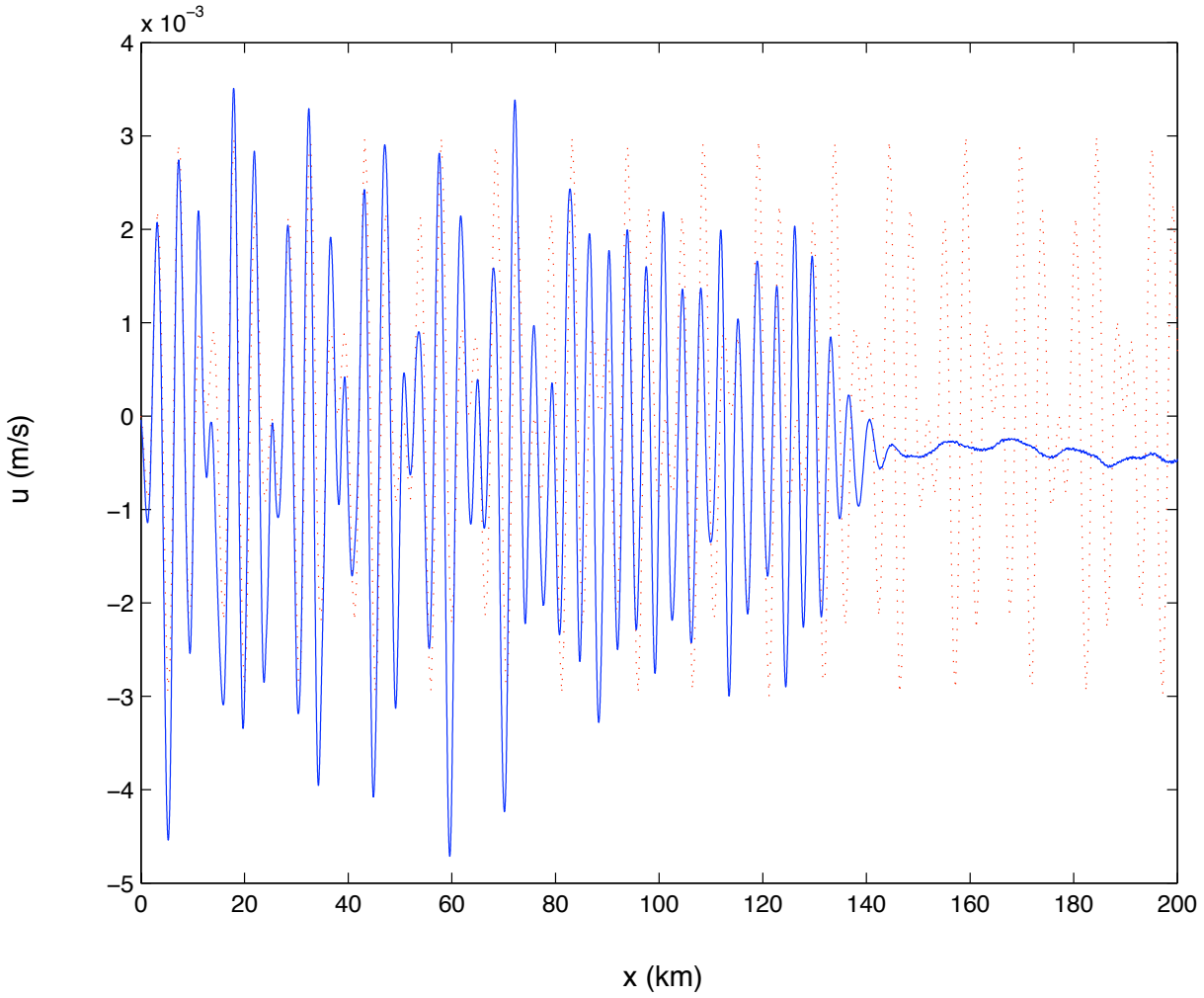

Figure 3.16: A closer look at (b) in fig(3.15). $f = 1.0 \times 10^{-4}$ s^{-1}, $N = 0.001$ s^{-1},$H = 1$ km. Blue solid: model output. Red dotted: amplitude DE solution.

the first six wave lengths; however, we find the theoretical result deviates to the left starting from the seventh wavelength. The same disagreement happens to the other two plots: (b) and (c).

The comparison of these two figures indicates that as the model becomes more nonlinear, the near-resonant theory provides less agreement with the nonlinear numerical simulation. In addition, we set up a few less nonlinear models with a smaller value of $\frac{F_a}{H\omega_{M_2}N}$ and find when

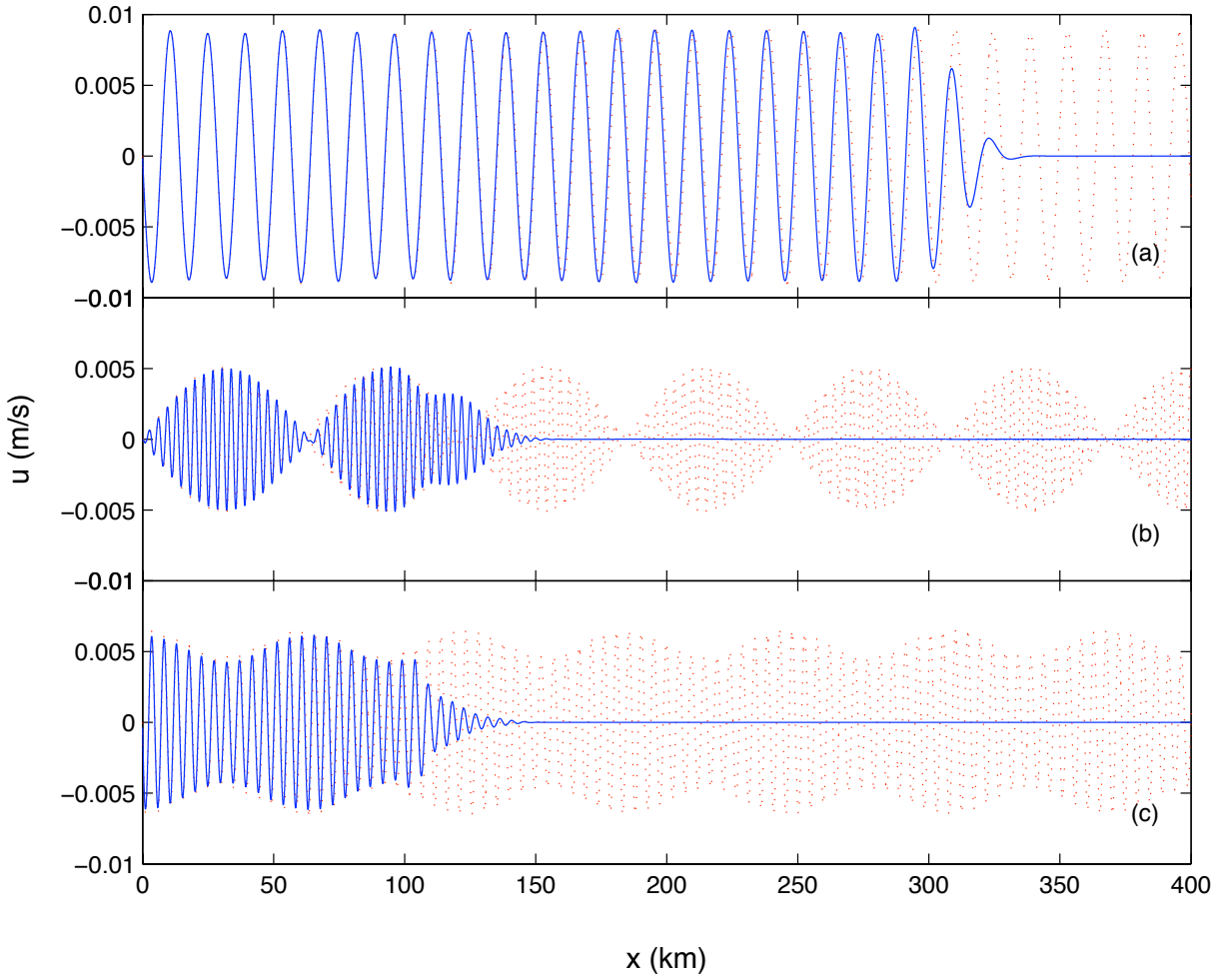

Figure 3.17: Plot of result of runs with the forcing amplitude half of the previous runs whose result is shown in figure 3.12. Here, $f = 0.2 \times 10^{-4}$ s^{-1}, $N = 0.001$ s^{-1}, $H = 1$ km. Blue solid: output of boundary forced model at 24 T_0. Red dotted: amplitude DE solution for near-resonance theory with the earth's rotation. (a) Harmonic 1 – mode 1. (b) Harmonic 2 – mode 2. (c) Harmonic 1 – mode 3.

the model becomes very linear, the near-resonant phenomenon disappears. Certainly, on the contrary, when the model becomes very nonlinear, the near-resonant theory also fails.

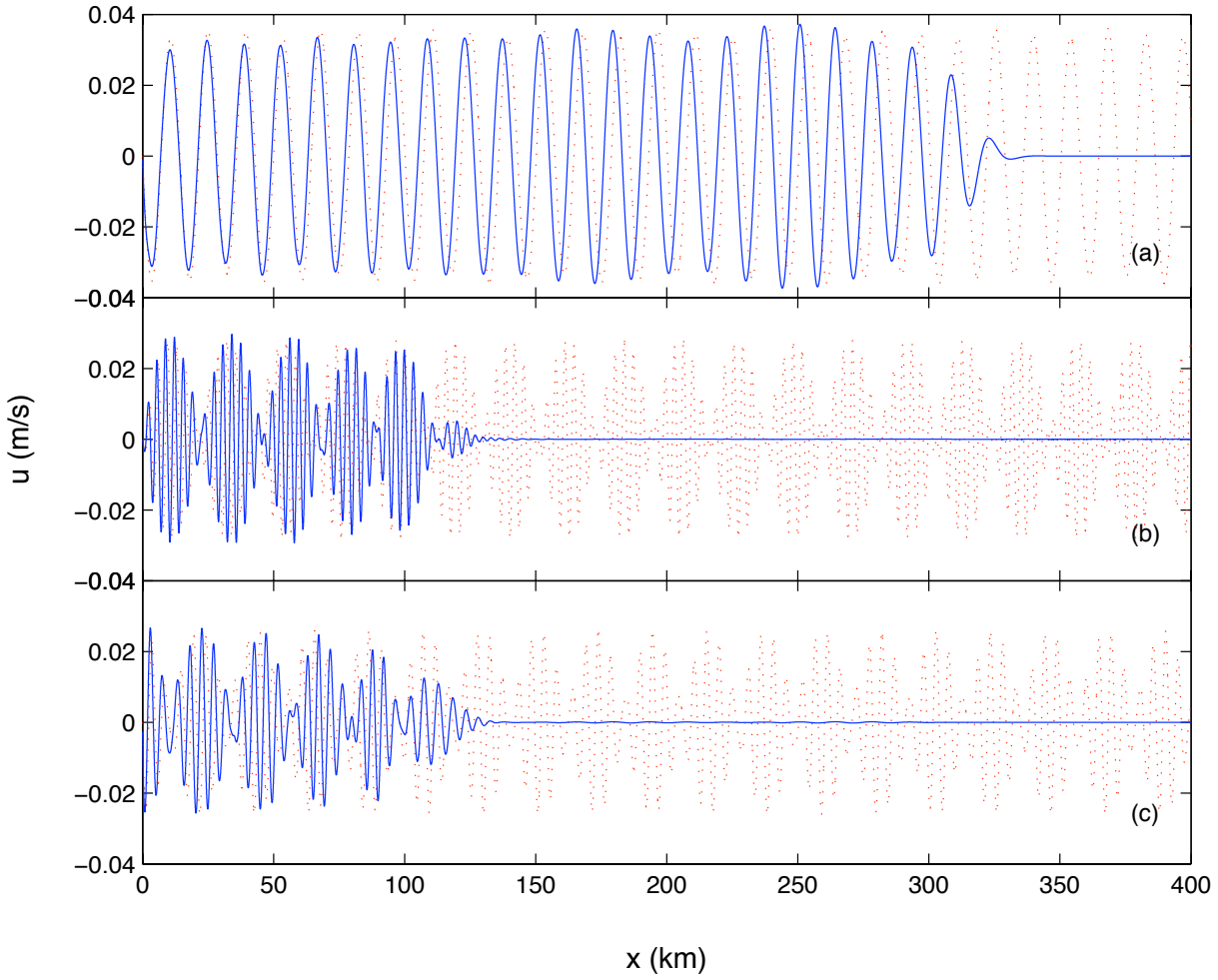

Figure 3.18: Plot of result of runs with the forcing amplitude twice of the previous runs whose result is shown in figure 3.12. Here, $f = 0.2 \times 10^{-4}$ s^{-1}, $N = 0.001$ s^{-1}, $H = 1$ km. Blue solid: output of boundary forced model at 24 T_0. Red dotted: amplitude DE solution for near-resonance theory with the earth's rotation. (a) Harmonic 1 – mode 1. (b) Harmonic 2 – mode 2. (c) Harmonic 1 – mode 3.

3.3 A Summary of the Figures

The results have been demonstrated in figures 3.5, 3.7 – 3.16, which are presented along the assumptions (hydrostaticity and negligible earth's roation) of the dispersion relation of internal

Figure	N (s^{-1})	Fa ($\frac{L}{T^2}$)	f (s^{-1})	$\frac{f}{\omega_{M_2}}$	$\frac{\omega_{M_2}}{N}$	$\frac{F_a}{H\omega_{M_2}N}$
3.5, 3.7–3.10	0.001	$0.018\omega_{M_2}$	0	0	0.14075	0.018
3.11	0.002	$0.036\omega_{M_2}$	0	0	0.070375	0.018
3.12	0.001	$0.018\omega_{M_2}$	0.2×10^{-4}	0.1421	0.14075	0.018
3.13	0.001	$0.018\omega_{M_2}$	0.4×10^{-4}	0.2842	0.14075	0.018
3.14	0.001	$0.018\omega_{M_2}$	0.6×10^{-4}	0.4263	0.14075	0.018
3.15, 3.16	0.001	$0.018\omega_{M_2}$	1.0×10^{-4}	0.7105	0.14075	0.018
3.17	0.001	$0.009\omega_{M_2}$	0.2×10^{-4}	0.1421	0.14075	0.0009
3.18	0.001	$0.036\omega_{M_2}$	0.2×10^{-4}	0.1421	0.14075	0.036

Table 3.3: A summary of the critical parameters of the numerical runs and the nondimensional parameters given by table 3.2. F_a is a typical amplitude of forced waves. In the numerical runs, we actually force two waves: the harmonic 1 – mode 1 wave and harmonic 1 – mode 3 wave on the left boundary. Here we choose the amplitude of the harmonic 1 – mode 1 wave as the typical amplitude (F_a). ω_{M_2} is the M_2 *tidal frequency*, which is 1.4075×10^{-4} s^{-1}.

waves. Here, we provide a table showing the different model parameters used in the different model runs as a convenience for comparing the different figures. The table also lists the values of non-dimensional parameters provided in table 3.2.

3.4 Parametric Subharmonic Instability

3.4.1 Appearance of PSI

In simulations of internal waves generated by boundary forcing, in order to cut down the running time and computer space, we save the velocity data after every tidal period $T_0 = 44640$ s. This save-time interval does not allow us to decompose the velocity into different harmonics, so, unlike the decomposition for the tide topography interaction runs, we only performed the modal decomposition, which provides the separation results of different modes. We did not do the harmonic decomposition and so different harmonics were kept together and not divided. Although in figure 3.12, 3.13, 3.14, and 3.15, we claim the three subplots of each figure are the plot of the three waves of distinct harmonics and modes in the near-resonant triad, the plot of the model output actually depicts the modes of all the harmonics, since we have not performed the harmonic decomposition. This trick works fine to demonstrate the near-resonant triads because the waves from the near-resonant triad capture the leading harmonics of mode 1, mode 2 and mode 3. Other harmonics of these modes serve as small amplitude because they have much smaller amplitudes than the leading ones. However, in these figures, in the region approximately between 150 km to 350 km where a harmonic 2 – mode 2 wave from near-resonance has not yet been obtained, a wave with small amplitude but long wavelength becomes the dominant wave. Curiosity and interest drive us to find out the physics behind the appearance of the front long wave.

Since the harmonic 1 – mode 3 wave does not appear to be related to this phenomenon, we modify and simplify the run by reducing the boundary forcing to only a harmonic 1 – mode 1 wave, such as one given the the mathematical expression

$$u_t = 0.018\omega_{M_2}\cos(\omega_{M_2}t)\cos(\frac{\pi}{H}). \tag{3.43}$$

By saving the output data after every tidal period and decomposing it into mode 1 through mode 10, we obtain the same front waves as in (3.12). If we plot the mode 2 wave from this run together with its counterpart from the run of two forced waves at the left boundary, we can find impressive agreement in the given region. This match drives us to suspect that the front long wave is a consequence of PSI of the harmonic 1 – mode 1 wave. To verify this hypothesis, we need to indentify that this front long wave is a progressive wave as well as identify the parent

wave and child waves.

The definition of a progressive wave is associated with that of a forced wave. Progressive waves are the waves that satisfy a dispersion relation and so can propagate freely with the group velocity determined by the dispersion relation; however, forced waves are those whose wavenumbers and frequency do not solve the dispersion relation, hence cannot propagate freely in the medium. More on the definition of progressive and forced waves can be found in Phillips [1967] and Leblond and Mysak [1978].

If we assume this front long wave is progressive wave, we can calculate the frequency of the wave by extracting information from the plot. To do so, we need to measure the wavelength (λ) from the plot and hence calculate the wavenumber ($k = \frac{2\pi}{\lambda}$). With this parameter and the given f and mode number in hand, we can obtain the frequency from the dispersion relation. To verify the assumption, one way is to run the numerical model again with decreasing the save-time interval (save_interval). A smaller save_interval will allow us to decompose the saved data into different harmonics.

We choose to calculate the frequency in the cases corresponding to figures 3.12, 3.13, and 3.14 and give the result in table (3.4). Then, we decompose the velocity data into different subharmonics so we can plot waves such as harmonic 0.16 – mode 2 wave if $f = 0.2 \times 10^{-4}$ s^{-1}. Consequently, we compare this wave with other mode 2 waves of different harmonics and find it has the largest amplitude in terms of the long front wave. The same result can be obtained for different other f values we worked on. This result is encouraging and satisfactory in informing us that the front long wave is a progressive wave and is likely to be generated from PSI. To further validate this hypothesis, we still need to find the parent wave and the child waves.

3.4.2 Which wave is the Parent Wave?

The boundary forced runs generate waves by mimicking the mechanism of internal waves generation by tide-topography interaction. Far away from the generation site, the first harmonic wave is the dominant wave. This can be demonstrated by a plot of the group velocity as in figure 3.19, where we see that harmonic 1, mode 1 has the second largest group velocity, which is slightly smaller (0.12%) as compared to the largest group velocity of the harmonic 1.1 – mode 1 wave. If now return to (b) in figure 3.12, 3.13, and 3.14, we see that the front long wave of mode 2 has gone almost as far as that of harmonic 1 – mode 1 wave. For example, when $f = 0.2 \times 10^{-4}\ s^{-1}$,

f	λ	k	$\frac{\omega}{\omega_{M_2}}$
$0.2 \times 10^{-4}\ s^{-1}$	80 km	7.85×10^{-5}	0.1676
$0.4 \times 10^{-4}\ s^{-1}$	38 km	1.65×10^{-4}	0.3401
$0.6 \times 10^{-4}\ s^{-1}$	18.2 km	3.45×10^{-4}	0.5772

Table 3.4: The wavelength (λ) of the long front wave under different f is measured directly from the plot. The wavenumbers k is calculated by $k = \frac{2\pi}{\lambda}$. The frequency is calculated from the dispersion relation $\omega^2 = \frac{N^2k^2+f^2m^2}{k^2+m^2}$ given $m = \frac{2\pi}{H}$ (mode-2 wave), where the fluid depth is $H = 1$ km. Note that the mode-2 front long wave of the case $f = 0.6 \times 10^{-4}$ does not a constant wavelength. We use the newest two three crests to calculate the wavelength.

shown by figure 3.12, the front long wave propagates to around 320 km. Since the group velocity for harmonic 1 – mode 1 is 0.2966 m/s, the distance this wave can travel after 24 tidal periods is 317.8 km. We might think that other waves with harmonic number close to 1 can also travel that far; however, the amplitude of the other waves are too small for us to take them as parent waves. Therefore, we claim that the harmonic 1 – mode 1 wave is the *parent wave*.

3.4.3 Which are the Child Waves?

We have determined that the parent wave for this PSI is the harmonic 1 – mode 1 wave and one of the child waves is a mode 2 wave by inspecting figure 3.12,3.13 and 3.14. If we use $\vec{k_0} = (k_0, m_0)$, $\vec{k'} = (k', m')$, $\vec{k''} = (k'', m'')$ and ω_0, ω', ω'' to denote the wavenumber vector and the frequency of the parents wave and two child waves respectively, then $m_0 = \pm\frac{\pi}{H}$ and $m' = \pm\frac{2\pi}{H}$. According to (2.11a), we have

$$k_0 = k' + k'', \tag{3.44}$$

$$m_0 = m' + m'', \tag{3.45}$$

we have $m'' = \pm m_0$ or $m'' = 3m_0$. From the (c) subplot of figure 3.12, 3.13, 3.14, we find that mode 3 is not involved in this PSI, so $m'' = \pm m_0$. We then need to employ (3.44) and the last resonant triad condition (2.11b) in order to find the two unknowns: ω' and ω''. In looking for the

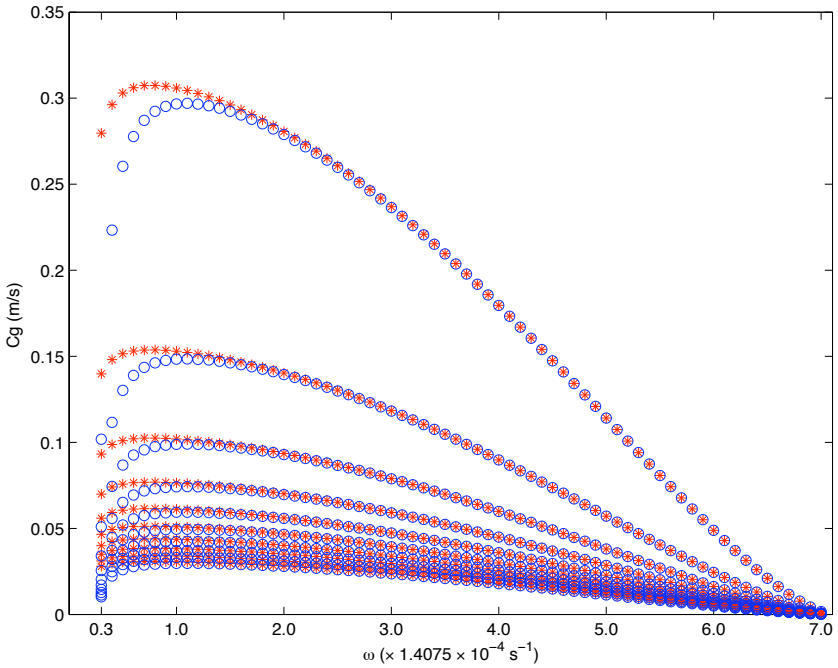

Figure 3.19: Plot of the group velocities of waves with frequencies of 0.3 times tidal frequency (harmonic 0.3) to that of 7 times tidal frequency ω_{M_2} (harmonic 7) with an interval of 0.1 times tidal frequency along the horizontal axis. These group velocities have been calculated with $f = 0.2 \times 10^{-4}\ s^{-1}$ (stars) and $f = 0.4 \times 10^{-4}\ s^{-1}$ (circles). Mode is depicted vertically, spanning from mode 1 (uppermost) to mode 10 (lowermost), leading us to conlcude that group velocity is inversely proportional to mode number.

unknowns, we also need to use the dimensional dispersion relationship

$$k = \pm m \left(\frac{\omega^2 - f^2}{N^2 - \omega^2} \right)^{\frac{1}{2}}. \tag{3.46}$$

Solving (2.11b), (3.44) manually is not an easy job, but gladly we have Maple to help us out.

It turns out that the child waves vary with f and the ratios of their frequency to that of the parent waves are listed in table (3.5). This result agrees with table (3.4), which is obtained from the numerical model output. What is worth mentioning is that when $f = 0$, Maple shows that we do not have solution for (3.44) – (3.45), leading us to the conclusion that the PSI phenomenon does not occur if we do not consider the rotational effects. This conclusion can be verified by the

f (s $^{-1}$)	$\frac{f}{\omega_0}$	$Re\{\frac{\omega'}{\omega_0}\}$	$Re\{\frac{\omega''}{\omega_0}\}$
$0.2 \times 10^{-4}\ s^{-1}$	0.1421	0.1662	0.8338
$0.4 \times 10^{-4}\ s^{-1}$	0.2842	0.3386	0.6614
$0.6 \times 10^{-4}\ s^{-1}$	0.4263	0.5711	0.4289

Table 3.5: The ratio of the frequency of the child waves to that of the parent wave given different f values. $Re(x)$ is to take the real part of a complex value x. In fact, when $f = 0.6 \times 10^{-4}$, the result shows complex ω' and ω''.

result of runs under $f = 0$, as we see in figure 3.10, 3.11 that no front wave appears.

CHAPTER 4

WEAKLY NONLINEAR INTERNAL WAVE MODELS

4.1 Internal Wave Models

A mathematical model is usually one or a set of equations describing the behaviour of a physical system. Mathematical models can be classified into two categories: linear and nonlinear models, depending on the nonlinearity of the equations. Internal wave models are associated with the Navier-Stokes equations [Kundu and Cohen, 2004; Leblond and Mysak, 1978] and the Euler equations [Lamb, 1994], whose adapted form and appropriate assumptions are described by (1.27a) – (1.27c) in chapter 1.

The earliest work on internal wave models dates back to several centuries ago was "under the umbrella of linear approximation" [Johnson, 1997]. The linear approximation applied in (1.27a) – (1.27c) is under the assumption that the perturbation fields have an infinitesimal amplitude so that we can ignore the nonlinear terms and hence obtain a set of linear equations. If we further assume linear stratification (constant buoyancy frequency N), then by substituting the conventional wave form $e^{i(kx+mz-\omega t)}$ into the linearized equations, we will obtain the dispersion relation, the phase speed, the group velocity and many other results in linear wave theory. For more description of linear internal wave models, we refer to [Kundu and Cohen, 2004; Gill, 1982; Craik, 1985].

Nonlinear internal wave models can be divided into weakly nonlinear and fully nonlinear models. Weakly nonlinear theory follows from the application of perturbation theory to nonlin-

ear problems, where we usually solve the linear (first-order) problem first and use the resulting solution to solve the higher-order problems where nonlinearity is initially addressed. Fully nonlinear models require solving the complete set of nonlinear governing equations.

An internal wave model described by (1.27a) – (1.27c) is actually fully nonlinear and cannot be solved analytically; however, thanks to numerical computation theory and fast computers nowadays, we can solve these equations numerically. In fact, IGW, the numerical code written by Kevin Lamb [Lamb, 1994] solves Euler equation to simulate internal waves generation by tide topography interaction at a time length of 24 tidal period. Another fully nonlinear model of two-layer fluid described by the MCC equation has been derived in Choi and Camassa [1999]. This equation has been modified to model multilayer fluid in Choi [2000] and been further studied in Jo and Choi [2002]. Helfrich [2007] has recently modified the MCC equation to include rotational effects without assuming a small rotational parameter.

4.2 Weakly Nonlinear Internal Wave Models

One of the earliest works devoted to weakly nonlinear internal wave models can be found in Benny [1966], where a KdV-type equation was derived in the context of long internal waves after the success of KdV-family equations used to describe shallow water surface waves. This KdV equation, which describes internal waves has since been under intensive studies. Many different terms have been added into this KdV equation to capture more details of the evolution of long internal waves. Much work has also been done to expand the coefficients of KdV-type equations to model wave motion in a fluid with slowly varying topography. Helfrich and Melville [2006]; Xiao [2006] both gave a short review of the various modified KdV equations such as Benjamin-Ono equation, Gardner equation and so on.

This chapter focuses on weakly nonlinear internal wave models which include the effect of the earth's rotation. In fact, in the review paper by Helfrich and Melville [2006], a section has been devoted to summarize previous works on this subject.

4.3 The Ostrovsky Equation: A Model with Small Rotational Effects

When Ostrovsky [1978] published his concise paper, he became the first to add a term incorporating the Coriolis force (the earth's rotation) into the KdV equation. This equation was hence named the Ostrovsky equation[1] to his credit and drew great attention from many researchers [Galkin and Stepanyants, 1991; Boyd, 2005]. Grimshaw et al. [2006] has used a generalized version of Ostrovsky equation to model internal waves on the Australian North West Shelf.

However, with its success and contribution on the one hand, the Ostrovsky equation is also notorious for its dispersion relation and its required rigid initial condition, which together make numerical simulation difficult without any artificial modification.

The Ostrovsky equation is used to model uni-directional wave motion with a small rotational effect. To derive this equation, Ostrovsky [1978] also kept the assumption of the KdV equation: waves are long compared to the length scale of stratification but short compared with length scale (Rossby radius) on which rotation is important. This assumption confines the KdV equation as well as this Ostrovsky equation to be only valid for waves with an intermediate range of wavenumber. The equation is usually written as

$$(A_t + cA_x - \mu r_{01} A_{xxx} - 2\epsilon r_{10} A A_x)_x = \frac{\delta}{2c} A, \tag{4.1}$$

where $A(x,t)$ describes the horizontal evolution of the wave, c is the linear, non-rotating, long-wave propagation speed, ϵ, μ and δ are small parameters representing the nonlinear, the dispersive and the rotational effects respectively, r_{01} and r_{10} are constants related to the background density. The expressions of r_{01} and r_{10} are given by Lamb and Yan [1996].

The dispersion relation of the linearized Ostrovsky equation is

$$\omega = \frac{\frac{\delta}{2c} + ck^2 + \mu r_{01} k^4}{k}, \tag{4.2}$$

from which, we can calculate the phase speed (c_p) and group velocity (C_g)

$$c_p = \frac{\frac{\delta}{2c} + ck^2 + \mu r_{01} k^4}{k^2}, \tag{4.3a}$$

$$C_g = \frac{ck^2 + 3\mu r_{01} k^4 - \frac{\delta}{2c}}{k^2}. \tag{4.3b}$$

[1] Sometimes, the Ostrovsky equation is called rotation modified KdV (RMKdV) equation.

From (4.2) and (4.3a) – (4.3b), we can see that as $k \to 0$, $\omega \to \infty$, $c_p \to \infty$ and $C_g \to \infty$, while as $k \to \infty$, $\omega \to \infty$, $c_p \to \infty$ and $C_g \to \infty$. These limits of ω, c_p and C_g are in fact unphysical and are not consistent with that of the exact dispersion relation[2]. This disagreement makes Ostrovsky equation an ineffective model for describing the evolution of internal waves, which usually includes internal tides with very small k and internal solitary waves with moderate k values.

To simulate (4.1) numerically, we can integrate it to obtain

$$A_t + cA_x - \mu r_{01} A_{xxx} - 2\epsilon r_{10} A A_x = \frac{\delta}{2c} \int_{-\infty}^{x} A(s,t) ds. \tag{4.4}$$

One often considers localized waves with the far field condition $A \to 0$ as $x \to \pm\infty$. If the waves have this property initially, then it will be kept at all later time since the group velocities are always assumed to be finite. This condition is expressed as

$$\int_{-\infty}^{\infty} A(x,t) dx = 0 \qquad \forall \ t. \tag{4.5}$$

If we attempt to simulate evolution of an internal solitary wave, with the initial condition given by

$$A(x,0) = \frac{\eta_0}{b + (1-b)\cosh^2(x)}, \tag{4.6}$$

where η_0 and b can be any constant, then (4.5) will not hold. Numerical simulation then results in a wave amplitude that grows over time. In fact, when simulating a solitary wave, in the far field we have $A_x \to 0$. Then the finite difference discretization of the first time step reads

$$A_1 - A_0 = \Delta t \frac{\delta}{2c} \int_{-\infty}^{\infty} A(x,0) dx \neq 0, \tag{4.7}$$

where A_0 and A_1 are the amplitude of initial time and first time step (Δt) respectively. Clearly, the amplitude will increase everywhere in the far field. A similar discretization after many (constant) time steps will lead to an unbounded $A(x,t)$. In many simulations (for example, in [Grimshaw et al., 2006]) of solitary waves by the Ostrovsky equation, an artificial step function is usually set in the far field in order to meet the initial condition (4.5).

[2]The complete analysis of the exact dispersion relation will be presented in section 4.4.

In the Ostrovsky equation, δ, the parameter characterizing the earth's rotation has been assumed to be small. However, under many circumstances (for example, the evolution of internal tides as studied in Gerkema and Zimmerman [1994]), it cannot be taken to be small. Hence, we need a new mathematical model which can account for the full rotational effects. New and Pingree [2000] have developed a new KdV-type theory to model the formation of internal solitary wave from internal tides in the Bay of Biscay. They compared the observed results with the numerical results of the new KdV-type theory and obtained goood agreement between the two. In their model derivation, they claim the horizontal wave form at the zeroth order to be $A = A_0 \cos\theta$ and consequently obtained the dispersion relation

$$\omega^2 = c_0^2 + \frac{f^2}{k^2}, \tag{4.8}$$

where c_0 is the phase speed of M_2 tide and f is the Coriolis parameter. Then, they can use $\frac{\partial}{\partial t} = -c\frac{\partial}{\partial x}$ where $c^2 = c_0^2 + \frac{f^2}{k^2}$ later in their derivation. This idea might work at a very early time of evolution of internal tides; however, when internal tides break into and interact with internal solitary waves, it is invalid to assume the leading order horizontal wave form is sinusoidal. Helfrich [2007] add full rotational effects in the MCC equation and witnessed several periods of decay and return of internal solitary waves until a localized new packet emerges. However, this model is confined to two-layer fluids with a constant depth. The MCC equation is a fully nonlinear model designed for large amplitude internal waves.

4.4 Analysis of the Exact Dispersion Relation

To obtain the exact dispersion relation, we return to the fundamental governing equations of internal waves. This section has been divided into two parts with the first part presenting the derivation of the actual linear dispersion relation and the second part investigating different Taylor expansions to approximate the exact dispersion relation.

4.4.1 The Exact Dispersion Relation

The Ostrovksy equation is useful for modelling waves of intermediate k, yet fails when k takes on very small and very large values. This property is largely due to its flawed dispersion relation.

In this section, we will inspect the fully nonlinear model, from which the Ostrovsky equation was derived under an appropriate approximation, and find the actual linear dispersion relation. Therefore, we can discuss the possible approximation to the linear dispersion relation.

Recall the non-dimensional governing equations (1.27a) – (1.27c) of internal waves

$$\begin{aligned} \frac{\partial}{\partial t}\psi_{zz} - b_x &= \delta v_z + \epsilon J(\psi, \psi_{zz}) - \mu \frac{\partial}{\partial t}\psi_{xx} + \epsilon\mu J(\psi, \psi_{xx}) && \text{(4.9a)} \\ v_t + \psi_z &= \epsilon J(\psi, v) && \text{(4.9b)} \\ b_t + N^2\psi_x &= \epsilon J(\psi, b). && \text{(4.9c)} \end{aligned}$$

If we assume the fluid to be hydrostatic, the governing equations are linearized to be

$$\begin{aligned} \frac{\partial}{\partial t}\psi_{zz} - b_x &= \delta v_z && \text{(4.10a)} \\ v_t + \psi_z &= 0 && \text{(4.10b)} \\ b_t + N^2\psi_x &= 0, && \text{(4.10c)} \end{aligned}$$

which can be simplified to read

$$\frac{\partial^2}{\partial t^2}\psi_{zz} + N^2\psi_{xx} + \delta\psi_{zz} = 0. \tag{4.11}$$

Solving (4.11) by substituting a separable solution $\psi(x, z, t) = B(x, t)\phi(z)$ yields the linear Klein-Gordon equation

$$B_{tt} - c^2 B_{xx} + \delta B = 0, \tag{4.12}$$

with the dispersion relation

$$\omega^2 = c^2k^2 + \delta, \tag{4.13}$$

and if $\omega > 0$,

$$\omega = (c^2k^2 + \delta)^{\frac{1}{2}}. \tag{4.14}$$

Here the dispersion relation satisfies $\omega \to \delta^{\frac{1}{2}}$ as $k \to 0$ and $\omega \to \infty$ as $k \to \infty$. A plot of the (4.13) with selected value of c and δ is displayed in figure 4.1. Two other lines are given in order to present the asymptotic behaviour of (4.13).

From (4.13), we calculate the phase speed c_p and group velocity C_g

$$c_p = \frac{(c^2k^2 + \delta)^{\frac{1}{2}}}{k}, \qquad C_g = \frac{c^2k}{(c^2k^2 + \delta)^{\frac{1}{2}}}, \tag{4.15}$$

with limits

$$\lim_{k\to 0} c_p = \infty, \qquad \lim_{k\to 0} C_g = 0, \tag{4.16}$$

$$\lim_{k\to \infty} c_p = c, \qquad \lim_{k\to \infty} C_g = c. \tag{4.17}$$

Comparing (4.16) and (4.17) to the limit of (4.2), (4.3a)-(4.3b), we find the limits of the dispersion relation for the Ostrovsky equation are inappropriate, as concluded in section 4.3. The disagreement is largely due to the assumption of δ being small when deriving Ostrovsky equation. Notice that in obtaining (4.13), we did not treat δ as a small parameter.

4.4.2 Approximation to the Exact Dispersion Relation

We would like to factor the operator equation

$$\frac{\partial^2}{\partial t^2} - c^2 \frac{\partial^2}{\partial x^2} + \delta = 0 \tag{4.18}$$

into two first order differential operators, so as to obtain a uni-directional leading-order equation[Lee and Beardsley, 1974; Lamb, 2005]; however, it can be shown that this operator is irreducible. Instead, we turn to Taylor expansions of the dispersion relation corresponding to (4.18) to find approximation to the dispersion relation. In accordance with the approximation, we can find a differential equation.

Recall the dispersion relation characterizing waves propagating in one direction is (4.13) and can be written as

$$\omega = \left(c^2k^2 + \delta\right)^{\frac{1}{2}} = \delta^{\frac{1}{2}} \left(1 + \frac{c^2k^2}{\delta}\right)^{\frac{1}{2}}, \tag{4.19}$$

$$= ck \left(1 + \frac{\delta}{c^2k^2}\right)^{\frac{1}{2}}. \tag{4.20}$$

The purpose of writing ω as (4.19) and (4.20) is because the Taylor expansion of $(1+x)^{\frac{1}{2}}$ has restriction $|x| < 1$. Under a different choice of δ, we need to choose either (4.19) or (4.20) to Taylor expand ω. In fact, for $|\frac{c^2k^2}{\delta}| < 1$, we need (4.19) to give

$$\omega \approx \delta^{\frac{1}{2}} + \frac{c^2k^2}{2\delta^{\frac{1}{2}}}; \tag{4.21}$$

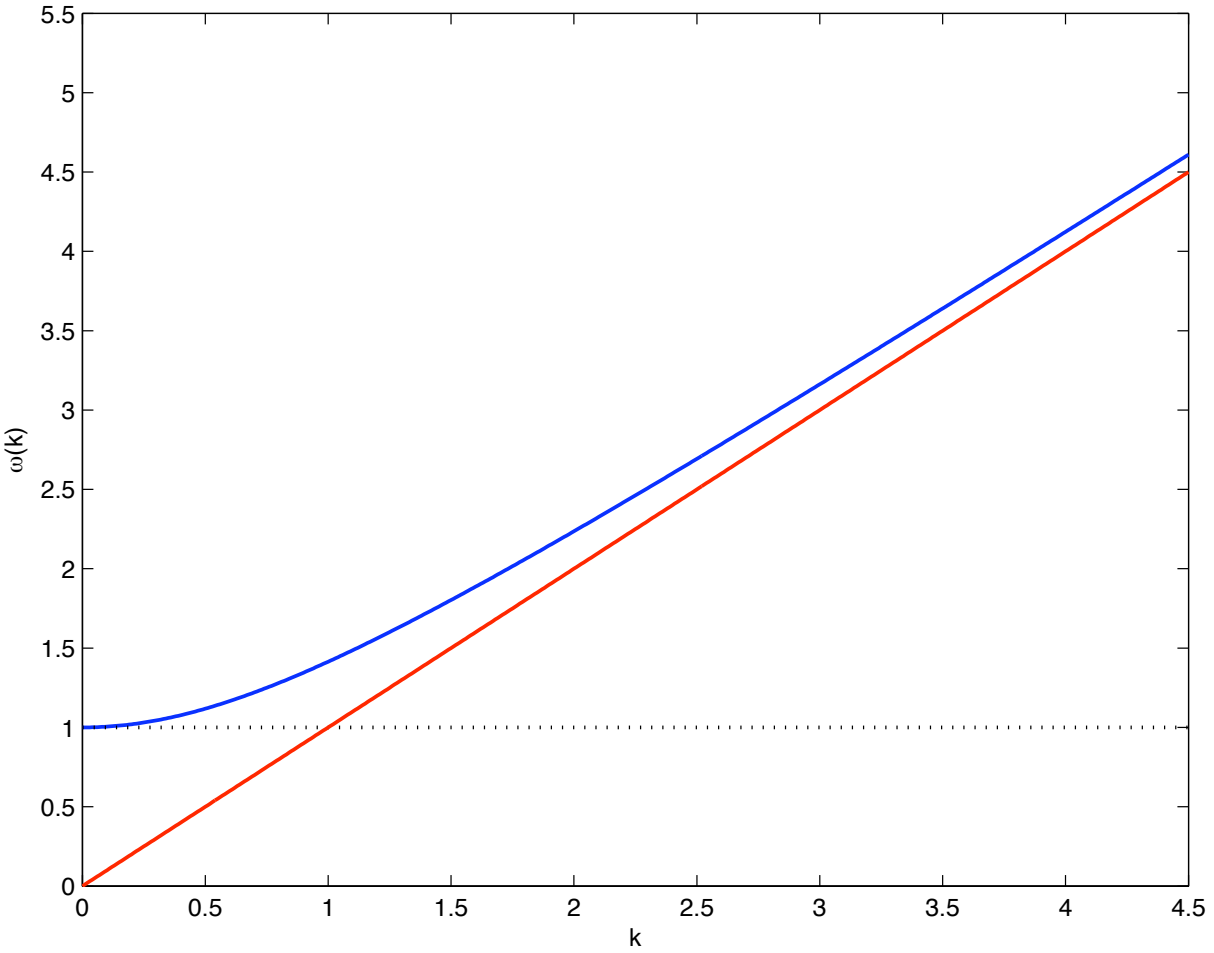

Figure 4.1: The blue line represents the plot of (4.14) with $c = 1$ and $\delta = 1$. The red line is the plot of dispersion of long wave equation: $\omega = ck$ and the dotted black line is that of inertial waves, sometimes called gyroscopic waves (Leblond and Mysak [1978], Chapter 2): $\omega = \sqrt{\delta}$, where the existence of the waves owes purely to the coriolis force. When k is very small, the dotted black line is a good approximation while when k is very large, the red line is a good approximation.

whereas for $|\frac{\delta}{c^2k^2}| < 1$, we use (4.20) to obtain

$$\omega \approx ck + \frac{\delta}{2ck}. \tag{4.22}$$

Note that when $|\frac{c^2k^2}{\delta}| < 1$ for regular solitary waves, δ usually cannot be assumed to be small, however when $|\frac{\delta}{c^2k^2}| < 1$, it is appropriate to consider δ as a small parameter.

It has already been discussed that a dispersion relation is obtained by substituting the wave form $e^{i(\vec{k}\cdot\vec{x}-\omega t)}$ into a linear differential equation. We can reverse this process to get a linear differential equation from a dispersion relation. Therefore, we find (4.21) corresponds to

$$\eta_t = -i\delta^{\frac{1}{2}}\eta + i\frac{c^2}{2\delta^{\frac{1}{2}}}\eta_{xx}, \tag{4.23}$$

and (4.22) gives

$$\eta_{xt} = -c\eta_{xx} + \frac{\delta}{2c}\eta, \tag{4.24}$$

or equivalently,

$$\eta_t = -c\eta_x + \frac{\delta}{2c}\int_{-\infty}^{x}\eta(x',t)dx', \tag{4.25}$$

which is the linearized version of Ostrovsky equation without consideration of the dispersive term η_{xxx}.

The aforementioned analysis explains why currently, in studies of the evolution of internal waves by using weakly nonlinear internal wave models, researchers tend to focus on either the generation of internal waves from internal tides, or simply the propagation of internal waves, especially that of internal solitary waves. The main reason is that in the life of internal waves, the importance of rotational effects changes, leading to big differences at times. However, the most widely used weakly nonlinear internal wave model is the Ostrovsky equation under the assumption that rotational effects are weak.

The idea of using two different mathematical equations during different stages of internal waves might work. However, the boundary of the different regimes is hard to define. The simplest example is that when internal tides break into solitary waves, internal tides actually interact with the internal solitary waves. Thus choosing the right equation is very difficult. Even if the stages are clearly separated, we still lack a model that matches all the different stages. All in all, it is desirable nowadays to have a weakly nonlinear model which is able to describe the life of internal wave.

We wonder if there is any other Taylor expansion that can merge two different cases together.

The dispersion relation in (4.19) can be also be written as

$$\begin{aligned} \omega &= (c^2k^2+\delta)^{\frac{1}{2}} && (4.26)\\ &= \left((ck+\delta^{\frac{1}{2}})^2 - 2ck\delta^{\frac{1}{2}}\right)^{\frac{1}{2}} && (4.27)\\ &= (ck+\delta^{\frac{1}{2}})\left(1-\frac{2ck\delta^{\frac{1}{2}}}{(ck+\delta^{\frac{1}{2}})^2}\right)^{\frac{1}{2}} && (4.28)\end{aligned}$$

Since $2ck\delta^{\frac{1}{2}} < (ck+\delta^{\frac{1}{2}})^2$ $(c,k,\delta>0)$, we get the Taylor expansion

$$\begin{aligned} \omega &\approx (ck+\delta^{\frac{1}{2}})\left(1-\frac{ck\delta^{\frac{1}{2}}}{(ck+\delta^{\frac{1}{2}})^2}\right) && (4.29)\\ &= (ck+\delta^{\frac{1}{2}}) - \frac{ck\delta^{\frac{1}{2}}}{ck+\delta^{\frac{1}{2}}}. && (4.30)\end{aligned}$$

It can be easily verified that as $k\to 0$, $\omega\to\delta^{\frac{1}{2}}$ and as $k\to\infty$, $\omega\to ck$. We also calculate c_p and C_g from (4.30) to be

$$\begin{aligned} c_p &= \frac{ck+\delta^{\frac{1}{2}}}{k} - \frac{c\delta^{\frac{1}{2}}}{ck+\delta^{\frac{1}{2}}}, && (4.31)\\ C_g &= c - \frac{c\delta}{(ck+\delta^{\frac{1}{2}})^2}, && (4.32)\end{aligned}$$

with $c_p\to\infty$, $C_g\to 0$ as $k\to 0$, and $c_p\to c$, $C_g\to c$ as $k\to\infty$. If we compare these limits with those of the actual linear dispersion given by (4.16)– (4.17) , we find that (4.30) is a very good approximation to (4.13)

The DE counterpart of this dispersion relation is

$$c\eta_{tx} + i\delta^{\frac{1}{2}}\eta_t = -c^2\eta_{xx} + \delta\eta - ic\delta^{\frac{1}{2}}\eta_x. \tag{4.33}$$

Notably, when $k\to 0$, ω can be approximated by just the first term in equation (4.30), so the DE counterpart is

$$\eta_t = -c\eta_x - i\delta^{\frac{1}{2}}\eta. \tag{4.34}$$

This DE is very interesting since it is the combination of equation (4.23) and (4.25). Also, (4.33) has imaginary coefficients for some terms as does the Nonlinear Schrödinger equation.

If we want to use (4.33) as the linearized equation of KdV-type equation, we might need to be innovative enough to explore KdV-type equation in a complex domain.

Overall, the exact dispersion relation (4.13) solves the linear Klein-Gordon equation (4.12) with the usual wave form $e^{i(kx-\omega t)}$. Both the dispersion relation and the linear Klein-Gordon equation are irreducible, leading to the difficulty of obtaining a first order DE to describe unidirectional wave propagation. However, the method of Taylor expansion provides us with different approximations of the exact dispersion relation, with which, we can find the approximate DE to the linear Klein Gordon equation. The dispersion relation of the Ostrovsky equation is a valid approximation when rotational effects are small. And a new proposed approximation given by (4.30) is effective in predicting the limits of the exact dispersion relation, thus potentially being a better approximation than that of the Ostrovsky equation. However, we need to bring KdV-type equations into the the world of complex functions and values to make use of this new dispersion relation.

4.5 A New RMKdV Equation

This section presents the derivation details of a new RMKdV equation, aiming to correct the flawed dispersion relation of the Ostrovsky equation. After the derivation, section 4.5.2 gives an analysis of this new RMKdV equation, the dispersion relation of which has been compared with most of the aforementioned dispersion relations. This comparison informs us of the advantages of the new RMKdV. In section 4.5.3 and 4.5.4, we talk about the shoaling effect as well as adding the shoaling effect to this new RMKdV equation to model wave motion in an inhomogenous fluid.

4.5.1 Derivation of the New RMKdV Equation

Again, the system of governing equations given by (1.27a) - (1.27c) is

$$\frac{\partial}{\partial t}\psi_{zz} - b_x = \delta v_z + \epsilon J\left(\psi, \psi_{zz}\right) - \mu\frac{\partial}{\partial t}\psi_{xx} + \epsilon\mu J\left(\psi, \psi_{xx}\right), \tag{4.35}$$

$$v_t + \psi_z = \epsilon J(\psi, v), \tag{4.36}$$

$$b_t + N^2\psi_x = \epsilon J(\psi, b), \tag{4.37}$$

with its asymptotic solution in perturbed form

$$\begin{aligned}
\psi &= \psi^{(0,0,0)} + \delta\psi^{(1,0,0)} + \epsilon\psi^{(0,1,0)} + \mu\psi^{(0,0,1)} + \epsilon^2\psi^{(0,2,0)} + \mathrm{O}(\epsilon^3, \delta^2, \mu^2), && (4.38)\\
v &= v^{(0,0,0)} + \delta v^{(1,0,0)} + \epsilon v^{(0,1,0)} + \mu v^{(0,0,1)} + \epsilon^2 v^{(0,2,0)} + \mathrm{O}(\epsilon^3, \delta^2, \mu^2), && (4.39)\\
b &= b^{(0,0,0)} + \delta b^{(1,0,0)} + \epsilon b^{(0,1,0)} + \mu b^{(0,0,1)} + \epsilon^2 b^{(0,2,0)} + \mathrm{O}(\epsilon^3, \delta^2, \mu^2). && (4.40)
\end{aligned}$$

The leading-order system of equations is

$$\begin{aligned}
\frac{\partial}{\partial t}\psi_{zz}^{(0,0,0)} - b_x^{(0,0,0)} &= 0, && (4.41)\\
v_t^{(0,0,0)} + \psi_z^{(0,0,0)} &= 0, && (4.42)\\
b_t^{(0,0,0)} + N^2\psi_x^{(0,0,0)} &= 0, && (4.43)
\end{aligned}$$

with (4.41) and (4.43) leading to

$$\frac{\partial^2}{\partial t^2}\psi_{zz}^{(0,0,0)} + N^2\psi_{xx}^{(0,0,0)} = 0. \tag{4.44}$$

Looking for separable solution of $\psi^{(0,0,0)} = B(x,t)\phi(z)$, we have

$$B_{tt} - c^2 B_{xx} = 0, \tag{4.45}$$

and the eigenvalue problem

$$\begin{aligned}
\phi_{zz} + \frac{N^2(z)}{c^2}\phi &= 0,\\
\phi(-1) = \phi(0) &= 0. && (4.46)
\end{aligned}$$

At $\mathrm{O}(\delta)$, if we perturb (4.45) as

$$B_{tt} - c^2 B_{xx} = \delta P(x,t), \tag{4.47}$$

and put the effect of ϵ and μ aside, we can simplify the governing equation (4.35) – (4.37) to read

$$\begin{aligned}
\frac{\partial}{\partial t}\psi_{zz} - b_x &= \delta v_z, && (4.48)\\
v_t + \psi_z &= 0, && (4.49)\\
b_t + N^2\psi_x &= 0, && (4.50)
\end{aligned}$$

which can be combined into

$$\frac{\partial^2}{\partial t^2}\psi_{zz} + N^2(z)\psi_{xx} = -\delta\psi_{zz}. \tag{4.51}$$

Taking the perturbation expressed by (4.47) into account, we obtain

$$\begin{aligned} \frac{\partial^2}{\partial t^2}\psi_{zz}^{(1,0,0)} + N^2(z)\psi_{xx}^{(1,0,0)} &= -\psi_{zz}^{(0,0,0)} - \left[\frac{\partial^2}{\partial t^2}\psi_{zz}^{(0,0,0)} + N^2(z)\psi_{xx}^{(0,0,0)}\right]_{\delta \text{ coefficient}} & (4.52)\\ &= -B\phi'' - P(x,t)\phi'', & (4.53) \end{aligned}$$

where we use $[A]_{\delta \text{ coefficient}}$ to describe the coefficient of the mathematical expression A. Later in this section, we will use this symbol to extract out the coefficient of ϵ, ϵ^2 and μ. To get a separable solution for this equation, we assume

$$P(x,t) = \gamma B(x,t) \tag{4.54}$$

and that

$$\psi^{(1,0,0)} = B^{(1,0,0)}(x,t)\phi^{(1,0,0)}, \tag{4.55}$$

hence turning (4.53) into

$$B_{tt}^{(1,0,0)}\phi_{zz}^{(1,0,0)} + N^2(z)B_{xx}^{(1,0,0)}\phi^{(1,0,0)} = -(1+\gamma)B\phi''. \tag{4.56}$$

Since

$$B_{tt}^{(1,0,0)} = c^2 B_{xx}^{(1,0,0)}, \tag{4.57}$$

to leading-order, (4.53) can be approximated by

$$B_{xx}^{(1,0,0)}(\phi_{zz}^{(1,0,0)} + \frac{N^2(z)}{c^2}\phi^{(1,0,0)}) = -\frac{1+\gamma}{c^2}B\phi''. \tag{4.58}$$

Choosing $B_{xx}^{(1,0,0)} = B$ leaves

$$\phi_{zz}^{(1,0,0)} + \frac{N^2}{c^2}\phi^{(1,0,0)} = -\frac{1+\gamma}{c^2}\phi''. \tag{4.59}$$

In order to solve for the two unknowns $B^{(1,0,0)}$ and $\phi^{(1,0,0)}$ in (4.58), we need to satisfy a solvability condition. Note that in the solution of the different higher-order problems, we will repeatedly use this solvability condition. We define the linear operator ℓ by

$$\ell = \frac{\partial^2}{\partial z^2} + \frac{N(z)^2}{c^2}. \tag{4.60}$$

It can be shown that ℓ is a self-adjoint operator as follows

$$\int_{-1}^{0}(\phi_{zz}^{(1,0,0)}+\frac{N^2}{c^2}\phi^{(1,0,0)})\phi dz = \int_{-1}^{0}\phi_{zz}^{(1,0,0)}\phi dz+\int_{-1}^{0}\frac{N^2}{c^2}\phi^{(1,0,0)}\phi dz \tag{4.61}$$

$$= \int_{-1}^{0}(\phi''+\frac{N^2}{c^2}\phi)\phi^{(1,0,0)}dz, \tag{4.62}$$

which is obtained by integrating by parts while applying the boundary condition that $\phi = \phi^{(1,0,0)} = 0$ at $z = 0$ and $z = -1$. Then with the leading-order eigenvalue equation (4.46), we have

$$\int_{-1}^{0}\ell(f(z))\phi dz = 0, \qquad \forall \quad f(x)\in C^2[-1,0] \quad \text{and} \quad f(-1)=f(0)=0. \tag{4.63}$$

Equation (4.63) is called the *solvability condition* for the eigenvalue problem (4.59).

The application of this solvability condition to (4.59) gives

$$\int_{-1}^{0}\frac{1+\gamma}{c^2}\phi''\phi dz = 0, \tag{4.64}$$

and hence

$$\gamma = -1, \tag{4.65}$$

because

$$\int_{-1}^{0}\phi\phi''dz = -\int_{-1}^{0}\phi'^2dz \neq 0. \tag{4.66}$$

Thus (4.47) becomes

$$B_{tt}-c^2B_{xx} = -\delta B. \tag{4.67}$$

The constants ϵ and μ are important for small perturbations too, taking the nonlinearity (ϵ) and non-hydrostaticity (μ) into account, we expand (4.47) into

$$B_{tt}-c^2B_{xx} = -\delta B+\epsilon R(x,t)+\mu Q(x,t)+\epsilon^2 S(x,t). \tag{4.68}$$

Notice here, (4.36) does not affect the governing equation at O($\epsilon, \epsilon^2, \mu$), so we do not need to list (4.36) and its derived form at O($\epsilon, \epsilon^2, \mu$).

At $O(\epsilon)$, the governing equation is then

$$\frac{\partial}{\partial t}\psi_{zz}^{(0,1,0)} - b_x^{(0,1,0)} = J\left(\psi^{(0,0,0)}, \psi_{zz}^{(0,0,0)}\right) - \left[\frac{\partial}{\partial t}\psi_{zz}^{(0,0,0)} - b_x^{(0,0,0)}\right]_{\epsilon \text{ coefficient}}, \quad (4.69)$$

$$b_t^{(0,1,0)} + N^2\psi_x^{(0,1,0)} = J\left(\psi^{0,0,0}, b^{(0,0,0)}\right) - \left[b_t^{(0,0,0)} + N^2\psi_x^{(0,0,0)}\right]_{\epsilon \text{ coefficient}}, \quad (4.70)$$

leading to

$$\frac{\partial^2}{\partial t^2}\psi_{zz}^{(0,1,0)} + N^2(z)\psi_{xx}^{(0,1,0)} = \frac{\partial}{\partial t}J\left(\psi^{(0,0,0)}, \psi_{zz}^{(0,0,0)}\right) + \frac{\partial}{\partial x}J\left(\psi^{(0,0,0)}, b^{(0,0,0)}\right) \quad (4.71)$$

$$- \left[\frac{\partial^2}{\partial t^2}\psi_{zz}^{(0,0,0)} + N^2(z)\psi_{xx}^{(0,0,0)}\right]_{\epsilon \text{ coefficient}}. \quad (4.72)$$

In order to carry out the algebra from the asymptotic analysis, we need an explicit form for $b^{(0,0,0)}$. In (4.43), ψ has a separable form, which drives us to assume

$$b^{(0,0,0)} = H(x,t)N^2(z)\phi. \quad (4.73)$$

Substituting this form of $b^{(0,0,0)}$ into (4.43), we obtain $H_t = -B_x$. We want to find a relation between B_t and B_x to express H in terms of B.

Recall that (4.45) gives $B_t = -cB_x$ if we only consider waves propagating rightward[3], so

$$H_t = -B_x = \frac{1}{c}B_t. \quad (4.74)$$

Given appropriate initial conditions, we get

$$H(x,t) = \frac{B(x,t)}{c}. \quad (4.75)$$

Substituting H back into $b^{(0,0,0)}$ leads to

$$b^{(0,0,0)} = \frac{B(x,t)N^2(z)\phi}{c} = -cB(x,t)\phi''. \quad (4.76)$$

With the explicit form of $b^{(0,0,0)}$, (4.72) becomes

$$\frac{\partial^2}{\partial t^2}\psi_{zz}^{(0,1,0)} + N^2(z)\psi_{xx}^{(0,1,0)} = \left(\frac{\partial}{\partial t}(BB_x) - c\frac{\partial}{\partial x}(BB_x)\right)(\phi\phi''' - \phi'\phi'') - R(x,t)\phi''$$

$$= -2c\frac{\partial}{\partial x}(BB_x)(\phi\phi''' - \phi'\phi'') - R(x,t)\phi''. \quad (4.77)$$

[3]Note we can also separately consider waves propagating leftward, but the result will not be affected dramatically.

Looking for a separable solutions for $\psi^{(0,1,0)}$, we let

$$R(x,t) = \alpha(BB_x)_x, \tag{4.78}$$

and

$$\psi^{(0,1,0)} = B^{(0,1,0)}(x,t)\phi^{(0,1,0)}. \tag{4.79}$$

If we assume that

$$B_{tt}^{(0,1,0)} = c^2 B_{xx}^{(0,1,0)}, \tag{4.80}$$

and

$$B_{xx}^{(0,1,0)} = \frac{\partial}{\partial x}BB_x = \frac{1}{2}\frac{\partial^2}{\partial x^2}B^2, \tag{4.81}$$

so

$$B^{(0,1,0)} = \frac{1}{2}B^2, \tag{4.82}$$

we then obtain

$$2c^2\left(\phi_{zz}^{(0,1,0)} + \frac{N^2}{c^2}\phi^{(0,1,0)}\right) = -2c(\phi\phi''' - \phi'\phi'') - \alpha\phi''. \tag{4.83}$$

This eigenvalue problem contains the self-adjoint operator ℓ. By applying the solvability condition as we have done in the algebra of O(δ), we obtain

$$\alpha = \frac{3c\int_{-1}^{0}\phi'^3 dz}{\int_{-1}^{0}\phi'^2 dz}. \tag{4.84}$$

At $O(\mu)$, we can find the expression of $Q(x,t)$ as well. The governing equations at this order are

$$\frac{\partial}{\partial t}\psi_{zz}^{(0,0,1)} - b_x^{(0,0,1)} = -\frac{\partial}{\partial t}\psi_{xx}^{(0,0,0)} - \left[\frac{\partial}{\partial t}\psi_{zz}^{(0,0,0)} - b_x^{(0,0,0)}\right]_{\mu \text{ coefficient}} \tag{4.85}$$

$$b_t^{(0,0,1)} + N^2\psi_x^{(0,0,1)} = -\left[b_t^{(0,0,0)} + N^2\psi_x^{(0,0,0)}\right]_{\mu \text{ coefficient}}, \tag{4.86}$$

which can be reduced to

$$\begin{aligned}\frac{\partial^2}{\partial t^2}\psi_{zz}^{(0,0,1)} + N^2(z)\psi_{xx}^{(0,0,1)} &= -\frac{\partial^2}{\partial t^2}\psi_{xx}^{(0,0,0)} - \left[\frac{\partial^2}{\partial t^2}\psi_{zz}^{(0,0,0)} + N^2(z)\psi_{xx}^{(0,0,0)}\right]_{\mu \text{ coefficient}} \\ &= -B_{ttxx}\phi - Q(x,t)\phi''. \end{aligned} \tag{4.87}$$

As we have done for previous orders, to find separable solutions, we set

$$Q(x,t) = \beta B_{ttxx} \tag{4.88}$$

and

$$\psi^{(0,0,1)} = B^{(0,0,1)}\phi^{(0,0,1)}, \tag{4.89}$$

with

$$B^{(0,0,1)} = c^2 B_{xx}, \tag{4.90}$$

then, (4.87) produces the equation

$$c^2(\phi_{zz}^{(0,0,1)} + N^2(z)\phi^{(0,0,1)}) = -(\phi - \beta\phi''). \tag{4.91}$$

The solvability condition of this type of eigenvalue problem leads to

$$\beta = -\frac{\int_{-1}^{0}\phi^2 dz}{\int_{-1}^{0}\phi'^2 dz}. \tag{4.92}$$

There are many cases when the nonlinear term vanishes and we need the cubic nonlinear term [Grimshaw et al., 2004; Holloway, 2002]. So, the following work is to present the steps that we follow in order to derive the cubic terms.

We now have

$$\psi = B\phi + \epsilon B^2\phi^{(0,1,0)} + \epsilon^2\psi^{(0,2,0)} + \cdots, \tag{4.93}$$

$$b = -cB\phi'' + \epsilon B^2 D^{(0,1,0)} + \epsilon^2 b^{(0,2,0)} + \cdots. \tag{4.94}$$

At $O(\epsilon^2)$, the system of governing equations is then

$$\begin{aligned}
(B_t\phi'' &+ cB_x\phi'') + \epsilon(2BB_t\phi_{zz}^{(0,1,0)} - 2BB_xD^{(0,1,0)}) + \epsilon^2\left(\frac{\partial}{\partial t}\psi_{zz}^{(0,2,0)} - b_x^{(0,2,0)}\right)\\
&= \epsilon J(B\phi, B\phi'') + \epsilon^2 J(B\phi, B^2\phi_{zz}^{(0,1,0)}) + \epsilon^2 J(B^2\phi^{(0,1,0)}, B\phi'')\\
(-cB_t\phi'' &+ N^2B_x\phi) + \epsilon(2BB_tD^{(0,1,0)} + 2BB_xN^2\phi^{(0,1,0)}) + \epsilon^2(b_t^{(0,2,0)} + N^2\psi_x^{(0,2,0)})\\
&= \epsilon J(B\phi, -cB\phi'') + \epsilon^2 J(B^2\phi^{(0,1,0)}, -cB\phi'') + \epsilon^2 J(B\phi, B^2D^{(0,1,0)})
\end{aligned}$$

which can be simplified as

$$\begin{aligned}\frac{\partial^2}{\partial t^2}\psi_{zz}^{(0,2,0)} + N^2(z)\psi_{xx}^{(0,2,0)} &= \aleph + \frac{\partial}{\partial t}J(B\phi, B^2\phi^{(0,1,0)}) + \frac{\partial}{\partial t}J(B^2\phi^{(0,1,0)}, B\phi'') \\ &+ \frac{\partial}{\partial x}J(B^2\phi^{(0,1,0)}, -cB\phi'') + \frac{\partial}{\partial x}J(B\phi, B^2D^{(0,1,0)}),\end{aligned}$$

where

$$\begin{aligned}\aleph &= [\underbrace{-(B_{tt}\phi'' + N^2B_{xx}\phi)}_{①}\underbrace{-\epsilon(2(BB_t)_t\phi_{zz}^{(0,1,0)} + 2(BB_x)_xN^2\phi^{(01,0)})}_{②} \\ &+ \underbrace{\epsilon\frac{\partial}{\partial t}J(B\phi, B\phi'') + \epsilon\frac{\partial}{\partial x}J(B\phi, -cB\phi'')}_{③}]_{\epsilon^2 \text{ coefficient}}. \end{aligned} \tag{4.95}$$

Before obtaining a closed-form expression of $\aleph$, recall the eigenvalue problem (4.83) from $O(\epsilon)$

$$2c^2(\phi_{zz}^{(0,1,0)} + \frac{N^2}{c^2}\phi^{(01,0)}) = -2c(\phi\phi''' - \phi'\phi'') - \alpha\phi'', \tag{4.96}$$

and the governing equation for B is

$$B_{tt} - c^2B_{xx} = -\delta B + \epsilon R(x,t) + \mu Q(x,t) + \epsilon^2 S(x,t), \tag{4.97}$$

where $R(x,t)$ and $Q(x,t)$ and $S(x,t)$ are higher order corrections. To simplify the problem, we restrict our consideration to the rightward propogating wave. The unidirectional KdV equation is then from Lamb and Yan [1996] and given by

$$B_t = -cB_x + \epsilon 2r_{10}cBB_x. \tag{4.98}$$

Because the O(ϵ) result contributes to a higher order O(ϵ^2), we need to include the nonlinear term in (4.98).

In (4.95), the equation has been divided into three parts (refer to appendix B for details on the derivation of ② and ③)

$$\begin{aligned}① &= -\epsilon\left[\alpha(BB_x)_x + \epsilon S(x,t)\right]\phi'' \\ ② &= -\epsilon\left[(2c^2(BB_x)_x - 4c^2\epsilon r_{10}(B^2B_x)_t + 4\epsilon r_{10}c(B^2B_x)_t)\phi_{zz}^{(0,1,0)} + 2(BB_x)_xN^2\phi^{(0,1,0)}\right] \\ &= -\epsilon\left[2c^2(BB_x)_x\left(\phi_{zz}^{(0,1,0)} + \frac{N^2}{c^2}\phi^{(0,1,0)}\right) + \epsilon(-4c^2r_{10}(B^2B_x)_x + 4r_{10}c(B^2B_x)_t)\phi_{zz}^{(0,1,0)}\right] \\ ③ &= \epsilon\left[((BB_x)_t - c(BB_x)_x(\phi\phi''' - \phi'\phi'')\right] \\ &= \epsilon\left[(-2c(BB_x))_x - 2\epsilon r_{10}c(B^2B_x)_x)(\phi\phi''' - \phi'\phi'')\right],\end{aligned}$$

so

$$\begin{aligned}
\aleph &= [\epsilon((BB_x)_x\left(-2c^2(\phi^{(0,1,0)}_{zz}+\frac{N^2}{c^2}\phi^{(01,0)}_{zz}\right)-2c(\phi\phi'''-\phi'\phi'')-\alpha\phi'')) \\
&+ \epsilon^2(-S(x,t)\phi''-(-4c^2r_{10}(B^2B_x)_x+4r_{10}c(B^2B_x)_t)\phi^{(0,1,0)}_{zz} \\
&- 2r_{10}c(B^2B_x)_x(\phi\phi'''-\phi'\phi''))]_{\epsilon^2 \text{ coefficient}} \\
&= -S(x,t)\phi''+4r_{10}c^2(B^2B_x)_x-4r_{10}c(B^2B_x)_t-2r_{10}c(B^2B_x)_x(\phi\phi'''-\phi'\phi''))
\end{aligned}$$

Note that we still have not yet got an expression for $D^{(0,1,0)}$. In order to find it, we refer back to (4.72) to relate $\psi^{(0,1,0)}$ and $b^{(0,1,0)}$. From the O(ϵ) derivation, we have

$$\psi^{(0,1,0)} = B^{(0,1,0)}\phi^{(0,1,0)} = B^2\phi^{(0,1,0)}, \tag{4.99}$$

where $\phi^{(0,1,0)}$ is the solution of

$$\phi^{(0,1,0)}_{zz}+\frac{N^2}{c^2}\phi^{(0,1,0)} = -\frac{1}{c}(\phi\phi'''-\phi'\phi'')-\frac{\alpha}{2c^2}\phi''. \tag{4.100}$$

To calculate $b^{(0,1,0)}$, we refer back to (4.69)

$$\frac{\partial}{\partial t}\psi^{(0,1,0)}_{zz}-b^{(0,1,0)}_x = J(\psi^{(0,0,0)},\psi^{(0,0,0)}_{zz})-\left[\frac{\partial}{\partial t}\psi^{(0,0,0)}_{zz}-b^{(0,0,0)}_x\right]_{\epsilon \text{ coefficient}}, \tag{4.101}$$

where

$$\begin{aligned}
b^{(0,1,0)}_x &= 2BB_t\phi^{(0,1,0)}_{zz}-BB_x(\phi\phi'''-\phi'\phi'')+\left[\frac{\partial}{\partial t}\psi^{(0,0,0)}_{zz}-b^{(0,0,0)}_x\right]_{\epsilon \text{ coefficient}} \\
&= -2cBB_x\phi^{(0,1,0)}_{zz}-BB_x(\phi\phi'''-\phi'\phi'')+2r_{10}cBB_x\phi'' \qquad (4.102)\\
&= BB_x[-2c\phi^{(0,1,0)}-(\phi\phi'''-\phi'\phi'')+2r_{10}c\phi'']. \qquad (4.103)
\end{aligned}$$

Here we have used (4.98). Assuming $b^{(0,1,0)} = B^2D^{(0,1,0)}$, we have

$$D^{(0,1,0)} = \frac{1}{2}[-2c\phi^{(0,1,0)}_{zz}-(\phi\phi'''-\phi'\phi'')+2r_{10}c\phi'']. \tag{4.104}$$

Now, (4.95) becomes

$$\begin{aligned}\frac{\partial^2}{\partial t^2}\psi_{zz}^{(0,2,0)} + N^2(z)\psi_{xx}^{(0,2,0)} &= (B^2B_x)_t(\phi\phi_{zzz}^{(0,1,0)} - 2\phi'\phi_{zz}^{(0,1,0)}) \\ &+ (B^2B_x)_t(2\phi^{(0,1,0)}\phi''' - \phi_z^{(0,1,0)}\phi'') \\ &+ c(B^2B_x)_x(\phi_z^{(0,1,0)}\phi'' - 2\phi^{(0,1,0)}\phi''') \\ &+ (B^2B_x)_x(\phi D_z^{(0,1,0)} - 2\phi' D^{(0,1,0)}) \\ &- S(x,t)\phi'' + (4r_{10}c^2(B^2B_x)_x - 4r_{10}c(B^2B_x)_t)\phi_{zz}^{(0,1,0)} \\ &- 2r_{10}c(B^2B_x)_x(\phi\phi''' - \phi'\phi''). \end{aligned} \tag{4.105}$$

Since to the leading order $(B^2B_x)_t = -c(B^2B_x)_x$, we let

$$S(x,t) = \lambda(B^2B_x)_x, \qquad \text{and} \qquad \psi^{(0,2,0)} = B^3\phi^{(0,2,0)}, \tag{4.106}$$

then (4.105) becomes

$$\begin{aligned}\phi_{zz}^{(0,2,0)} + \frac{N^2}{c^2}\phi^{(0,2,0)} &= -\frac{1}{3c}(\phi\phi_{zzz}^{(0,1,0)} - 2\phi'\phi_{zz}^{(0,1,0)}) - \frac{1}{3c}(2\phi^{(0,1,0)}\phi''' - \phi_z^{(0,1,0)}\phi'') \\ &+ \frac{1}{3c}(\phi_z^{(0,1,0)}\phi'' - 2\phi^{(0,1,0)}\phi''') + \frac{1}{3c^2}(\phi D_z^{(0,1,0)} - 2\phi' D^{(0,1,0)}) \\ &- \lambda\phi'' + \frac{8}{3}r_{10}\phi_{zz}^{(0,1,0)} - \frac{2}{3c}r_{10}(\phi\phi''' - \phi'\phi''). \end{aligned} \tag{4.107}$$

We can then use the solvability condition of (4.107) to obtain the expression of λ.

To sum up, the equation for B with the higher order corrections is

$$B_{tt} - c^2B_{xx} = -\delta B + \alpha\epsilon(BB_x)_x + \beta\mu B_{ttxx} + \epsilon^2\lambda(B^2B_x)_x, \tag{4.108a}$$

$$\text{subject to} \qquad \alpha = \frac{3c\int_{-1}^0 \phi'^3 dz}{\int_{-1}^0 \phi'^2 dz}, \quad \text{and} \quad \beta = -\frac{\int_{-1}^0 \phi^2 dz}{\int_{-1}^0 \phi'^2 dz}. \tag{4.108b}$$

4.5.2 Analysis of the New RMKdV Equation

The new rotation modified KdV equation given by (4.108a) – (4.108b) has advantages over the Ostrovsky equation in that we have not violated the asymptotic properties of the exact dispersion relation for a very small k for the new equation. If we use the leading-order governing equation $B_t = -cB_x$ to approximate the RHS in (4.108a), the linearized evolution equation is

$$B_{tt} - c^2B_{xx} = -\delta B + \beta\mu B_{ttxx}, \tag{4.109}$$

with dispersion relation

$$\omega^2 = \frac{c^2k^2 + \delta}{\beta\mu k^2 + 1}. \tag{4.110}$$

In the limit as $k \to 0$, we have $\omega \to \delta^{\frac{1}{2}}$. The phase speed ($c_p$) and group velocity ($C_g$) are then

$$c_p = \left(\frac{c^2k^2 + \delta}{k^2(\beta\mu k^2 + 1)}\right)^{\frac{1}{2}}, \tag{4.111a}$$

$$C_g = \frac{c^2k - \beta\mu\delta k}{(c^2k^2 + \delta)^{\frac{1}{2}}\,(\beta\mu k^2 + 1)^{\frac{3}{2}}}, \tag{4.111b}$$

with $c_p \to \infty$, $C_g \to 0$ as $k \to 0$. The asymptotic behaviour of ω, c_p and C_g as $k \to 0$ agrees well with that predicted by the exact dispersion relation; yet upon analysing, we will find that the limits as $k \to \infty$ are not as desired. However, this new RMKdV equation would work well to model internal wave ranging with large wavelength to moderate wavelength, which is common in an oceanic environment.

Numerical simulations of (4.108a) – (4.108b) do not have as rigid a restriction on the initial condition as the Ostrovsky equation explained in section 4.3. However, in the derivation of this equation, we have assumed wave is propagating rightward and so we need to choose appropriate initial conditions to satisfy this assumption. Note that since the DE (4.108a) is second order, we need two initial conditions for the numerical simulation.

4.5.3 On Shoaling Effects

In deriving the modified KdV equation, it is necessary to assume the homogeneity of the fluid. If the waves experience shoaling, we usually assume the fluid depth is slowly varying. Shoaling waves are waves that propagate from deep water to shallow water. This phenomenon is essential in many coastal areas such as the Massachusetts Bay and the Bay of Biscay. Research with regard to shoaling can be found in Djordjevic and Redekopp [1978]; Small [2001]; Small and Hornby [2004].

In Small [2001] and Pelinovsky et al. [1994], an energy flux conservation law along ray tubes was used to derive the shoaling term.The energy flux along a ray tube is

$$F = \Delta \int_{-H(x)}^{0} pu dz, \tag{4.112}$$

where Δ is the wave front length, p is the pressure, u is the horizontal velocity and the water depth $H(x)$ is a slowly varying function of x.

Since the change in the background environment is assumed to be slow compared to the typical wave length scale, we can use the linear pressure and velocity

$$p = \rho B c^2 \frac{\partial \phi}{\partial z}, \qquad u = cB\frac{\partial \phi}{\partial z}, \tag{4.113}$$

and hence

$$F = \Delta \int_{-H(x)}^{0} \rho c^3 B^2 \left(\frac{\partial \phi}{\partial z}\right)^2 dz. \tag{4.114}$$

Energy flux is conserved along the ray tubes, so $\frac{\partial F}{\partial x} = 0$. In fact,

$$\frac{\partial F}{\partial x} = \Delta_x B^2 \int_H^0 \rho c^3 \left(\frac{\partial \phi}{\partial z}\right)^2 dz + 2\Delta B B_x \int_{-H}^0 \rho c^3 \left(\frac{\partial \phi}{\partial z}\right)^2 dz + \Delta B^2 \frac{\partial M}{\partial x}, \tag{4.115a}$$

where

$$M = \int_{-H}^{0} \rho c^3 \left(\frac{\partial \phi}{\partial z}\right)^2 dz, \tag{4.116}$$

and

$$\frac{\partial M}{\partial x} = \int_{-H}^{0} \frac{\partial}{\partial x}\left(\rho c^3 \left(\frac{\partial \phi}{\partial z}\right)^2\right) dz + H_x \left(\Delta \rho c^3 \left(\frac{\partial \phi}{\partial x}\right)\right)|_{z=H(z)}. \tag{4.117}$$

By equating (4.115a) to 0, we obtain

$$B_x = -\frac{1}{2}\left(\frac{\Delta_x}{\Delta} B\right) - \frac{1}{2}\left(\frac{M_x}{M} B\right). \tag{4.118}$$

This equation does not reveal any information about B, but as in the KdV family equations, we are interested in knowing B_t, or sometimes B_{tt}. Therefore, we need to dig out the equation by making some approximations

$$B_x = \frac{\partial B}{\partial t}\frac{\delta t}{\delta x} = \frac{B_t}{\frac{\delta x}{\delta t}}. \tag{4.119}$$

To the leading order, $\frac{\delta x}{\delta t} = c$, so

$$B_t = -\frac{c}{2}\left(\frac{\Delta_x}{\Delta} B\right) - \frac{c}{2}\left(\frac{M_x}{M} B\right), \tag{4.120}$$

and

$$B_{tt} = -\frac{c^2}{2}\left(\frac{\Delta_x}{\Delta} B_x\right) - \frac{c^2}{2}\left(\frac{M_x}{M} B_x\right) \tag{4.121}$$

is the leading order equation that describes the shoaling effect.

4.5.4 Variable Coefficient RMKdV Equation

By coupling the result of the RMKdV equation with the shoaling effect, we will have the Ve-RMKdV equation

$$B_{tt} = c^2 B_{xx} - \delta B + \epsilon\alpha(BB_x)_x + \mu\beta B_{ttxx} + \epsilon^2\lambda(B^2 B_x)_x - \frac{c^2}{2}\left(\frac{M_x}{M}B_x\right). \tag{4.122}$$

Note here, we only use one of the two terms in (4.121) since the model we are trying to build up is 2D, hence Δ_x is zero. In (4.122), the coefficients are slowly varying functions of x instead of constants.

CHAPTER 5

CONCLUSION

5.1 Summary

The effects of the earth's rotation on internal waves has been discussed in this thesis with respect to two topics of nonlinear internal wave theory: near-resonant triads and weakly nonlinear models.

The near-resonant internal wave triad phenomenon in this thesis was firstly observed among three waves in two plots (figure 3.2 and 3.3) of the decomposition of horizontal velocity of internal waves generated by tide-topography interaction. The same phenomenon was obtained from a simpler numerical run where internal waves were generated by forcing waves directly at the left boundary. The three waves: the harmonic 1 – mode 1, the harmonic 2 – mode 2 and the harmonic 1 – mode 3 wave formed an internal wave triad and were found to satisfy the near-resonance condition when either the detuning of the frequency or the wavenumber are sufficiently small. The main results of the near-resonant theory were demonstrated by a system of six PDEs, which, with hydrostatic ($\mu = 0$) and non-rotating ($f = 0$) assumptions, can be converted into the canonical wave amplitude equations of exact resonant triads.

Numerical runs with different parameters (buoyancy frequency N, the Coriolis force f and the forcing amplitude F_a) have been done and their results have been summarized in table 3.3. When the model is not sufficiently nonlinear, the near-resonant phenomenon disappears, since resonance and near-resonance are from nonlinear wave interaction. On the other hand, when the nonlinearity parameter of the model is very large, the derived near-resonant internal wave triad theory does not apply since resonant and near-resonant theories are weakly-nonlinear theories

based on the assumption that the wave amplitude is not too large. When the model can be treated as weakly-nonlinear, near-resonant theory is very effective in predicting the wave form of the internal wave triad.

Furthermore, when the rotational effect is included (f is nonzero), we find that the mode-2 waves have a low-frequency front. By analysing the mechanism and applying parametric subharmonic instability (PSI) theory, we find that the front long wave is the product of an exact resonant triad.

The rotational effects of weakly-nonlinear models were first studied by Ostrovsky. The resulting equation he developed became the first KdV-type equation taking the earth's rotation into account. This equation is used for a uni-directional wave model and is most successful when the wavenumber is moderate. However, the Ostrovsky equation fails to model waves with small wavenumber due to its imperfect dispersion relation. This thesis, in its second part, gives an analysis of the exact dispersion relation for fully nonlinear internal wave governing equations and provides a derivation of a new rotational modified equation whose dispersion relation has some nice properties and obeys the exact dispersion relation for waves with both small and moderate wavenumbers.

5.2 Conclusion

The near-resonant internal wave triad theory is mainly embodied in the amplitude equations of six PDEs. This system of equations are effective in predicting the wave amplitude (envelope) when the internal waves are weakly nonlinear. In the figures presented in chapter 3, we can see the incredible overlap between the numerical and theoretical result. However, this effectiveness also varies with the nonlinearity of internal waves. For the specific forced wave runs or the tide topography interaction run, nonlinearity is represented by the ratio shown in table 3.2. Comparing figures 3.17 and 3.18, which depict waves of different nonlinearity, we can see that when the waves are sufficiently nonlinear and near-resonance occurs, the effectiveness of our theory is very satisfactory; however, when the the nonlinearity parameter is too big, even if we still obtain near-resonance, our theory becomes less effective, but is still capable of predicting the wave form of the first few tidal periods.

In this thesis, the earth's rotation is described by a f- plane. As we change the value of f

in the numerical runs, we find that when $f \neq 0$, a front long wave appears in the plot of mode 2 wave. The envelope and wavenumber of this front long wave varies with f. Work has been done to show that the new front long wave originates from PSI of the harmonic 1 – mode 1 wave. PSI is a type of exact resonance, so, even with the limited information of parent wave and child wave, we are still able to predict the frequency and hence wavenumber of the child waves by the resonant triad condition. This technique predicts that no similar PSI occurs when $f = 0$.

Another branch of studies of nonlinear internal wave theory is weakly nonlinear models characterized by KdV-type equations. The pioneer of the rotation modified equation is the Ostrovsky equation, but it is largely used in describing propagation of internal solitary waves. Aiming to use one sole equation to model two processes of internal wave evolution: generation and propagation of internal waves, we derived a new RMKdV equation, whose dispersion relation has been shown to possess better properties than that of the Ostrovsky equation. The new RMKdV equation is second-order but its wave solution should be rightward propagating in accord with the assumptions used for the derivation. Numerical simulations of this RMKdV equation should be easier without the rigid initial condition from the Ostrovsky equation (refer to the section 4.3 for the rigid initial condition). Modification of this new RMKdV equation to model shoaling internal waves has also been suggested in this thesis.

5.3 Future Work

Several extensions to the work of this thesis are possible:

- We have focused on wave-wave interactions among three waves. It would be interesting to look at near-resonant interaction of four or more waves.
- We have pointed out that the developed near-resonant theory is effective when the model is weakly nonlinear. As the model becomes too nonlinear, the near-resonant theory becomes invalid. More work is needed in finding the range of the nonlinearity parameter so we will be able to test if our theory is applicable to any new model result.
- We have already verified that the low-frequency long waves at the mode-2 wave front occurring for the cases when $f \neq 0$ results from the PSI of the harmonic 1 – mode 1 wave. We have also found the parent wave and child waves for different f by using the resonant

triad condition. But no result has been obtained to predict the envelopes of the three waves in this PSI. Future work can be done to find and solve the amplitude equations as what have been done for the near-resonant triad.

- We have derived the KdV-type equation to model internal waves with the consideration of the earth's rotation. We have not performed numerical simulation of this RMKdV equation. Future work should be done to apply this equation to model internal solitary wave generation and shoaling.

- Our RMKdV equation has been derived under the assumption that the earth' rotation is small. In appendix C, we have explained that the same technique used in this derivation fails if the Coriolis effect is not small. New methods are needed to derive an effective model without the assumption of small rotation. Or, possibly, numerical simulation are needed to show that this RMKdV equation is valid even when the earth's rotation is not small.

APPENDIX A

A NOTE ON THE DETUNING $\triangle k$

The dimensional k is given by

$$k = \pm m \left(\frac{\omega^2 - f^2}{N^2 - \omega^2} \right)^{\frac{1}{2}}, \tag{A.1}$$

which can be written as

$$k = \pm m \frac{\omega}{N} (1 - \frac{f^2}{\omega^2})^{\frac{1}{2}} (1 - \frac{\omega^2}{N^2})^{-\frac{1}{2}}. \tag{A.2}$$

According to this Taylor expansion

$$(1+x)^a = 1 + ax + \frac{a(a-1)}{2!}x^2 + \cdots + \frac{a(a-1)(a-2)\cdots(a-n+1)}{n!}x^n + \cdots, \tag{A.3}$$

where $|x| < 1$, we have

$$k = \pm m \frac{\omega}{N} \left\{ \left[1 - \frac{1}{2}\frac{f^2}{\omega^2} + \mathrm{O}((\frac{f^2}{\omega^2})^2) \right] \left[1 + \frac{1}{2}\frac{\omega^2}{N^2} + \mathrm{O}((\frac{\omega^2}{N^2})^2) \right] \right\}, \tag{A.4}$$

which can be also written

$$k = \pm m \left\{ \frac{\omega}{N} + \frac{1}{2}\frac{\omega^3}{N^3} - \frac{1}{2}\frac{f^2}{N\omega} + \mathrm{O}(\frac{\omega}{N}(\frac{f^2}{\omega^2})^2, (\frac{\omega^2}{N^2})^3) \right\} \tag{A.5}$$

For the wave triad given by (2.11a) – (2.11b), we use k_1, k_2 and k_3 to denote harmonic 2 – mode 2, harmonic 1 – mode 3 and harmonic 2 – mode 2 wave and we use the k_j ($j = 1, 2, 3$) to make

sure that three three waves have same positive phase speed. Then we will have

$$k_1 = -2m_0\left\{\frac{2\omega_{M_2}}{N}+4\frac{\omega_{M_2}^3}{N^3}-\frac{1}{4}\frac{f^2}{N\omega_{M_2}}+\cdots\right\}, \tag{A.6a}$$

$$k_2 = 3m_0\left\{\frac{\omega_{M_2}}{N}+\frac{1}{2}\frac{\omega_{M_2}^3}{N^3}-\frac{1}{2}\frac{f^2}{N\omega_{M_2}}+\cdots\right\}, \tag{A.6b}$$

$$k_3 = m_0\left\{\frac{\omega_{M_2}}{N}+\frac{1}{2}\frac{\omega_{M_2}^3}{N^3}-\frac{1}{2}\frac{f^2}{N\omega_{M_2}}+\cdots\right\}, \tag{A.6c}$$

where we use ellipsis $\cdots$ to represent the higher order terms.

Δk is calculated by summing up (A.6a) – (A.6c)

$$\Delta k = m_0\left\{-4\frac{\omega_{M_2}^3}{N^3}-\frac{3}{2}\frac{f^2}{N\omega_{M_2}}+\mathrm{O}((\frac{f^2}{\omega_{M_2}^2})^2,(\frac{\omega_{M_2}^2}{N^2})^2)\right\}. \tag{A.7}$$

In the numerical model, we chose

$$f = 0.2\times10^{-4}\ s^{-1}, \tag{A.8a}$$

$$\omega_{M_2} = 1.4075\times10^{-4}\ s^{-1}, \tag{A.8b}$$

$$m_0 = 6.283\times10^{-3}\ m^{-1}, \tag{A.8c}$$

$$N = 1.0\times10^{-3}\ s^{-1}, \tag{A.8d}$$

In fact, (A.8a) gives a typical value for f, which has also been selected to be $0.4\times10^{-4}\ s^{-1}$, $0.6\times10^{-4}\ s^{-1}$ and etc.

By using (A.8a) – (A.8d) in (A.7), we can see that Δk is at the order of $10^{-4}\ m^{-1}$. If we keep (A.8b) – (A.8d) and let f take on the value $1.0\times10^{-4}\ s^{-1}$, we still get Δk to be $\mathrm{O}(10^{-3}\ m^{-1})$. This explains why we still get good agreement with the result in figure 3.15.

APPENDIX B

DERIVATION DETAILS OF THE CUBIC NONLINEAR TERM IN THE RMKDV EQUATION

In this appendix, we provide the derivation details of $\aleph$ in (4.95).

$$\begin{aligned}
(BB_t)_t &= (B(-cB_x + 2\epsilon r_{10} cBB_x))_t = (-cBB_x + 2\epsilon r_{10} cB^2 B_x)_t \\
&= -c(BB_x)_t + 2\epsilon r_{10} c(B^2 B_x)_t = -c(B_t B_x + BB_{xt}) + 2\epsilon r_{10} c(B^2 B_x)_t \\
&= -c((-cB_x + 2\epsilon r_{10} cBB_x)B_x + B(-cB_x x + 2\epsilon r_{10} c(BB_x)_x)) + 2\epsilon r_{10} c(B^2 B_x)_t \\
&= c^2(B_x^2 + BB_{xx}) - c(2\epsilon r_{10} cBB_x^2 + 2\epsilon r_{10} cB(BB_x)_x) + \epsilon 2 r_{10} c(B^2 B_x)_t \\
&= c^2(BB_x)_x - 2c^2\epsilon r_{10}(B^2 B_x)_x + 2\epsilon r_{10} c(B^2 B_x)_t \qquad \text{(B.1)}
\end{aligned}$$

We extract this following equation from the above equation

$$(BB_x)_t = -c(BB_x)_x + 2c^2\epsilon r_{10}(B^2 B_x)_x. \qquad \text{(B.2)}$$

APPENDIX C

AN ATTEMPT TO INCLUDE FULL ROTATIONAL EFFECTS

The success of the derivation of a new RMKdV in section 4.5 is largely owing to the fact that we have kept the assumption of a small δ. In this appendix, we will present the difficulty brought by not making this assumption.

If the rotation term δ is small, according to the governing equations given by (1.27a) – (1.27c), we have the leading order equations

$$\begin{aligned} \frac{\partial}{\partial t}\psi_{zz}^{(0,0)} - b_x^{(0,0)} - \delta v_z^{(0,0)} &= 0, && \text{(C.1a)} \\ v_t^{(0,0)} + \psi_z^{(0,0)} &= 0, && \text{(C.1b)} \\ b_t^{(0,0)} + N^2\psi_x^{(0,0)} &= 0, && \text{(C.1c)} \end{aligned}$$

which can be reduced to

$$\frac{\partial^2}{\partial t^2}\psi_{zz}^{(0,0)} + N^2\psi_{xx}^{(0,0)} + \delta\psi_{zz}^{(0,0)} = 0. \qquad \text{(C.2)}$$

Looking for separable solutions for $\psi = B\phi$, we have

$$B_{tt} - c^2 B_{xx} + \delta B = 0, \qquad \text{(C.3)}$$

and the eigenvalue problem,

$$\begin{aligned} \phi_{zz} + \frac{N^2(z)}{c^2}\phi &= 0 \\ \phi(-1) = \phi(0) &= 0. \end{aligned} \qquad \text{(C.4a)}$$

We assume

$$v^{(0,0)} = G(x,t)\phi' \quad \text{and} \quad b^{(0,0)} = H(x,t)N^2(z)\phi, \tag{C.5}$$

then $G_t = -B$, and$H_t = -B_x$. Going back to equation(C.1a), we obtain the leading order equation for B, G and H,

$$B_t\phi'' - H_x N^2\phi = \delta G\phi''. \tag{C.6}$$

Plugging $N(z)\phi = -c^2\phi''$ into (C.6) then gives

$$\begin{aligned} B_t + c^2 H_x &= \delta G(x,t), && \text{(C.7a)}\\ G_t &= B(x,t), && \text{(C.7b)}\\ H_t &= -B_x(x,t), && \text{(C.7c)} \end{aligned}$$

which governs B at the leading order. To derive the equation at higher order, we assume

$$\begin{aligned} B_t + c^2 H_x &= \delta G + \epsilon R(x,t) + \mu Q(x,t), && \text{(C.8a)}\\ G_t &= B(x,t) && \text{(C.8b)}\\ H_t &= -B_x(x,t), && \text{(C.8c)} \end{aligned}$$

Notice that G and H still solve (C.7b) and (C.7c), except that now B is the solution of (C.8a). At $O(\epsilon)$, the governing equations become

$$\frac{\partial}{\partial t}\psi_{zz}^{(1,0)} - b_x^{(1,0)} - \delta v_z^{(1,0)} = J(\psi^{(0,0)}, \psi_{zz}^{(0,0)}) - [\frac{\partial}{\partial t}\psi_{zz}^{(0,0)} - b_x^{(0,0)} \quad - \quad \delta v_z^{(0,0)}]_{\epsilon \text{ term}} \tag{C.9a}$$

$$\frac{\partial}{\partial t}v^{(1,0)} + \psi_z^{(1,0)} = J(\psi^{(0,0)}, v^{(0,0)}) - [v_t^{(0,0)} + \psi_z^{(0,0)}]_{\epsilon \text{ term}} \tag{C.9b}$$

$$\frac{\partial}{\partial t}b^{(1,0)} + N^2\psi_x^{(1,0)} = J(\psi^{(0,0)}, b^{(0,0)}) - [b_t^{(0,0)} + N^2\psi_x^{(0,0)}]_{\epsilon \text{ term}} \tag{C.9c}$$

Since (C.8a) is to modify B_t to a higher order, the ϵ term in (C.9a) is $R(x,t)\phi''$; however, ϵ terms in (C.9b) and (C.9c) do not exist according to (C.8b) and (C.8c).

$$\begin{aligned} J(\psi^{(0,0)}, \psi_{zz}^{(0,0)}) &= BB_x(\phi\phi''' - \phi'\phi''), && \text{(C.10a)}\\ J(\psi^{(0,0)}, v^{(0,0)}) &= B_x G\phi\phi'' - BG_x\phi'^2 && \text{(C.10b)}\\ J(\psi^{(0,0)}, b^{(0,0)}) &= B_x(-Hc^2)\phi\phi''' - B(-H_x c^2)\phi'\phi'' && \text{(C.10c)} \end{aligned}$$

The governing equation can be simplified from (C.9a) – (C.9c) to one differential equation

$$\begin{aligned}\frac{\partial^2}{\partial t^2}\psi_{zz}^{(1,0)} + N^2\psi_{xx}^{(1,0)} + \delta\psi_{zz}^{(1,0)} &= \frac{\partial}{\partial t}\left(BB_x\right)\left(\phi\phi''' - \phi'\phi''\right) - \frac{\partial}{\partial t}R(x,t)\phi'' \\ &+ \frac{\partial}{\partial x}\left(-B_xHc^2\right)\phi\phi''' + \frac{\partial}{\partial x}(BH_xc^2)\phi'\phi'' \\ &+ \delta\frac{\partial}{\partial z}(B_xG\phi\phi'' - BG_x\phi'^2). \end{aligned} \tag{C.11}$$

Notice that (C.11) has the same form of (C.2) except it is inhomogenous in that the RHS is likely not zero. A comparison of this situation with that of section 4.5 leads us to find a solvability condition, so that we will be able to solve for $R(x,t)$ and $\psi^{(1,0)}(x,t)$ in one sole equation (C.11). Similarly, we need the self-adjoint operator ℓ that allows us to use the zero boundary conditions (C.4a). Suppose that on the LHS of (C.11), we can factor out the self-adjoint operator $\ell = \frac{\partial^2}{\partial z^2} + \frac{N(z)^2}{c^2}$ which was also defined in (4.60), then we need to find an appropriate $R(x,t)$ to allow integration of the RHS is zero. In fact, we find

$$\int_{-1}^{0}\phi(\phi\phi''')dz = \int_{-1}^{0}\phi'^3dz, \tag{C.12a}$$

$$\int_{-1}^{0}\phi(\phi'\phi'')dz = -\frac{1}{2}\int_{-1}^{0}\phi'^3dz, \tag{C.12b}$$

$$\int_{-1}^{0}\phi\phi''dz = -\int_{-1}^{0}\phi'^2dz. \tag{C.12c}$$

We need

$$\begin{aligned}\frac{\partial}{\partial t}\left(BB_x\right)\left(\frac{3}{2}\int_{-1}^{0}\phi'^3dz\right) &+ \frac{\partial}{\partial t}R(x,t)\left(\int_{-1}^{0}\phi'^2dz\right) + \delta B_xG\left(\frac{1}{2}\int_{-1}^{0}\phi'^3dz\right) \\ +\delta BG_x\left(\int_{-1}^{0}\phi'^3dz\right) &- \frac{\partial}{\partial x}\left(B_xHc^2\right)\int_{-1}^{0}\phi'^3dz - \frac{\partial}{\partial x}\left(BH_xc^2\right)\left(\frac{1}{2}\int_{-1}^{0}\phi'^3dz\right) = 0\end{aligned} \tag{C.13}$$

Therefore,

$$\frac{\partial}{\partial t}R(x,t) = -\alpha\left(\frac{3}{2}\frac{\partial}{\partial t}(BB_x) + \frac{1}{2}\delta B_xG + \delta BG_x - \frac{\partial}{\partial x}(B_xHc^2) - \frac{1}{2}\frac{\partial}{\partial x}(BH_xc^2)\right), \tag{C.14}$$

where

$$\alpha = \frac{\int_{-1}^{0}\phi'^3dz}{\int_{-1}^{0}\phi'^2dz}. \tag{C.15}$$

We have assumed that LHS of (C.11) has to factor as the self-adjoint operator ℓ. In order to meet this condition, let

$$\psi^{(1,0)} = B^{(1,0)}\phi^{(1,0)}, \tag{C.16}$$

then

$$\frac{\partial^2}{\partial t^2}\psi^{(1,0)}_{zz} + \delta\psi^{(1,0)}_{zz} + N^2\psi^{(1,0)}_{xx} = (\frac{\partial^2}{\partial t^2}B^{(1,0)} + \delta B^{(1,0)})\phi^{(1,0)}_{zz} + N(z)^2 B^{(1,0)}_{xx}\phi^{(1,0)}, \tag{C.17}$$

we so should have

$$\frac{\partial^2}{\partial t^2}B^{(1,0)} + \delta B^{(1,0)} = c^2 B^{(1,0)}_{xx} \tag{C.18}$$

The aforementioned result was obtained under a few assumptions, the most important assumption being that the operator $\frac{\partial^4}{\partial t^2 \partial z^2} + \delta\frac{\partial^2}{\partial z^2} + N^2\frac{\partial^2}{\partial x^2}$ on the LHS has ℓ as a factor. To verify this assumption, we need to show that the RHS of (C.11) is separable, so that the self-ajoint operator exists.

Unfortunately, we have not been able to verify that the RHS of (C.11) is separable.

Bibliography

Armstrong, J. A., Bloembergen, N., Ducuing, J., and Pershan, P. (1962). Interaction between light waves in a nonlinear dielectric. *Physical Review*, 127(2):1918–1939.

Bell, J. B. and Marcus, D. J. (1989). A second-order projection method for variable-density flows. *J. Comp. Phys.*, 85(2):257–283.

Bender, C. M. and Orszag, S. A. (1999). *Advanced Mathematical Methods for Scientists and Engineers: Asymptotic Methods and Perturbation Theory*. Springer.

Benny, D. J. (1966). Long nonlinear waves in fluid flows. *Journal of Mathematics and Physics*, 45:52 – 63.

Boyce, W. E. and Diprima, R. C. (1997). *Elementary differential equations and boundary value problems*. John Wiley and Sons, Inc., New York, sixth edition.

Boyd, J. P. (2005). Ostrovsky and hunter's generic wave equation for weakly dispersive waves: matched asymptotic and pseudospectral study of the paraboloidal travelling waves (corner and near-corner waves). *Euro. Jnl of Applied Mathematics*, 16:65–81.

Choi, W. (2000). Modeling of strongly nonlinear internal waves in a multilayer system. In *Proceedings of the Fourth Intl. Conf. on Hydrodynamics*, pages 453 – 458, Yokohama Univeresity, Japan.

Choi, W. and Camassa, R. (1999). Fully nonlinear internal waves in a two-fluid system. *Journal of Fluid Mechanics*, 396:1–36.

Craik, A. D. D. (1985). *Wave Interactions and fluid flows*. Cambridge University Press.

Djordjevic, V. D. and Redekopp, L. G. (1978). The fission and disintegration of internal solitary waves moving over two-dimensional topography. *Journal of Physical Oceanography*, 8:1016–1024.

Doodson, A. T. (1921). The harmonic development of the tide-generating potential. *Proceedings of the Royal Society of London*, 100(704):305 – 329.

Galkin, V. N. and Stepanyants, Y. A. (1991). On the existence of stationary solitary waves in a rotating fluid. *J. Appl. Maths Mechs*, 55(6):939–943.

Garrett, C. and Kunze, E. (2007). Internal tide generation in the deep ocean. *Ann. Rev. Fluid Mech.*, 39:57–87.

Garrett, C. and Munk, W. (1979). Internal waves in the ocean. *Ann. Rev. Fluid Mech.*, 11:339–69.

Gerkema, T. (1996). A unified model for the generation and fission of internal tides in a rotating ocean. *Journal of Marine Research*, 54(3):421–450.

Gerkema, T. and Zimmerman, J. T. F. (1994). Generation of nonlinear internal tides and solitary waves. *Journal of Physical Oceanography*, pages 1081–1094.

Gill, A. E. (1982). *Atmosphere-Ocean Dynamics*, volume 30. International Geophysics series.

Grimshaw, R., Pelinovksy, E., Talipova, T., and Kurkin, A. (2004). Simulation of the transformation of internal solitary waves on oceanic shelves. *Journal of Physical Oceanography*, 34.

Grimshaw, R., Pelonovsky, E., Stepanyants, Y., and Talipova, T. (2006). Modelling internal solitary waves on the Australian north west shelf. *Marine and Freshwater Research*, 57:265–272.

Hasselmann, K. (1962). On the non-linear energy transfer in a gravity wave spectrum. *Journal of Fluid Mechanics*, 12:481–500.

Helfrich, K. R. (2007). Decay and return of internal solitary waves with rotation. *Physics of Fluids*, 19:026601–9.

Helfrich, K. R. and Melville, W. K. (2006). Long nonlinear internal waves. *Annual Review of Fluid Mechanics*, 38:395–425.

Holloway, P. (2002). Internal tide transformation and oceanic internal solitary waves. In *Environmental Stratified Flows*. Kluwar Academic Publishers, Norwell, Massachusetts.

Jeffrey, A. (1999). *Advanced Engineering Mathematics*. Springer.

Jo, T. C. and Choi, W. (2002). Dynamics of strongly nonlinear internal solitary waves in shallow water. *Studies in applied mathematics*, 109:205–227.

Johnson, R. S. (1997). *A Modern Introduction to the Mathematical Theory of Water Waves*. Cambridge University Press.

Koudella, C. R. and Staquet, C. (2005). Instability mechanism of a two-dimensional progressive internal gravity wave. *Journal of Fluid Mechanics*, 548:165–196.

Kundu, P. K. and Cohen, I. M. (2004). *Fluid Mechanics*. Academic Press.

Lamb, K. G. (1994). Numerical experiments of internal wave generation by strong tidal flow across a finite amplitude bank edge. *Journal of Geophysical Research*, 99:848–864.

Lamb, K. G. (2002). A numerical investigation of solitary internal waves with trapped cores formed via shoaling. *Journal of Fluid Mechanics*, 451:109–144.

Lamb, K. G. (2005). Course note of AM 732: Asymptotic analysis and perturbation theory. unpublished.

Lamb, K. G. (2007a). Course note of AM 863: Hydrodynamic stability and turbulence. unpublished.

Lamb, K. G. (2007b). Tidally generated near-resonant internal gravity waves triads at a shelf break. *Geophysical Research Letters*. submitted.

Lamb, K. G. and Yan, L. (1996). The evolution of internal wave undular bores: comparison of a fully nonlinear numerical model with weakly nonlinear theory. *Journal of Physical Oceanography*, 26(12).

Leblond, P. H. and Mysak, L. A. (1978). *Waves in the Ocean*, volume 20. Elsevier Oceanography Series.

Lee, C.-Y. and Beardsley, R. C. (1974). The generation of long nonlinear internal wavs in a weakly stratified shear flow. *Journal Geophysical Research*, 79:453–462.

Martin, S., Simmons, W., and Wunsch, C. (1972). The excitation of resonant triads by single internal waves. *Journal of Fluid Mechanics*, 53:17–44.

McComas, H. C. and Bretherton, F. P. (1977). Resonant interaction of oceanic internal waves. *Journal of Geophysical Research*, 82:1397–1412.

McEwan, A. D. and Robinson, R. M. (1975). Prametric instability of internal gravity waves. *Journal of Fluid Mechanics*, 67:667–687.

McGoldrick, L. F. (1965). Resonant interactions among capillary-gravity waves. *Journal of Fluid Mechanics*, 21:305–331.

McGoldrick, L. F. (1970). An experiment on second-order capillary-gravity resonant wave interactions. *Journal of Fluid Mechanics*, 40:251–271.

McGoldrick, L. F. (1972). On the rippling of small waves: a harmonic non-linear nearly resonant interaction. *Journal of Fluid Mechanics*, 52:725–751.

Mellor, G. L. (1996). *Introduction to Physical Oceanography*. Springer.

Nayfeh, A. H. (1973). *Perturbation Methods*. Wiley.

Nayfeth, A. H. (1971). Third harmonic resonance in the interactinon of capillary and gravity waves. *Journal of Fluid Mechanics*, 48:385–395.

Neef, L. (2004). Triad resonance as a mechanism for internal wave. Technical report, Woods Hole Oceanographic Institution.

New, A. L. and Pingree, R. D. (2000). An intercomparison of internal solitary waves in the Bay of Biscay and resulting from korteweg-de vries-type theory. *Progress in Oceanography*, 45:1–38.

Ostrovsky, L. (1978). Nonlinear internal waves in a rotating ocean. *Oceanography (Engl. Transl.)*, 18(119).

Pedlosky, J. (1987). *Geophysical Fluid Dynamics*. Springer.

Pelinovsky, E., Stepanyants, Y. A., and Talipova, T. (1994). Simulation of nonlinear internal wave propagation in horizontal in homogeneous ocean. *Atmospheric and Oceanic Physics*, 30(1).

Phillips, O. M. (1960). On the dynamics of unsteady gravity waves of finite amplitude, part 1. the elementary interactions. *Journal of Fluid Mechanics*, 9:193–217.

Phillips, O. M. (1967). Theoretical and experimental studies of gravity wave interactions. *Proceedings of the Royal Society of London.*, 299:104 – 119.

Phillips, O. M. (1981). Wave interaction – the evolution of an idea. *Journal of Fluid Mechanics*, 106:215 – 227.

Press, W. H., Flannery, B. P., Teukolsky, S. A., and Vetterling, W. T. (1992). *Numerical Recipes in C: The Art of Scientific Computing*. Press Syndicate of the University of Cambridge, second edition.

Small, J. (2001). A nonlinear model of the shoaling and refraction of interfacial solitary waes in the ocean. part one: Development of the model and investigations of the shoaling effect. *Journal of Physical Oceanography*, 19:755–772.

Small, R. J. and Hornby, R. P. (2004). A comparison of weakly and fully non-linear models of the shoaling of a solitary internal wave. *Ocean Modelling*, 8:395–416.

Smith, L. M. and Lee, Y. (2005). On near resonances and symmetry breaking in forced rotation flows at moderate rossby number. *Journal of Fluid Mechanics*, 515:111–142.

Staquet, C. and Sommeria, J. (2002). Internal gravity waves: from instability to turbulence. *Annual Review of Fluid mechanics*, 34:559–593.

Tabei, A., Akylas, T., and Lamb, K. G. (2004). Nonlinear effects in reflecting and colliding internal wave beams. *Journal of Fluid Mechanics*, 526:217–243.

Thorpe, S. A. (1966). On wave interactions in a stratified fluid. *Journal of Fluid Mechanics*, 24:737–751.

Williams, E. E. F., Kunze, E. L., and MacKinnon, J. A. (2007). Bispectra of internal tides and parametric subharmonic. *Journal of Physical Geography*. submitted.

Xiao, W. (2006). Shoaling internal solitary waves: comparisons between weakly and fully nonlinear numerical models. Master's thesis, University of Waterloo, Waterloo, Ontario, Canada.